



# GRAĐEVINSKI MATERIJALI I KONSTRUKCIJE

## BUILDING MATERIALS AND STRUCTURES

Volume 67  
March 2024

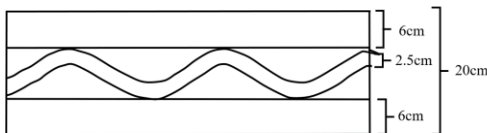
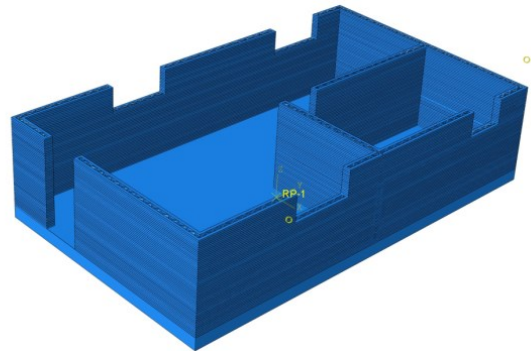
ISSN 2217-8139 (Print)  
ISSN 2335-0229 (Online)  
UDK: 06.055.2:62-  
03+620.1+624.001.5(49  
7.1)=861

# 1

---

Society for Materials and Structures Testing of Serbia  
University of Belgrade Faculty of Civil Engineering  
Association of Structural Engineers of Serbia

---



**CONTENTS**

Peyman Narjabadifam, Somayeh Mollaei, Ehsan Noroozinejad Farsangi, Yahya Talebi Somahe <b>Numerical Analysis of Seismic Behavior of an Arched-Roof 3D-Printed Building</b> Article 2300014P <b>Original scientific paper</b> .....	1
Reda Sadouri, Hocine Kebir, Mustafa Benyoucef <b>Enhancing mechanical properties and crack resistance of earth-sand building materials through alfa fiber reinforcement: an experimental investigation</b> Article 2300015R <b>Original scientific paper</b> .....	17
Rajkumar Ratnaraju <b>Experimental investigation of buried flexible HDPE pipe</b> Article 2300016R <b>Original scientific paper</b> .....	29
Geetha Ramalingam, Vijayalakshmi Ramalingam, Prakash Ramaiah, Sathia Ramalinam <b>Concrete crack analysis using a deep belief convolutional neural network</b> Article 2300017R <b>Original scientific paper</b> .....	37
<b>IN MEMORIAM – Prof. Mihailo Muravljov, PhD</b> <b>December 19, 1937 – January 11, 2024</b> .....	47
Guide for authors.....	50

**EDITORIAL BOARD**

**Editor-in-Chief**

Professor **Snežana Marinković**  
University of Belgrade, Faculty of Civil Engineering, Institute  
for Materials and Structures, Belgrade, Serbia  
e-mail: [sneska@imk.grf.bg.ac.rs](mailto:sneska@imk.grf.bg.ac.rs)

**Deputy Editor-in-Chief**

Professor **Mirjana Malešev**  
University of Novi Sad, Faculty of Technical Sciences,  
Department of Civil Engineering, Novi Sad, Serbia  
e-mail: [miram@uns.ac.rs](mailto:miram@uns.ac.rs)

**Associate Editor**

Dr. **Ehsan Noroozinejad Farsangi**  
Department of Civil Engineering,  
The University of British Columbia, Vancouver, Canada  
e-mail: [ehsan.noroozinejad@ubc.ca](mailto:ehsan.noroozinejad@ubc.ca)

**Members**

Professor **Jose M. Adam**  
ICITECH, Universitat Politècnica de Valencia, Valencia,  
Spain

Dr **Ksenija Janković**  
Institute for Testing Materials – Institute IMS, Belgrade,  
Serbia

Professor Academician **Yatchko P. Ivanov**  
Bulgarian Academy of Sciences, Institute of Mechanics,  
Sofia, Bulgaria

Professor **Tatjana Isaković**  
University of Ljubljana, Faculty of Civil and Geodetic  
Engineering, Ljubljana, Slovenia

Professor **Michael Forde**  
University of Edinburgh, Institute for Infrastructure and  
Environment, School of Engineering, Edinburgh, United  
Kingdom

Professor **Vlastimir Radonjanin**  
University of Novi Sad, Faculty of Technical Sciences,  
Department of Civil Engineering, Novi Sad, Serbia

**Predrag L. Popovic**  
Vice President, Wiss, Janney, Elstner Associates, Inc.,  
Northbrook, Illinois, USA

Professor **Zlatko Marković**  
University of Belgrade, Faculty of Civil Engineering,  
Institute for Materials and Structures, Belgrade, Serbia

Professor **Vladan Kuzmanović**  
University of Belgrade, Faculty of Civil Engineering,  
Belgrade, Serbia

Professor Emeritus **Valeriu A. Stoian**  
University Politehnica of Timisoara, Department of Civil  
Engineering, Research Center for Construction  
Rehabilitation, Timisoara, Romania

Secretary:

**Slavica Živković**, Master of Economics  
Society for Materials and Structures Testing of Serbia, 11000 Belgrade, Kneza Milosa 9  
Telephone: 381 11/3242-589; e-mail: [office@dimk.rs](mailto:office@dimk.rs), veb sajt: [www.dimk.rs](http://www.dimk.rs)

English editing:

Professor **Jelisaveta Šafranč**, University of Novi Sad, Faculty of Technical Sciences, Novi Sad, Serbia

Technical support:

**Stoja Todorović**, e-mail: [saska@imk.grf.bg.ac.rs](mailto:saska@imk.grf.bg.ac.rs)

Dr **Vilma Ducman**  
Head of Laboratory for Cements, Mortars and  
Ceramics, Slovenian National Building and Civil  
Engineering Institute, Ljubljana, Slovenia

Assistant Professor **Ildiko Merta**  
TU Wien, Faculty of Civil Engineering, Institute of  
Material Technology, Building Physics, and Building  
Ecology, Vienna, Austria

Associate Professor **Ivan Ignjatović**  
University of Belgrade, Faculty of Civil Engineering,  
Institute for Materials and Structures, Belgrade, Serbia

Professor **Meri Cvetkovska**  
University "St. Kiril and Metodij", Faculty of Civil  
Engineering, Skopje, Macedonia

Dr **Anamaria Feier**  
University Politehnica of Timisoara, Department for  
Materials and Manufacturing Engineering, Timisoara,  
Romania

Associate Professor **Jelena Dobrić**  
University of Belgrade, Faculty of Civil Engineering,  
Institute for Materials and Structures, Belgrade, Serbia

Dr **Vladimir Gocevski**  
Hydro-Quebec, Mécanique, structures et architecture,  
Ingénierie de production, Montréal (Québec), Canada

Dr **Nikola Tošić**  
MSCA Individual Fellow, Civil and Environmental  
Engineering Department, Universitat Politècnica de  
Catalunya (UPC), Barcelona, Spain

## Aims and scope

Building Materials and Structures aims at providing an international forum for communication and dissemination of innovative research and application in the field of building materials and structures. Journal publishes papers on the characterization of building materials properties, their technologies and modeling. In the area of structural engineering Journal publishes papers dealing with new developments in application of structural mechanics principles and digital technologies for the analysis and design of structures, as well as on the application and skillful use of novel building materials and technologies.

The scope of Building Materials and Structures encompasses, but is not restricted to, the following areas: conventional and non-conventional building materials, recycled materials, smart materials such as nanomaterials and bio-inspired materials, infrastructure engineering, earthquake engineering, wind engineering, fire engineering, blast engineering, structural reliability and integrity, life cycle assessment, structural optimization, structural health monitoring, digital design methods, data-driven analysis methods, experimental methods, performance-based design, innovative construction technologies, and value engineering.

<b>Publishers</b>	Society for Materials and Structures Testing of Serbia, Belgrade, Serbia, veb sajt: <a href="http://www.dimk.rs">www.dimk.rs</a> University of Belgrade Faculty of Civil Engineering, Belgrade, Serbia, <a href="http://www.grf.bg.ac.rs">www.grf.bg.ac.rs</a> Association of Structural Engineers of Serbia, Belgrade, Serbia, <a href="http://dgks.grf.bg.ac.rs">dgks.grf.bg.ac.rs</a>
<b>Print</b>	Razvojno istraživački centar grafičkog inženjerstva, Belgrade, Serbia
<b>Edition</b>	quarterly
<b>Peer reviewed journal</b>	
<b>Journal homepage</b>	<a href="http://www.dimk.rs">www.dimk.rs</a>
<b>Cover</b>	Finite element model of the 3-D printed building from <i>Numerical Analysis of Seismic Behavior of an Arched-Roof 3D-Printed Building</i> by Peyman Narjabadifam, Somayeh Mollaei, Ehsan Noroozinejad Farsangi and Yahya Talebi Somahe
<b>Financial support</b>	Ministry of Education, Science and Technological Development of Republic of Serbia University of Belgrade Faculty of Civil Engineering Institute for testing of materials-IMS Institute, Belgrade Faculty of Technical Sciences, University of Novi Sad, Department of Civil Engineering Serbian Chamber of Engineers

CIP - Каталогizacija u publikaciji  
Narodna biblioteka Srbije, Beograd

620.1

**GRAĐEVINSKI materijali i konstrukcije** = Building materials and structures / editor-in-chief Snežana Marinković  
. - God. 54, br. 3 (2011)- . - Belgrade : Society for Materials and Structures Testing of Serbia : University of Belgrade, Faculty of Civil Engineering : Association of Structural Engineers of Serbia, 2011- (Belgrade : Razvojno istraživački centar grafičkog inženjerstva). - 30 cm

Tromesečno. - Je nastavak: Materijali i konstrukcije  
= ISSN 0543-0798. - Drugo izdanje na drugom medijumu:  
Građevinski materijali i konstrukcije (Online) = ISSN 2335-0229  
ISSN 2217-8139 = Građevinski materijali i konstrukcije  
COBISS.SR-ID 188695820



## Numerical Analysis of Seismic Behavior of an Arched-Roof 3D-Printed Building

Peyman Narjabadifam<sup>1)</sup>, Somayeh Mollaei<sup>\*1)</sup>, Ehsan Noroozinejad Farsangi<sup>\*2)</sup>, Yahya Talebi Somahe<sup>1)</sup>

<sup>1)</sup> University of Bonab, Department of Civil Engineering, Velayat Highway, Bonab, East Azerbaijan, Iran

<sup>2)</sup> Urban Transformations Research Centre (UTRC), Western Sydney University, NSW, Australia

### Article history

Received: 23 October 2023

Received in revised form:

23 December 2023

Accepted: 19 January 2024

Available online: 05 February 2024

### Keywords

3D-Printed Concrete (3DPC) buildings,  
earthquake,  
seismic safety,  
phenomenological modeling

### ABSTRACT

3D-Printed Concrete (3DPC) can reduce the consumption of materials, construction costs, and implementation time, as well as increase sustainability. Seismic safety is one of the necessities of any structure in a high earthquake hazard zone. The lack of scientific and engineering studies in this area would highlight the importance of studying seismic safety in 3DPC building structures. This paper is focused on the basic specifications of 3DPC buildings under earthquake excitations. The authors conducted a thorough theoretical study due to the pilot nature of the research. A prescriptive evaluation was conducted based on the existing seismic regulations for similar structures. The main goal of the research was to create the necessary platform for applied studies, which was achieved through theoretical investigations and prescriptive evaluations. For this purpose, the finite element modeling of a 3DPC building with an arch roofing system was implemented and analyzed using ABAQUS software. Based on the main results, the most remarkable weakness of such a structure was the material's poor tension behavior. The arrangement of the internal partitions (infill walls), the shear performance of the walls, and the relative displacement of the components were other effective factors of the 3DPC building under seismic loads. The results showed that the truss-like performance of the arch roof in the considered 3DPC building probably caused the undesirable structural responses under the seismic loads.

## 1 Introduction

Using 3D-Printed Concrete (3DPC) in buildings can reduce the use of materials, costs, and construction time and increase the sustainability of the building. This technology has other futuristic advantages, such as the ease of transferring the building even to other planets [1-3]. Due to the on-site construction and use of local materials, 3D printing of the buildings significantly reduces transportation costs [4]. This method also substantially reduces adverse environmental effects such as high energy use, greenhouse gas emissions, water use, and waste production in the construction process [5]. The other significant advantage of this technology is the construction of structures with free forms, which requires complex, heavy, and expensive molding systems in ordinary construction methods [6, 7].

Contour Crafting (CC) technology was developed for the first time by Khoshnevis [8], which was among the first examples of 3D printing using concrete materials. 3D printing technology is a set of sciences that includes the disciplines of material, architectural, structural, mechanical, and software engineering and was created to print structures and pieces on a real scale [9]. 3D printing technology is used in most industries, including aerospace, automotive, medicine, weaponry, and the construction industry [10].

Concrete is the most popular material used in 3D-printed buildings. The essential characteristics of concrete materials used in 3D printing construction include the rheological or fresh properties as well as the hardened properties of the concrete [11, 12]. Most of the materials used in the 3DPC mixture are locally available materials, and the desired properties are achieved by chemical additives. However, most common mortars in 3D-printed buildings consist of microsilica, ordinary Portland cement, fly ash, river sand (up to 2 mm grain size), and polypropylene microfibers [4].

In previous studies, factors affecting the rheological properties of the printed concrete material have been studied, such as time interval, extrusion rate, layer thickness, material composition, fibers, nozzle tip geometry, etc., [3, 6, 7, 12, 13, 14]. Ahmed Saleh [3] evaluated the feasibility of concrete in 3D printing construction. He concluded that 3D concrete printing has a promising future in construction. Jeong et al. [6] proposed a model to derive the rheological properties of the 3D-printed concrete material. It was proven that using sisal fibers in printed mortar led to a higher yield stress and cohesiveness of the mix [7]. Bukvić et al. [12] reviewed the pumpability and printability properties of fresh printable concrete in past research.

\* Corresponding author:

E-mail address: [s.mollaei@ubonab.ac.ir](mailto:s.mollaei@ubonab.ac.ir) & [ehsan.noroozinejad@westernsydney.edu.au](mailto:ehsan.noroozinejad@westernsydney.edu.au)

Khoshnevis [8] reviewed the basic concepts in the construction of a 3D-printed building. The study results showed that the increasing voids in the layers, the lightness of the material, as well as the use of a layered dome form inspired by traditional methods in the bed of modern materials, could be helpful in practical applications [8]. Van et al. [13] studied the interlayer bonding in printed construction. They found that the application of a robust system for 3D concrete printing was as vital as the material properties [13]. Also, Bos et al. [15] conducted a study to reinforce printed concrete using steel cables. They showed that steel reinforcement was a feasible method to achieve improved material behavior.

Martens et al. [16] conducted a study to optimize the material mixture and topology of the structure for 3D-printed buildings. Also, Hojati et al. [17] conducted studies on different mixtures of printed materials, including native materials on Mars. Their studies showed that native materials on Mars have a high potential for printing buildings there. Also, using long fibers can increase the structure's efficiency [17]. Daniel et al. [18] studied the possibility of improving the strength of layers. Their studies showed that shorter time intervals and increased contact area were helpful in improving interlayer bonding [18]. Skibicki et al. [19] tested some novel compositions for printed building materials at different temperatures. Their proposed methods had enhancing effects on the curing time of the printed materials and led to a higher speed of the construction process. Padnis and Shariff [20] proposed a numerical method to calculate the critical buckling height of the 3D-printed walls. They validated the proposed method using test results. Li et al. [14] reviewed the experimental testing on the fresh-state and hardened properties of the materials in 3D-printed concrete.

Pudjisuryadi et al. [1] studied the weaknesses of printed structural beams. They concluded that the use of small-scale samples may not be suitable to predict the behavior of the printed structures. Federowicz et al. [21] investigated the shrinkage of 3D-printed cement materials and the deformations caused by this shrinkage at different time intervals. They showed that the application of anti-shrinkage admixtures did not change the compressive strength of the hardened material. Olobokola [22] investigated the difference between the results of finite element analysis (FEA) and analytical models for 3D-printed components. The study showed a close correlation between manual calculations and computer analyses. Pekuss et al. [23] studied 3D-printed columns with different geometrical complexities. Wang et al. [24] studied the interface properties of the printed concrete layers. The ultimate tensile strength and shear strength of 3D-printed concrete were increased by using steel rebars and fiber reinforcement in the printed material.

Chang et al. [25] proposed a model with a new failure criterion for numerical modeling of 3D-printed concrete. Licciardello et al. [26] conducted experimental studies on the hardening behavior of printed concrete walls. Gebhard et al. [11] investigated the bending behavior of printed beams. Duarte et al. [27] investigated the geometric form of printed buildings. They showed that load-bearing wall systems with shell and arch forms were desirable geometries [27]. Pan et al. [28] investigated the effects of raw material properties on the interlayer bond of printed concrete at different time intervals. Xiao et al. [29] proposed the idea of using recycled materials in 3D-printed buildings.

Recently, Xiao et al. [30] reviewed the literature on appropriate geometric forms and structures for 3DPC

buildings. Essebyty et al. [31] investigated the sustainability of 3D-printed buildings in a case study. They showed that the seismic performance of the building was similar to that of an unreinforced masonry building. In another study, Zhang et al. [32] investigated the 3D-printed walls under Gaussian-static loading conditions. Their study proved that the 3DCP building reinforced with FRP textile had desirable mechanical properties. One study on the structural design of printed buildings subject to dynamic loadings is that by Aghajani Delavar et al. [33], who studied the design, modeling, and analysis of 3D-printed walls under dynamic horizontal loads. They proposed analytical equations to forecast the behavior of 3D-printed walls under in-plane seismic loading, which OpenSees numerical results validated.

Reviewing the literature on 3DPC buildings proved that the seismic performance and nonlinear behavior of those buildings have not been widely studied. Most previous studies in this field have focused on the mixture plans and construction methods of 3DPC structures. While seismic safety is one of the basic needs of any structure located in an earthquake-prone environment, printed structures are no exception to this.

Investigating the seismic safety of 3D-printed buildings could be helpful to expand the practical applications of those structures. This issue was considered in this study. This research attempted to determine the basic needs and characteristics of earthquake engineering in 3D-printed structures. Here, defining a prescriptive evaluation process for the seismic safety of printed structures and providing a practical model for a detailed evaluation of the seismic safety of these structures were pursued. For this purpose, an extensive theoretical study was conducted using technical literature related to printed structures. In the following, the existing seismic regulations were used for loading, analysis, and modeling of the considered 3DPC building. Then, a practical phenomenological model was proposed for a 3D-printed structure using ABAQUS finite element software.

## 2 Materials and methods

The initial hypothesis in this study was that the basic needs of earthquake engineering in printed structures mainly include control of accelerations. Also, another hypothesis of the authors was that a prescriptive evaluation process of printed buildings can be defined based on the existing building seismic criteria. The research process and results are described and discussed in the following parts.

### 2.1 3D-printed structure considered in the study

As shown in Figure 1a, the considered model was a barrel vault structure with dimensions of  $10 \times 6$  m and a wall height of 3 m with an arch roofing form. The geometric and material properties of the considered building were selected with minimum discontinuity. Therefore, any reinforcements or different material types were not taken into account. The existing 3D printing technologies can guarantee the implementation of the whole building, from the foundation to the rooftop, without human intervention. Hence, the considered 3D-printed structure can be implemented without any human intervention and in all directions, even on other planets. According to previous studies, the arching system is one of the recommended forms for 3D-printed structures [8, 27]. As shown in Figure 1b, on each of the longitudinal perimeter walls (y direction), two openings were considered as windows, and one opening was created as a door at the

transverse end of the building. Also, two inner infill walls were modeled in the considered building. The layers of the walls and roof of the model had a truss-like structure with a 20 cm width. As shown in Figures 1c to 1e, the cross-section of the walls and arch was a two-row truss-like form with a width of 6cm in each row and a distance of 8 cm from each other. The rows were connected by zigzagged grids with a width of 2.5 cm. A cross-section with parallel filaments and a grid pattern between them is widely used for 3D-printed structures [34]. The thickness of every printing layer was assumed to be 4 cm. The specific weight of the printing concrete was 2100 kg/cm<sup>3</sup>.

The maximum height of the arch at the highest point was 3 m. The dimensions of the foundation were 10 × 6 m, with a thickness of 30 cm. The 3D-printed perimeter walls were assumed to be the lateral and gravitational load-bearing systems of the studied structure. Also, it was assumed that 3D printing technology without human intervention was used in the construction process. Therefore, all the rheological properties of the concrete material were assumed to be isotropic and homogenous. During the construction of the structure, no additional stresses had been applied to the structure due to the movement of the nozzle or its vibrations, so no stress reduction had been considered in the material model.

## 2.2 Loading of the structure

The regulations used in this study included National Building Regulations of Iran parts 6, 8, and 9 [35-37], which are dedicated to seismic loading and the design and execution requirements of masonry and reinforced concrete buildings, respectively. Also, the Organization of Strategic Planning and Supervision of Iran publications No. 740 and 360 [38, 39] were used in this study, which includes guidelines for seismic evaluation and rehabilitation of buildings. It should be noted that the lack of specialized regulations was the most essential and fundamental limitation of this study. Also, the lack of previous studies on the behavior of 3D-printed structures under the conditions of natural disasters was another limitation.

Here, a residential building was investigated, which was located in Tabriz city, Iran, and on the third soil type. Therefore, according to Iranian seismic standard criteria No. 2800 [40], its experimental period of vibration can be obtained using Equation 1. Based on the mentioned criteria, the equivalent lateral force is the most commonly used technique for seismic analysis.

$$T = 0.08H^{0.75} \quad (1)$$

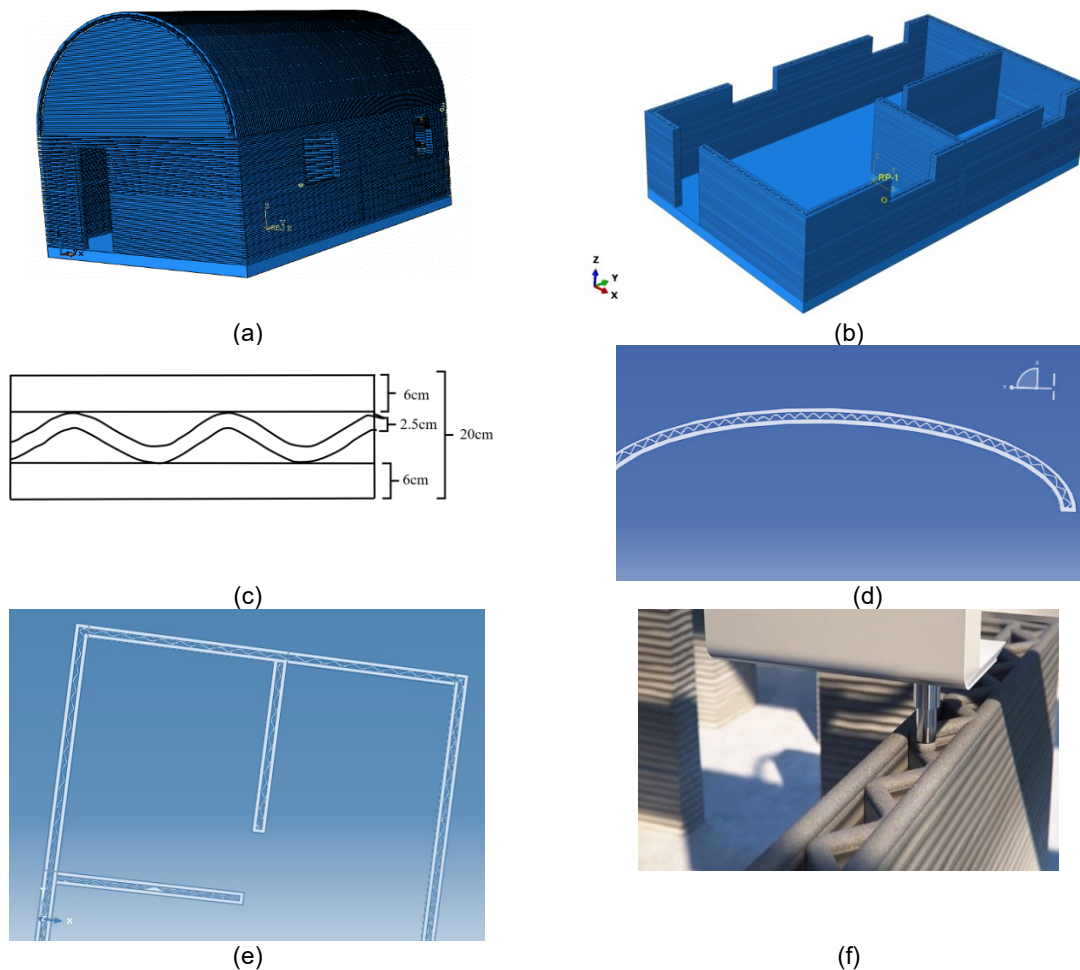


Figure 1. Finite element model of the considered building in this study: a) 3D-printed building; b) building plan; c) cross-section of the arch and walls; d) a layer of the modeled arch roof; e) a layer of the modeled walls; f) schematic printing process of the parallel filament with internal grids

Where  $T$  is the main period of vibration(s), and  $H$  is the height of the building (m).

The reflection coefficient of the building is a parameter that is used for calculating the seismic coefficient of the building, and it can be calculated by Equation (2).

$$B = B_1 N \quad (2)$$

Where  $B_1$  is the spectral shape factor (SSF) and  $N$  is the spectral correction factor.  $B_1$  is also calculated by Equation (3).

$$B_1 = \begin{cases} S_o + (S - S_o + 1) \left(\frac{T}{T_o}\right); & 0 < T < T_o \\ S + 1; & T_o < T < T_s \\ (S + 1) \left(\frac{T}{T_o}\right); & T > T_o \end{cases} \quad (3)$$

Where  $T$  is the main period of the building (s), and  $T_o$ ,  $T_s$ ,  $S$ , and  $S_o$  are parameters that depend on the soil type and the seismic zone of the region.

Considering that 3D-printed buildings are not part of any structural systems classified in the existing seismic regulations, and given that this research is a pilot study, the behavior factor of  $R$  can be considered equal to 1. This is a conservative assumption.

Given the values of  $A$ ,  $B$ , and  $R$ , the seismic coefficient of the building can be obtained from Equation (4).

$$C = ABIR \quad (4)$$

Where  $A$  is the design acceleration,  $B$  is the reflection coefficient,  $I$  is the importance coefficient, and  $R$  is the coefficient of the behavior of the building. The seismic characteristics of the considered building are tabulated in Table 1.

Table 1. Seismic characteristics of the building (based on the regulations [38-40])

A	B	I	R	C	W
0.35	2.75	1	1	0.9625	55784kg

Snow loading, as a live load on the arched roof, was calculated according to the National Building Regulations of Iran Part 6 [33] by Equation (5).

$$Pr = 0.7CsCtCeIPg \quad (5)$$

Where  $Pr$  is the snow load on the arch per square centimeter of the horizontal projection of the surface,  $Ce$  is the snow removal coefficient,  $Ct$  is the temperature condition coefficient,  $Pg$  is the weight of the snow layer on the horizontal projection of the ground, and  $C_s$  is the slope coefficient of the roof.

The ultimate limit state load combinations were applied according to Equation (6) [35].

$$D + 1.5L + 1.2(Lr \text{ or } S \text{ or } Rr) + 1.2(w \text{ or } 0.7E) \quad (6)$$

Where  $D$  is the dead load of the building,  $L$  is the live load on the floors,  $Lr$  is the live load on the arch,  $S$  is the snow load,  $Rr$  is the rain load,  $E$  is the design earthquake load, and  $w$  is the maximum wind load.

The foundation shear force caused by the earthquake refers to the sum of the lateral forces of the earthquake, which is applied to the foundation of the building according to Equation (7).

$$V = CW \quad (7)$$

Where  $V$  is the floor shear force and  $W$  is the effective seismic weight (including the dead load and the weight of facilities and infill walls as well as a percentage of the live and snow loads) [38-40].

The foundation shear force is distributed by the height of the building by Equation (8).

$$Fi = \frac{Wh}{Wh} V \quad (8)$$

Where  $Fi$  is the lateral force at the level of the floor,  $w$  is the weight of the floor, including the weight of the arch and half of the weight of the walls and columns above and below the roof, and  $h$  is the height of the roof from the base level.

### 2.3 Shear resistance force of the wall [10]

The shear stress in 3D-printed structures can be defined as Equation (9) using Mohr–Coulomb theory.

$$\tau = \sigma \tan(\phi) + Cc \quad (9)$$

Where  $\tau$  is the resistant shear stress in the wall,  $\sigma$  is the normal stress due to the weight of the upper layers,  $\phi$  is the internal friction angle, and  $Cc$  is cohesion. The value of  $\sigma$  is calculated by Equation (10).

$$\sigma = \rho h \quad (10)$$

Where  $\rho$  is the concrete density, and  $h$  is the height of the wall.

To obtain the shear stress, the value of  $Cc$  should be determined by Equation (11).

$$C_c = \frac{(1 - Ky) + (1 + Ky)\sin(\Phi)}{2\cos(\Phi)} \sigma \quad (11)$$

The value of  $Ky$  is equal to the Poisson ratio of the material.

#### 2.3.1 The friction force [10]

The maximum frictional stress is obtained from Equation (12).

$$Fcr(i) = \frac{\mu Vg}{Lbi} \quad (12)$$

Where  $Fcr(i)$  is the maximum interlayer frictional stress,  $\mu$  is the coefficient of internal friction,  $Vg$  is the gravity load caused by dead and live loads on the wall,  $L$  is the length of the multilayer beam or wall, and  $bi$  is the inner surface of the wall or multilayer beam.

### 2.4 FEA

The dynamic analysis of the structure under earthquake excitation was performed using the finite element software by introducing the ground displacement time history at the base level of the building. In this analysis, the damping ratio can be assumed to be 5%, unless it can be shown that other values are more suitable for the structure [40]. Currently, there is no consensus about how to select and scale the earthquake motions for code-based design and evaluation of the seismic performance of buildings using nonlinear response history analysis [41].

The finite element modeling of the 3D-printed structure was implemented using ABAQUS software following the criteria discussed in the National Building Regulations of Iran, Part 8 [36]. In the following, the loading of the structure

and the ultimate state load combination were defined. Tabas earthquake records were used as the design earthquake in this study. Finally, non-linear time history analysis of the structure was done, and the results were evaluated.

2.4.1 ABAQUS software [42]

ABAQUS is a commercial package for computer-aided FEA of structures. The Explicit solver is one of several multipurpose solvers in ABAQUS that uses the explicit integration method to solve problems with a high degree of nonlinearity, such as complex contact interactions and severe transient loads. In this study, the explicit solver of ABAQUS is used to analyze the considered 3D-printed building under seismic loads.

2.4.2 Material model

In the previous studies, no special constitutive model for 3DPC has been introduced yet [43]. According to past studies, the numerical simulation methods for masonry and other layered structures can be considered for 3DPC [44]. The material model used in this study was plain cement concrete (PCC) (not reinforced). Therefore, the Concrete Damage Plasticity (CDP) model was used to define the non-linear behavior of the material, which is available in the material library of ABAQUS. In order to obtain the inelastic behavior of the material, damaged elasticity, and isotropic tensile, and compressive plasticity can be used in the CDP

model. According to Equation (13), the total strain tensor  $\epsilon$  consists of two elastic and plastic parts.

$$\epsilon = \epsilon_{el} + \epsilon_{pl} \tag{13}$$

Where  $\epsilon$  is the total strain tensor,  $\epsilon_{el}$  is the strain tensor of the elastic region, and  $\epsilon_{pl}$  is the plastic strain tensor.

In this model, isotropic hardening variables are expressed by inelastic compressive strain, cracking strain, including plastic hardening strain, and residual strain due to the damage. Hardening variables are used to control the crack development or failure level. Figure 2 shows the uniaxial compressive and tensile behaviors of the concrete material in the CDP model.

In Figure 2,  $\sigma_{cu}$  is the ultimate compressive strength,  $\sigma_{co}$  is the compressive strength,  $\epsilon_{in}$  is the inelastic strain, and  $\sigma_c$  is the compressive strength of concrete.  $\sigma_t$  is the tensile stress,  $\sigma_{to}$  is the tensile strength,  $\epsilon_p$  is the plastic strain tensor, and  $\epsilon_t$  is the tensile strain. The compressive and tensile behavior of the unconfined concrete can be calculated based on the formulas presented in the literature [45].

Table 2 shows the specifications of the concrete material used in the 3D-printed structure model in this study. In this model, the results of previous studies on the behavior of unconfined plain concrete [45] have been used, which were assumed to be similar to the material behavior of the 3D-printed concrete considered here. In Table 2,  $f_{c0}$  is the initial uniaxial compressive yield stress,  $K$  is the shape parameter, and  $\rho$  is the mass density of the material.

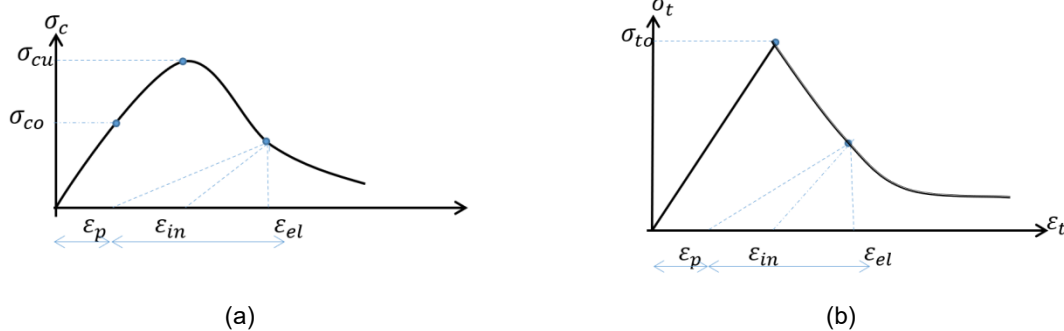


Figure 2. Concrete behavior: a) incompression; b) intension [45]

Table 2. Specifications of the concrete material model

Elasticity parameters		plasticity parameters	
Young's modulus(kg/cm <sup>2</sup> )	250000	dilation angle (°)	30
f <sub>c0</sub>	234	eccentricity	0.1
Poisson ratio	0.24	f <sub>b0</sub> /f <sub>c0</sub>	1.16
Friction coefficient	1.94	K	0.67
φ	20	viscosity parameter	0
		ρ (kg/m <sup>3</sup> )	2100
compressive behavior		Compressive damage	
yield stress (kg/cm <sup>2</sup> )	inelastic strain	damage parameter	inelastic strain
104.2	0	0	0
130.52	0.000077	0	0.000077
152.9	0.00017	0	0.00017
171.03	0.00028	0	0.00028
185.58	0.00042	0	0.00042

195.78	0.00057	0	0.00057
201.9	0.00074	0	0.00074
203.94	0.00093	0	0.00093
200	0.0011	0.01	0.0011
195	0.0013	0.04	0.0013
185	0.0016	0.09	0.0016
170	0.0018	0.16	0.0018
152	0.0021	0.25	0.0021
130.5	0.0024	0.36	0.0024
104	0.0028	0.49	0.0028
73.42	0.0031	0.64	0.0031
32.6	0.0035	0.81	0.0035
tensile behavior		tension damage	
yield stress (kg/cm <sup>2</sup> )	cracking strain	damage parameter	cracking strain
20	0	0	0
0.02	0.00094	0.99	0.00094

Interfacial forces between the printed layers were introduced to the model using Equations (9)-(12). As mentioned before, each printing layer with a 4 cm thickness was subject to the bonding resistance of the face and the weight of the upper layers. FE modeling of the printing layers is illustrated in Figure 3.

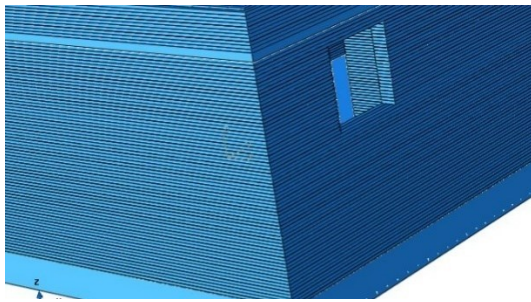
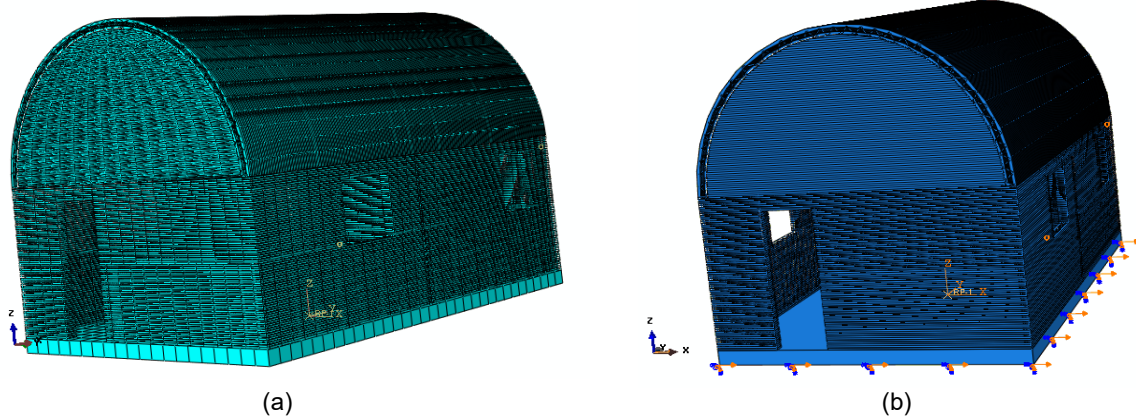


Figure 3. FE modeling of the consecutive printed layers

### 2.4.3 Boundary conditions and meshing

The nodes of the foundation floor were fully restrained against displacement and rotation in all directions. In the STEP of the earthquake excitation, the time history record of the earthquake was applied to the foundation nodes as boundary conditions (BCs). At the same time, the other degrees of freedom were still restrained. In order to avoid convergence problems in the software, three-dimensional HEX (8-node brick) elements with average dimensions of 30×30×30 cm were used to model the solid layers of the cross section. Also, the zigzagged grids between the two were modeled using 4-noded shell elements. Figure 4 shows the meshing of the FE model as well as the BCs defined in the analysis steps.



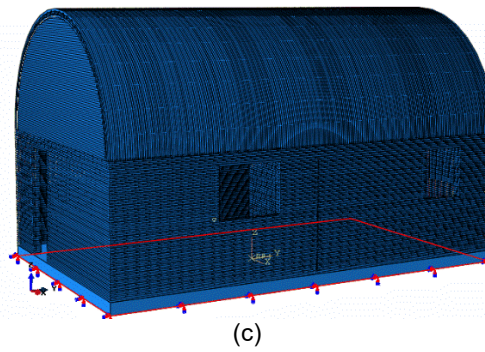


Figure 4. FE modeling of the considered building: a) meshing of the model; b) BCs for earthquake load step; c) BCs for initial and gravity load step.

In the analysis procedure of the model, a separate static general STEP was defined for gravity loads. A dynamic load STEP was assigned to the seismic loads as well, and the multi-step analysis was implemented. The results of the analyses were summarized and discussed in the following.

#### 2.4.4 Seismic excitation

To put the earthquake loads on the building, the horizontal part of the earthquake accelerogram close to the Tabas fault, which has the details shown in Table 3 and Figure 5, was used. It came from a peer site [46]. Due to the time-consuming explicit analysis procedure in ABAQUS as well as the large number of elements in the considered model, only the records of severe ground motions from the earthquake were used here (Figure 6).

Table 3. Characteristics of the Tabas earthquake records

Spectral ordinate	event	year	station	Mag Mechanism
SRSS	Tabas,iran	1978	Bajestan	7.3
SRSS	Tabas,iran	1978	Boshrooyeh	7.3
SRSS	Tabas,iran	1978	Dayhook	7.3
SRSS	Tabas,iran	1978	Ferdows	7.3
SRSS	Tabas,iran	1978	Kashmar	7.3
SRSS	Tabas,iran	1978	Sedeh	7.3
SRSS	Tabas,iran	1978	tabas	7.3

### 3 Results and Discussion

This section reviews the study findings regarding how seismic excitation affected the behavior of the 3D-printed structure. Here, the horizontal seismic excitation was applied once along the x-axis (transverse direction of the building) and the y-axis (longitudinal direction). The effects of external loading, cracks propagation, and the severity of damage to the structure during the earthquake were evaluated. In the following, the failure pattern of the structure was investigated. Finally, possible solutions to deal with the structural damages were presented according to the regulations and previous studies.

In this study, due to the lack of facilities to construct the 3D-printed structure as well as the lack of results of experimental studies on this type of structure, it was not possible to validate FEA results compared to the laboratory data. Hence, the results of all analyses were interpreted theoretically according to scientific principles and theoretical engineering considerations. Also, according to the design of the research model following the Iranian National Building Regulations, all the responses of the structure were controlled by those regulations.

FEA performed by Tahmasebinia et al. [47] on a model of a 3D-printed structure with arch roofing showed that the joints between the arch and walls and the foot of the arches were always the most critical positions under gravitational loads. These results are consistent with the results of the upcoming research. In the following parts, those results will be provided and discussed.

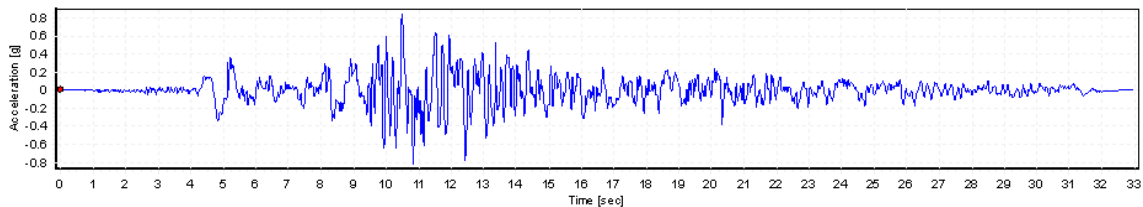


Figure 5. The Tabas earthquake accelerogram

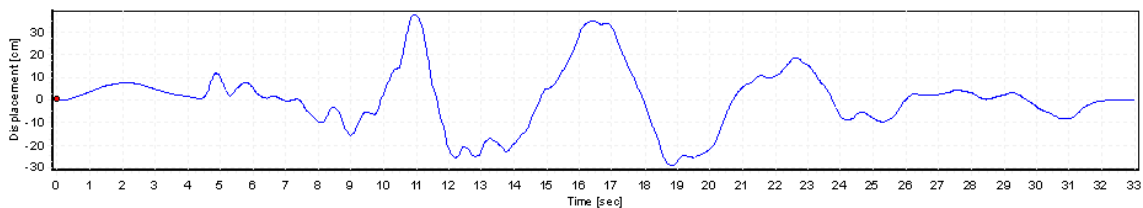


Figure 6. Strong ground movements of the Tabas earthquake records

3.1 Deformations and displacements

Figure 7 shows the structural elements before and after the seismic excitation along the x-axis (transverse direction of the building). Therefore, the undeformed shape of the elements is visible behind the deformed shape, as shown in Figure 7. The largest deformation occurred in the elements of the arch (the connection points to the wall) and in the connection points of the base of the walls to the foundation, where there is a sudden change in the geometry of the layers.

3.2 Deformation and stress in the arch system

Under seismic excitation along the x-axis, the von Mises stress quantities in the arch of the building along the path, as shown in Figure 8a, are drawn in Figure 8b. Due to symmetry in the structure and seismic excitation, only half of the arch span has been checked. Figure 8b shows that the von Mises stress has increased significantly in both halves of the arch. This result is rational because a shallow arch behaves like a beam under uniform loading conditions [48].

Figure 8c illustrates the variations in von Mises stress in the arch along the considered path in the z-direction (height

of the structure). As shown in Figure 9c, the stress at the arc's beginning shows a higher value. But gradually, from the edge to the end of the first third of the arch, the stress reduces significantly. Then, in the middle third of the arch, a significant increase is observed again. Given that von Mises stress is used for normal, shear, and combined stress, as shown in Figure 8, it is concluded that the behavior of the arch corresponds to the behavior of a beam under a uniform load.

Figure 9a illustrates the variations in the displacement of the arch elements in the x-direction proportional to the distance along the arc, drawn along the same path as demonstrated in Figure 9a. The displacement shown in Figures 9a and b demonstrates that the failure occurred almost at the beginning of the arch. Also, the amount and trend of displacement in the x- and z-directions are very similar. So, at the beginning of the arc, the slope of displacement changes in the x-direction is much steeper than the displacement slope in the z-direction. This difference is due to the presence of a support in the z-direction. In the x direction, due to being in alignment with the lateral force as well as the gap space between the two faces of the truss section of the wall, higher displacement occurs.

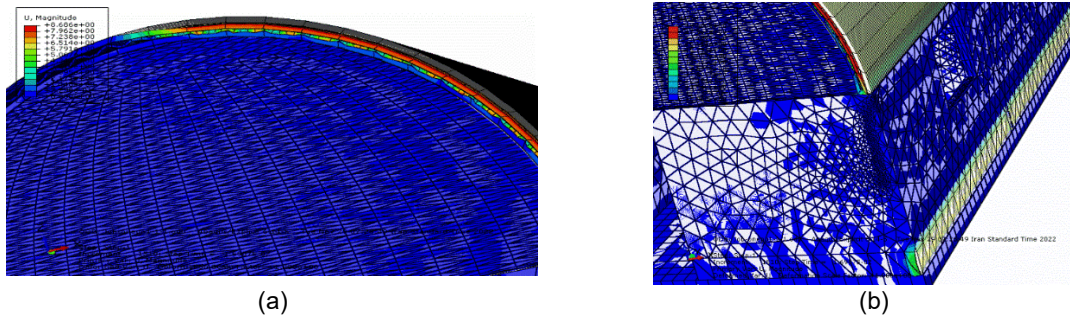


Figure 7. Deformed and undeformed elements of: a) the arch; b) the body of the structure

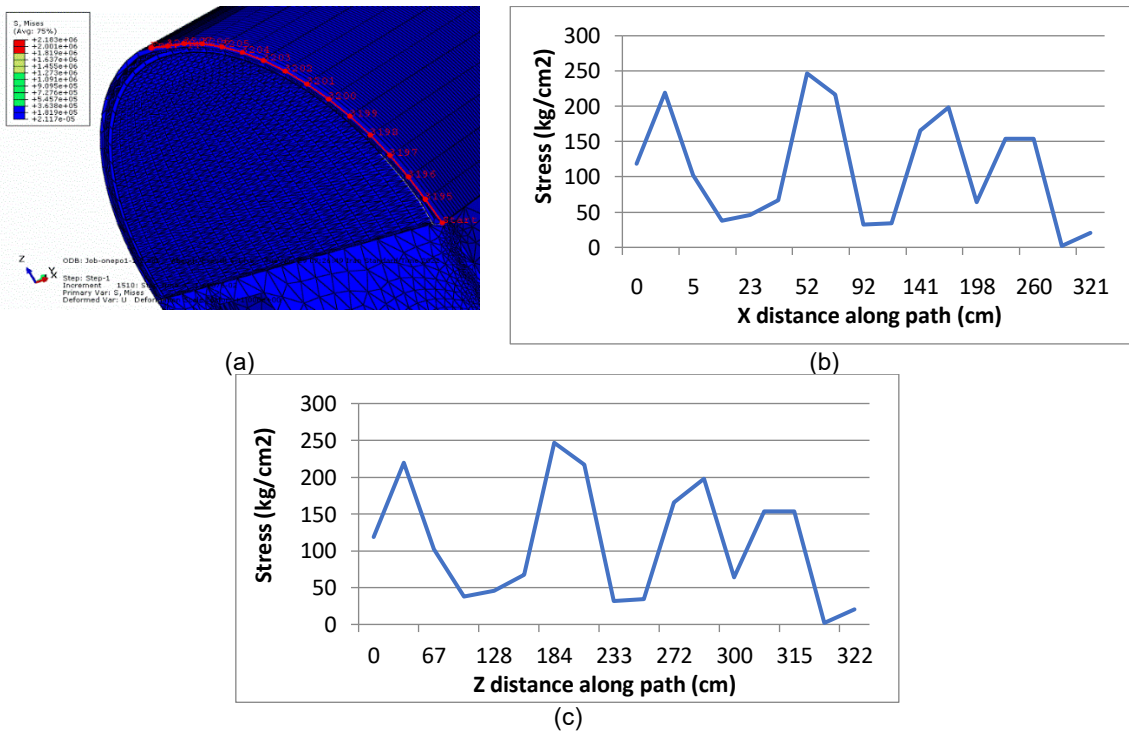


Figure 8. a) The considered path on the arch; b) von Mises stress variations in the x-direction; c) von Mises stress variations in the z-direction

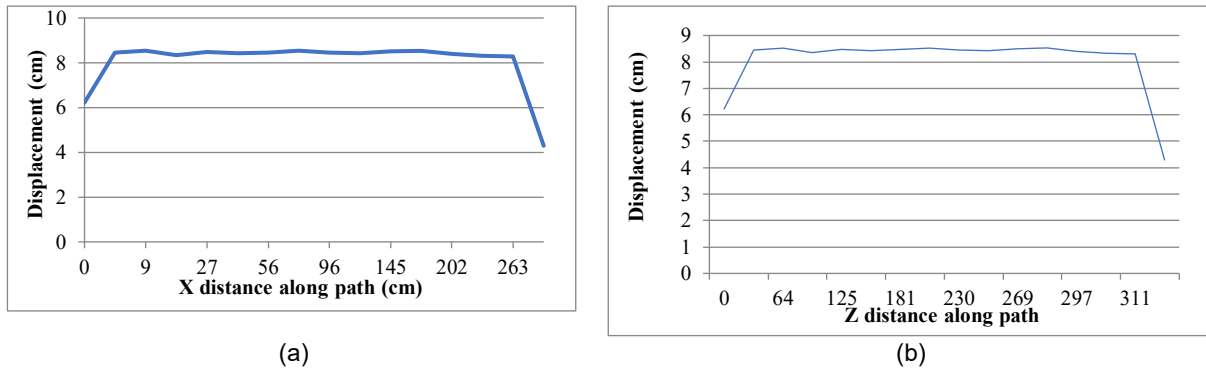


Figure 9. Displacement variations in the arch proportional to the distance from the beginning of the arch in the: a) x-direction; b) z-direction

By comparing Figures 8 and 9, it can be said that the stresses increase significantly in the middle of the arch. On the other hand, the high amount of displacement at the beginning of the arch has led to failure at this point. Therefore, at the beginning of the arch, i.e., at the connections of the arch and the wall of the building, there is a need to strengthen and/or replace the geometry or materials. In order to solve this problem, it is better to combine different arc radii in the arch or other roofing forms with a uniform change in the connection to the walls. In previous studies, other geometric shapes have been proposed for the roof of 3D-printed buildings [8, 49].

The maximum response value of the support reactions, as demonstrated in Figure 10a, is equal to  $1.102 \times 10^5$  kgf ( $1.081 \times 10^6$  N). This was recorded in one of the middle nodes of the building's foundation, which has reached the

point of yielding and failure in terms of resistance. On the other hand, the maximum plastic strain occurred in one of the middle nodes at the joint of the internal partition to the perimeter wall of the building (Figure 10b). The place where the maximum deformations occurred was on the edge of the partition wall connected to the perimeter wall. This reveals the critical effect of partition walls and their connection to the structure. Observations revealed that the highest stress in the structure occurred in the middle part of the longitudinal wall, perpendicular to seismic excitation. This point is precisely where the interior partition is connected to the perimeter wall of the building. Therefore, this also indicates the importance of placement and the existence of partitions in 3-D printed structures.

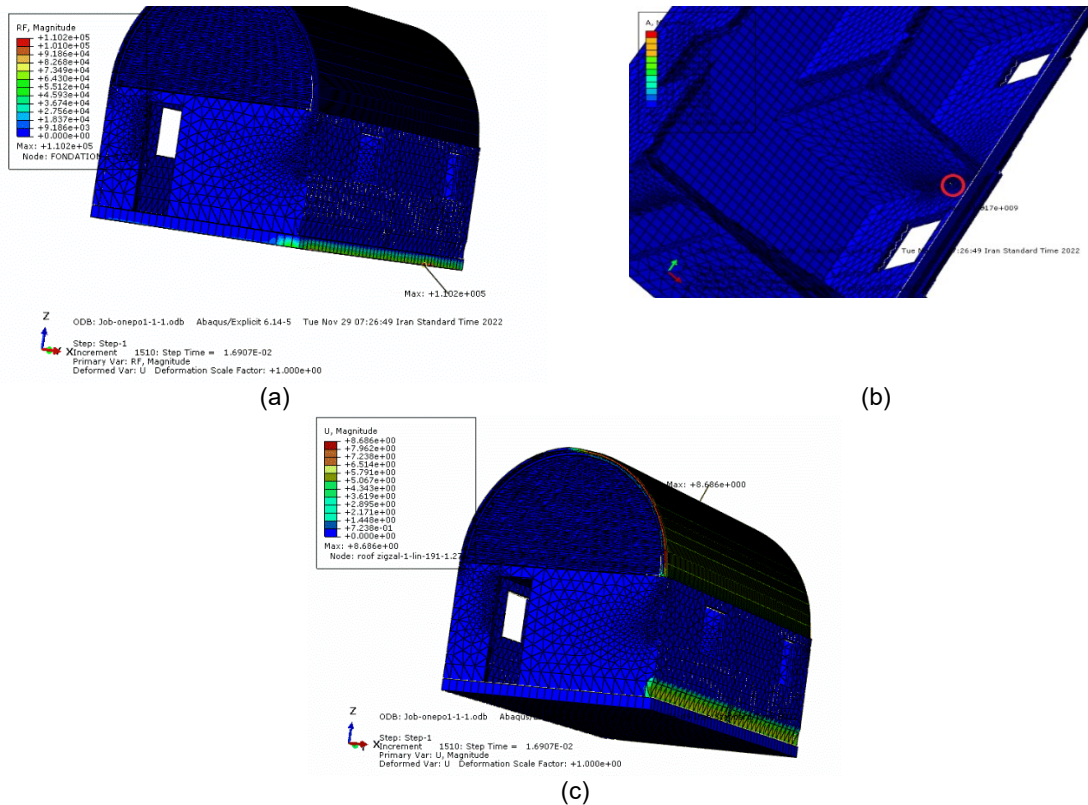


Figure 10. Extreme values of: a) support reactions; b) plastic strains; c) displacements

Figure 10c shows that the highest displacement in the structure is related to the grids located between the two layers of the arch. Most of the time, components of truss-like sections undergo buckling and instability before reaching the yield point. These large deformations cause structural collapse in the truss-like section components before reaching the yield condition. The walls of the model in this study also follow the pattern of truss behavior. In most cases, the arch is vulnerable due to the large displacement of the structure. This can be seen more clearly if the deformation is magnified, as shown in Figure 11.

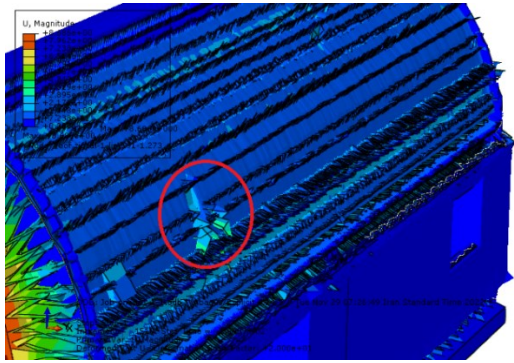


Figure 11. Maximum damage to the structure (magnified deformations)

### 3.2 Stress and displacement in the foundation

Under seismic excitation along the x-axis (transverse direction of the building), as shown in Figure 12a, a path was considered in the structure foundation in the direction of the y-axis for the changes in stress and reactions in the support (building foundation). Figures 12b, c, and d show the variations in von Mises stress, plastic strain, and support reaction forces in the considered path, respectively. Figure 11c shows that approximately 800 cm from the beginning of the path, along the length of the structure, the stress has the highest value. Also, at the beginning and end of the path, the amount of stress is found to be very large in the structure's foundation.

As shown in Figure 12d, the support force in the structure foundation near the distance of 800 centimeters from the beginning of the path has the highest value, as shown in the stress diagram. The presence of internal infill walls and their connection to the external walls on this side of the building can be the main cause of asymmetries in the stress and strain responses as well as the reactions in the foundation.

In the printing process of 3D structures, all the building components are executed layer by layer. Therefore, the partitions inside the building cannot be considered separately from the (lateral or gravitational) load-bearing system. This internal partitioning affects the behavior of the structure. Therefore, the thickness of the partition walls, their location, and their length are very significant issues.

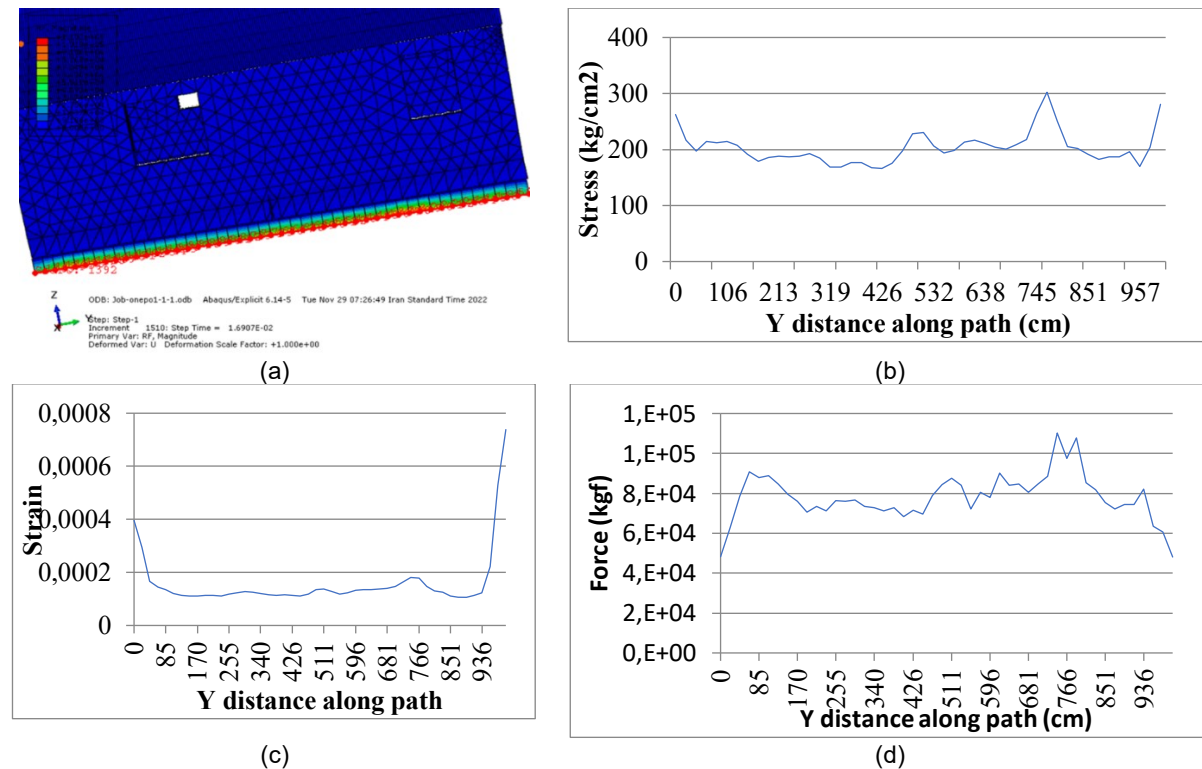


Figure 12. a) The considered path on the support; b) stress in the y direction; c) plastic strain, d) support reactions

### 3.3 Stress and displacement in the longitudinal direction of the structure

Under seismic excitation along the x-axis (the transverse direction of the building), Figure 13a shows the considered path in the arch. The diagram of the variations of the von Mises stress in the radial direction is drawn in Figure 13b. According to Figure 13b, in the middle part of the diagram, the value of the stress has reached zero in some elements. In the displacement diagram (Figure 13c), at the same point, the displacement response is at its peak value. As shown in Figure 13d, collapse has occurred at this point, indicating that failure (instability) has occurred due to large deformations. Therefore, it can be concluded that the structure needs to control displacement and strengthen the materials or sections used at the maximum displacement points.

It was observed that the highest base reaction was created at the beginning of the wall, i.e., at the connection zone of two external perpendicular walls. The reason for this is probably related to the shear behavior of the wall parallel to the direction of seismic excitation.

### 3.4 Seismic excitation in the longitudinal direction

In the case where the horizontal seismic excitation is defined along the y-axis (longitudinal direction of the building), as shown in Figure 14a, the damage to the roof of the structure is significant. Therefore, there are human life risks for the users of 3D-printed structures with truss-like sections. Therefore, if these structures are used in areas with very high seismic hazards, the necessary measures should be taken into account. As shown in Figure 14b, the roof of the structure has broken, and most of the zigzagged grids between the two layers of the arch are separated. As shown in Figure 14c, despite applying a high friction coefficient among the layers of the model, the sliding of the arch is evident on its supports. The sliding of the arch on the supports causes damage to the walls located in the inner part of the arch. Therefore, concentrated bending occurs in the arch, depending on the number of separating walls located in the internal parts of it.

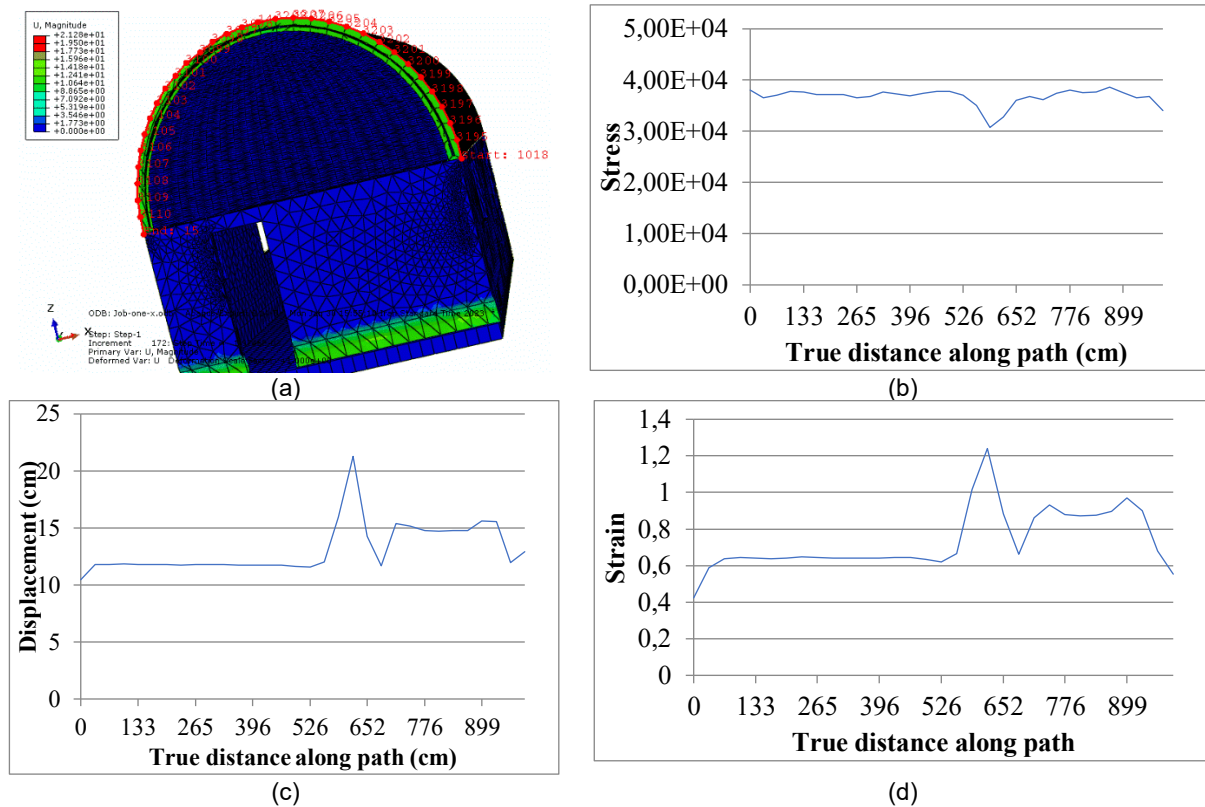


Figure 13. a) The considered path on the arch; b) von Mises stress; c) displacement; d) strain in the radial direction

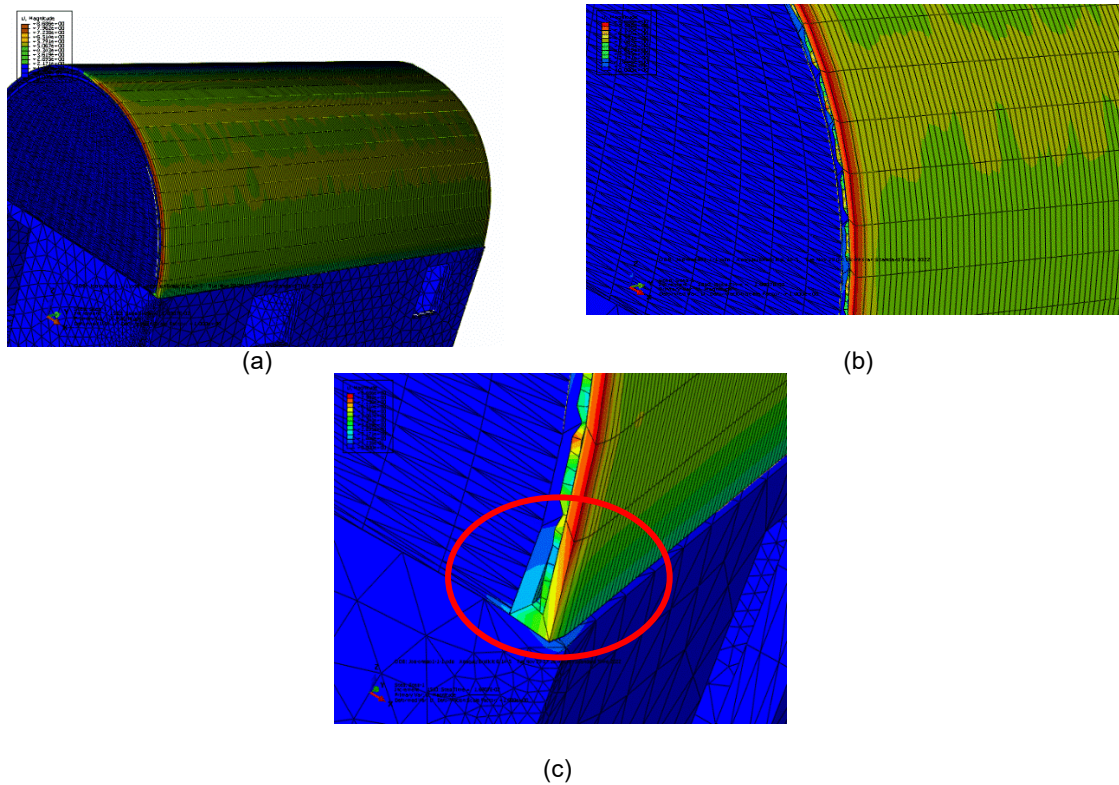


Figure 14. Seismic excitation on the length of the building, a. damage to the arch, b. damage to the grids between the windows, c. slipping of the arch over the living room

Adding rebars is one of the ways to increase the tensile strength and thus improve the behavior of the roof of 3D-printed buildings [15]. Although several studies have been conducted in this field, the practical application of this method requires complex technologies and expensive machinery, which leads to an increase in the total price of the printed structures. Another way is by adding fibers, especially long fibers, to the mixture of printing materials [14, 17]. It should be noted that excess use of those fibers can cause problems in the extrusion process. Therefore, some limitations should be considered when adding fibers to the mix [7].

Studies have shown that using smaller components and elements increases the load-bearing strength and reduces the stress concentration in 3DPC structures [1]. One of the cases that can improve the structural roof resistance is the

reduction in the density of the concrete, which causes a lighter structure and thus reduces the seismic loads.

### 3.5 Shear force in the longitudinal direction

As shown in Figures 15a and b, the wall, which is considered the gravitational and lateral load-bearing system, is removed from the system, and the building faces complete collapse. Therefore, in the case of using this type of 3D-printed structure in areas with high and very high seismic risks, the necessary measures should be taken into account. For this purpose, the shear resistance of the walls should be increased, especially at the connection points to the foundation.

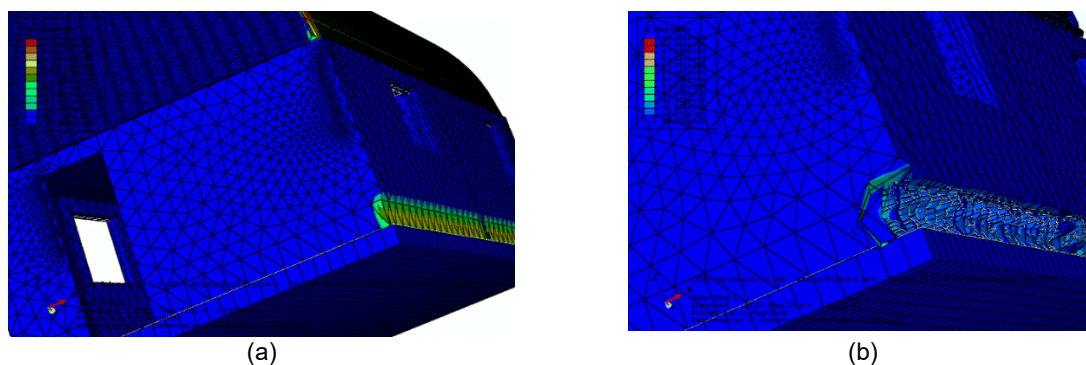


Figure 15. Shear damage to the foot of the walls under earthquake loading in the longitudinal direction of the structure: a) damage contours; b) magnified image of the wall's damage

One of the factors affecting the shear force applied to 3D-printed structures is the bond at the layer's interface. One of the critical solutions to the insufficient interface shear resistance is using steel rebars or fasteners [24]. As well, more suitable geometric shapes for the layers, for example, V-shaped forms that are placed inside each other, can be utilized [49]. Also, the design of short shear walls can be very effective.

#### 4 Conclusion

Seismic safety is one of the basic needs of any structure located in an earthquake-prone environment. Printed structures are no exception to this rule. In this study, the behavior of a 3DPC building was investigated. The structure has a truss-like cross-section and is located in an area with very high relative risk. The Tabas earthquake records were selected as seismic excitations here. First, the basic needs of earthquake engineering for 3D-printed buildings were determined by extensive theoretical studies. Given the pilot nature of this study, a large part of the work included the same theoretical studies. Then, a prescriptive evaluation was done based on the regulations of similar structures. In the following, the safety methods of 3DPC buildings were discussed, and seismic evaluation was done using the results of explicit FEA by ABAQUS software.

According to the results, the displacement response played the most critical role in the structural failure. Most of the parts of the structure suffered damage and buckling due to local displacements before reaching the yield stress. The reason for this was the truss-like sections. In the state of seismic excitation along the length of the structure, tensile performance was dominant in the components. Due to the inherent weakness of concrete material in tension, the failure was higher than in the state where the seismic excitation was along the width of the structure. When the force of the earthquake was applied along the width of the structure, the arch roof of the structure had compressive behavior. The results of the analysis showed that the location of load-bearing and non-load-bearing walls (infill walls) was very significant. The presence of walls was very influential on the performance of the supports (building foundation). According to the results, the following can be suggested regarding the seismic behavior of 3DPC buildings:

- According to the hypotheses of this study, the structural components had a very low displacement and deformation capacity due to the functional properties of the materials. As a result, limiting and controlling displacements and rotations is a necessity.

- Using shear walls, 3D-printed structures can be secured against earthquake loads.

- Existing finite element software can be used to achieve a detailed and practical evaluation of 3D-printed structures to some extent.

For further studies and to complete this research, the authors decided to address materials with better tensile capacity and other types of 3D-printed structural models, such as printed buildings with limited human intervention under seismic loads.

#### References

- [1] Pudjisuryadi, P., Antoni, A., & Chandra, J. (2020, September). Review on 3D printed concrete as structural beam members. In IOP Conference Series: Materials Science and Engineering (Vol. 930, No. 1, p. 012045). IOP Publishing.
- [2] Schuldt, S. J., Jagoda, J. A., Hoisington, A. J., & Delorit, J. D. (2021). A systematic review and analysis of the viability of 3D-printed construction in remote environments. *Automation in Construction*, 125, 103642.
- [3] Ahmed Saleh, A. E. (2019). 3D Printing in Architecture, Engineering and Construction (Concrete 3D printing). *Engineering Research Journal*, 162, 119-137.
- [4] Allouzi, R., W. Al-Azhari, and R. Allouzi. (2020). Conventional construction and 3D printing: A comparison study on material cost in Jordan. *Journal of Engineering*.
- [5] Mohammad, M., E. Masad, and S.G. Al-Ghamdi. (2020). 3D concrete printing sustainability: A comparative life cycle assessment of four construction method scenarios. *Buildings*, 10(12), p. 245.
- [6] Jeong, H., Han, S. J., Choi, S. H., Lee, Y. J., Yi, S. T., & Kim, K. S. (2019). Rheological property criteria for buildable 3D printing concrete. *Materials*, 12(4), 657.
- [7] Bohuchval, M., Sonebi, M., Amziane, S., & Perrot, A. (2019). Rheological properties of 3D printing concrete containing sisal fibres. *Academic Journal of Civil Engineering*, 37(2), 249-255.
- [8] Khoshnevis, B. (2004). Automated construction by contour crafting—related robotics and information technologies. *Autom. Constr.*, 13, 5–19.
- [9] Jagoda, J., Diggs-McGee, B., Kreiger, M., & Schuldt, S. (2020). The viability and simplicity of 3D-Printed construction: A military case study. *Infrastructures*, 5(4), 35.
- [10] Suiker, A. S. J. (2018). Mechanical performance of wall structures in 3D printing processes: Theory, design tools and experiments. *International Journal of Mechanical Sciences*, 137, 145-170.
- [11] Gebhard, L., Mata-Falcón, J., Anton, A., Dillenburger, B., & Kaufmann, W. (2021). Structural behaviour of 3D printed concrete beams with various reinforcement strategies. *Engineering Structures*, 240, 112380.
- [12] Bukvić, O., Radonjanin, V., Malešev, M., & Laban, M. (2020). Basic fresh-state properties of extrusion-based 3D printed concrete. *Građevinskimaterijali i konstrukcije*, 63(4), 99-117.
- [13] Van Zijl, G., Suvash, C. Suvash, C.P., Ming, J., Tan, M.J. (2016). Properties of 3D printable concrete. In *Proceedings of the 2nd International Conference on Progress in Additive Manufacturing*, Singapore.
- [14] Li, Z., Hojati, M., Wu, Z., Piasente, J., Ashrafi, N., Duarte, J. P., Nazarian, S., Bilén, S. G., Memari, A. M. & Radlińska, A. (2020). Fresh and hardened properties of extrusion-based 3D-printed cementitious materials: A review. *Sustainability*, 12(14), 5628.
- [15] Bos, F. P., Ahmed, Z. Y., Jutinov, E. R., & Salet, T. A. (2017). Experimental exploration of metal cable as reinforcement in 3D printed concrete. *Materials*, 10(11), 1314.

- [16] Martens, P., Mathot, M., Bos, F., & Coenders, J. (2018). Optimising 3D printed concrete structures using topology optimisation. In *High Tech Concrete: Where Technology and Engineering Meet: Proceedings of the 2017 fib Symposium*, held in Maastricht, The Netherlands, June 12-14, 2017 (pp. 301-309). Springer International Publishing.
- [17] Hojati, M., Nazarian, S., Duarte, J. P., Radlinska, A., Ashrafi, N., Craveiro, F., & Bilen, S. (2018). 3D printing of concrete: A continuous exploration of mix design and printing process. 42st International Association for Housing (IAHS).
- [18] Tay, Y. W. D., Ting, G. H. A., Panda, B. I. R. A. N. C. H. I., He, L. E. W. E. I., & Tan, M. J. (2018, May). Bond strength of 3D printed concrete. In *Proceedings of the International Conference on Progress in Additive Manufacturing*, Singapore (pp. 14-17).
- [19] Skibicki, S., M. Kaszyńska, and M. Techman. (2018). Maturity testing of 3D printing concrete with inert microfiller. in *MATEC Web of Conferences*. EDP Sciences.
- [20] Phadnis, K., M. Shariff, and D. Menon. (2020). Optimal Rate of Printing of 3D Printed Concrete Columns and Walls to Avoid Buckling. in *IOP Conference Series: Materials Science and Engineering*. IOP Publishing.
- [21] Federowicz, K., Kaszyńska, M., Zieliński, A., & Hoffmann, M. (2020). Effect of curing methods on shrinkage development in 3D-printed concrete. *Materials*, 13(11), 2590.
- [22] Zainab, Olubukola. (2020). Exploring the Potential of 3D printing for Building Houses in Nigeria and Brief Numerical Analysis of Lintels in 3D Printed Houses. Graduate School of Science and Engineering Ritsumeikan University.
- [23] Pekuss, R., A. Ančupane, and B.G. de Soto. (2021). Quantifying the complexity of 3D printed concrete elements. in *ISARC. Proceedings of the International Symposium on Automation and Robotics in Construction*. IAARC Publications.
- [24] Wang, L., Ma, G., Liu, T., Buswell, R., & Li, Z. (2021). Interlayer reinforcement of 3D printed concrete by the in-process deposition of U-nails. *Cement and Concrete Research*, 148, 106535.
- [25] Chang, Z., Xu, Y., Chen, Y., Gan, Y., Schlangen, E., & Šavija, B. (2021). A discrete 25 model for assessment of buildability performance of 3D-printed concrete. *Computer-Aided Civil and Infrastructure Engineering*, 36(5), 638-655.
- [26] Licciardello, L., Reggia, A., Metelli, G., & Plizzari, G. A. (2021, November). Investigation of the Structural and Thermal Behaviour of 3D Printed Concrete Walls. In *Symposium on concrete and concrete structures* (pp. 18-19).
- [27] Duarte, G., Brown, N., Memari, A., & Duarte, J. P. (2021). Learning from historical structures under compression for concrete 3D printing construction. *Journal of Building Engineering*, 43, 103009.
- [28] Pan, T., Jiang, Y., He, H., Wang, Y., & Yin, K. (2021). Effect of structural build-up on interlayer bond strength of 3D printed cement mortars. *Materials*, 14(2), 236.
- [29] Xiao J, Zou S, Yu Y et al. 3D recycled mortar printing: System development, process design, material properties and on-site printing. *Journal of Building Engineering* 2020; 32. <https://doi.org/10.1016/j.jobe>
- [30] Xiao, J. Z., Liu, H. R., Ding, T., & Ma, G. W. (2021). 3D printed concrete components and structures: An overview. *Sustain. Struct*, 1(000006), 10-54113.
- [31] Es-sebyty, H., Igouzal, M., & Ferretti, E. (2022). Improving stability of an ecological 3D-printed house - a case study in Italy. *Journal of Achievements in Materials and Manufacturing Engineering*, 111(1), 18-25.
- [32] Zhang, D., Feng, P., Zhou, P., Xu, W., & Ma, G. (2023). 3D printed concrete walls reinforced with flexible FRP textile: Automatic construction, digital rebuilding, and seismic performance. *Engineering Structures*, 291, 116488.
- [33] Delavar, M. A., Chen, H., & Sideris, P. Design of 3D Printed Concrete Walls under In-Plane Seismic Loading. in *12<sup>th</sup> National Conference on Earthquake Engineering (12NCEE)*, Earthquake Engineering Research Institute (EERI), Salt Lake City, Utah, USA, 27 June – 1 July 2022.
- [34] García-Alvarado, R., Moroni-Orellana, G., & Banda-Pérez, P. (2021). Architectural evaluation of 3D-printed buildings. *Buildings*, 11(6), 254.
- [35] Iranian National Building Codes Compilation Office (2020) INBC-Part 6: Structures Loading. Ministry of Housing and Urban Development (MHUD), Tehran, Iran.
- [36] Iranian National Building Codes Compilation Office (2020) INBC-Part 8: Design and Construction of Masonry Buildings. Ministry of Housing and Urban Development (MHUD), Tehran, Iran.
- [37] Iranian National Building Codes Compilation Office (2014) INBC-Part 9: Design and Construction of Reinforced Concrete Buildings. Ministry of Housing and Urban Development (MHUD), Tehran, Iran.
- [38] Vice Presidency for Strategic Planning and Supervision, (2018). Instructions for Seismic Evaluation and Rehabilitation of Conventional Existing Masonry Buildings (Code No. 740). Tehran, Iran.
- [39] Vice Presidency for Strategic Planning and Supervision, (2018). Instruction for Seismic Rehabilitation of Existing Buildings (Code No. 360), 1<sup>st</sup> Rev. Tehran, Iran.
- [40] Building and Housing Research Center (BHRC). (2015). Iranian Code of Practice for Seismic Resistant Design of Buildings: Standard No. 2800-05, 4th Ed, Iran.
- [41] Haselton, C. B., Whittaker, A. S., Hortacsu, A., Baker, J. W., Bray, J., & Grant, D. N. (2012, September). Selecting and scaling earthquake ground motions for performing response-history analyses. In *Proceedings of the 15th world conference on earthquake engineering* (pp. 4207-4217). Oakland, CA, USA: Earthquake Engineering Research Institute.
- [42] Abaqus v. 6.14 Documentation; Dassault SystemesSimulia Corporation: Providence, RI, USA, 2014.
- [43] Xiao, J., Liu, H., Ding, T. (2021). Finite element analysis on the anisotropic behavior of 3D printed concrete under compression and flexure. *Additive Manufacturing*, 39, 101712.
- [44] van den Heever, M., Bester, F., Kruger, J., & van Zijl, G. (2022). Numerical modelling strategies for reinforced 3D concrete printed elements. *Additive Manufacturing*, 50, 102569.

- [45] Hafezolghorani, M., Hejazi, F., Vaghei, R., Jaafar, M. S. B., & Karimzade, K. (2017). Simplified damage plasticity model for concrete. *Structural engineering international*, 27(1), 68-78.
- [46] Center for Engineering Strong Motion Data, CESMD. <http://www.strongmotioncenter.org>
- [47] Tahmasebinia, F., Niemelä, M., EbrahimzadehSepasgozar, S. M., Lai, et al. (2018). Three-dimensional printing using recycled high-density polyethylene: Technological challenges and future directions for construction. *Buildings*, 8(11), 165.
- [48] Dym, C.L. and H.E. Williams, Stress and displacement estimates for arches. *Journal of structural engineering*, 2011. 137(1): p. 49-58.
- [49] Babafemi, A. J., Kolawole, J. T., Miah, M. J., Paul, S. C., & Panda, B. (2021). A concise review on interlayer bond strength in 3D concrete printing. *Sustainability*, 13(13), 7137.





## Original scientific paper

**Enhancing mechanical properties and crack resistance of earth-sand building materials through alfa fiber reinforcement: an experimental investigation**Reda Sadouri<sup>\*1)</sup>, Hocine Kebir<sup>2)</sup>, Mustafa Benyoucef<sup>1)</sup><sup>3)</sup> LRDDS, Cadi-Ayyad University, Faculty of Sciences and Technics, Department of Applied Physics, Marrakesh, Morocco<sup>4)</sup> Laboratoire Roberval - Université de Technologie de Compiègne, BP 20529 - 60205 Compiègne Cedex, France*Article history*

Received: 17 November 2023

Received in revised form:

21 December 2023

Accepted: 26 December 2023

Available online: 07 February 2024

*Keywords*Earth construction;  
Alfa fiber;  
Shrinkage;  
Mechanical strength;  
SEM**ABSTRACT**

This paper investigates enhancing the mechanical properties and crack resistance of earth-sand building materials by incorporating Alfa fibers, derived from the Alfa plant. Earth-based construction materials, known for their sustainability, face challenges in mechanical performance and cracking. The study explores a composite of earth (60 wt%) and sand (40 wt%) reinforced with Alfa fibers of varying lengths and rates. Tensile strength and water absorption of the fibers were assessed, and prismatic specimens (40x40x160 mm<sup>3</sup>) with different cutting lengths were tested. Results inform the potential of Alfa fibers for improving earth-based material performance.

Incorporating 2% wt of Alfa fibers reduced the unit weight of the composite from 1849 kg/m<sup>3</sup> to 1632 kg/m<sup>3</sup>, resulting in a slight material weight decrease. Compared to unreinforced adobe specimens, fibrous samples exhibited lower linear shrinkage rates and improved mechanical behavior, with 2% wt of 3 cm fibers showing optimal performance. The fibers effectively impeded crack propagation, with both length and content influencing crack attenuation. However, microstructural observation revealed poor fiber/matrix adhesion, negatively impacting adobe specimen compactness despite enhanced mechanical properties.

**1 Introduction**

Around the world, buildings are constructed from a wide variety of materials. When access to concrete, timber, and crushed stone is limited, the most commonly used material is soil. For thousands of years, earthen houses have been built around the globe [1].

In recent years, there has been a lot of interest in the use of vegetable fibers as a possible reinforcement in adobe as a building material. Several fibers [2]–[7] have been incorporated to improve the properties of bricks [8] and also to gradually change out conventional construction materials in an attempt to decrease building large carbon footprints. The addition of this kind of material negatively impacts the compressive strength characteristics of the composite. Nevertheless, the incorporation of a minor quantity of fibers with short lengths could be used as reinforcement and effectively address this shortcoming with a significant increase in strength [9], [10].

Given the fact that natural soil is the most eco-friendly material that is typically used to produce bricks, combining vegetable fibers with it could be deemed one of the most promising methods for greening the construction sector. Several researchers around the globe are inspired to try creating intelligent, lightweight, and alternative materials with

this basic mixture because it takes advantage of the earth's high thermal mass and the substantial influence of agro-aggregates on the hygrothermal efficiency of adobe bricks [11]. Additionally, the utilization of vegetable fibers is more advantageous in developing countries, where they are available at a low cost and their manufacture requires a small amount of energy. Besides, they do not contribute to pollution.

A series of experimental studies have been conducted on the physical and mechanical properties of earth brick composite. They have shown the benefits of the incorporation of vegetable fibers (coconut, straw, jute, flax, bamboo, cane, etc.) [2], [3], [5]–[7], [9], [12]–[15]. Also, in order to create theoretical analytical models for earth composites [16], [17], the impact of synthetic fibers on the soil matrix has also been investigated [18]–[20]. The primary factors that significantly impact the properties of earth composites are the kind, durability, water absorption, and tensile strength of the fibers, in addition to their length and weight percentage replacement in the composite [2].

The type of fiber has a significant impact on the impermeability of the bricks, which depends on the percentage of lignin in the fiber. The impermeability of vegetable fiber increases with its lignin content. The brick shrinkage that occurs during the drying process of adobe

\* Corresponding author:

E-mail address: [r.sadouri@uca.ma](mailto:r.sadouri@uca.ma)

samples could vary greatly depending on the earth mixture and the addition of fibers to the soil matrix to prevent the formation of shrinkage cracks [21]. Less shrinkage occurs when fibers with higher bonds are more resistant [8]. Furthermore, the crack resistance of earth reinforced with fibers is directly related to the tensile strength of the fibers [22]. This paper does not address the long-term stability of this aspect, but it does investigate the physical and mechanical properties of adobe bricks reinforced with Alfa fibers. The length of the fiber directly influences the reinforcement force, which is equal to or less than the fiber tensile strength, by determining the pullout resistance of the incorporated fiber in the earth matrix. Several studies support this statement. A study by Mustapha et al. used both experiments and computer simulations to look into how natural fibers pull away from an earth-based matrix. They discovered that the interfacial crack driving force is equal to the interfacial fracture toughness, which changes non-linearly with the internal crack lengths and the elastic properties of the materials. This means that the fiber pull-out loads probably won't depend linearly on the fiber embedment length [23]. The total weight ratio of fibers controls the reinforcement's intensity; for small quantities, the reinforcement's strength goes up as the number of fibers increases. However, as the fibers become so widespread randomly they weaken the matrix, decreasing the strength of reinforced adobe composites [2], [3]. Finally, other studies have highlighted that incorporating natural fiber increases the ductility, fracture resistance, and energy absorption properties of earthen materials [24], [25]. The fiber length was also found to have a notable influence on ductility and the post-fracture response of the material for large deflection levels of the material [24].

The motivation for this research stems from the need to develop construction materials that not only align with sustainable building practices but also exhibit improved mechanical strength and durability. By exploring the potential benefits of Alfa fiber reinforcement, we aim to contribute to the evolution of earth-based building materials into high-performance, environmentally friendly alternatives.

This experimental investigation involves a systematic exploration of the mechanical properties and crack

resistance of earth-sand composites reinforced with Alfa fibers. The study encompasses evaluations of fiber characteristics, such as tensile strength and water absorption, to gain insights into their behavior within the composite matrix. Additionally, prismatic specimens with varying fiber lengths and content ratios undergo rigorous testing to assess the impact of Alfa fibers on the overall performance of the material.

The outcomes of this research are anticipated to provide valuable insights into the feasibility and effectiveness of Alfa fiber reinforcement in earth-sand building materials. Such advancements hold the potential to reshape construction practices by offering sustainable alternatives with enhanced structural attributes. As we delve into this experimental investigation, we anticipate uncovering new possibilities for the development of resilient, environmentally conscious building materials.

## 2 Experimental:

### 2.1 Characterization of raw materials

#### 2.1.1 Alfa fibers

The Alfa fibers, from the *Stippa Tenacissima* L [26], thrive in the dry regions of North Africa and the South of Europe. It belongs to the graminaceous family and grows to a height of about 1m in Morocco. The Alfa plant grew in abundance in many regions, primarily in the north-eastern part of the country. The fibers used in this study were harvested from the region of "Oujda". Before their use in the composite, the fibers were cleaned to remove any dust and impurities deposited on the surface, then they were cut at different lengths (1, 2, and 3 cm). Fig. 1 shows the cut Alfa fiber studied in this paper.

According to Ajouguim [26], and A.B. Mabrouk [27], Alfa fibers are mainly composed of cellulose, hemicellulose, lignin, and extractable elements. The chemical composition of used Alfa fiber is given in Table 1, and its properties are presented in Table 2. Fig. 2 shows the structure of the Alfa plant observed through scanning electronic microscopy



Figure 1. Cut Alfa fiber

(SEM). Based on longitudinal stem observation, the SEM observations show that Alfa stems have a hairless and soft appearance with numerous dusts and impurities (wax, fat, etc.) that are located on the surface (Fig. 2b). Additionally, the SEM of the fiber cross section indicates that this plant has a cellular structure with pores (Fig. 2a). This type of vegetal fiber's void network morphology provides promise for creating Adobe composites with improved thermal performance and low unit weight. Beyond surface visualization, the SEM analysis allows us to measure the diameter as well.

The earth used in this study was collected from the 'AitOurir' (31° 33' 54" nord, 7° 40' 05" ouest) located in Al Haouz Province, at the foot of the Atlas Mountains, around 40 km east of the city of Marrakesh. This soil was used in the past by local builders to manufacture Adobe bricks, and it is characterized by its abundance and availability in the area.

The mineralogical composition reveals that the soil contains dominant quartz, with other constituents including illite, augite, and plagioclase. The soil was sieved to obtain elements less than 2 mm in size. The granulometric size distribution of the soil, which was obtained by sieving and hydrometer analyses carried out following ASTM standard D422 [28], is given in Table 3a. Concerning ASTM particle size limits, the soil has 23% clay, 40.3% silt, and 36.70% sand. Table 3a reports the Density and Atterberg limits of the used soil. The soil might be classified as CL, i.e., inorganic clay with medium plasticity and medium liquid limit, in the Unified Soil Classification System [29]. Table 3b. presents the properties of crushed sand brought from a local quarry near Marrakesh city and tested according to AFNORD standard [28]. The diffractograph of the used sand reveals the dominance of quartz, together with other constituents including plagioclase and tridymite.

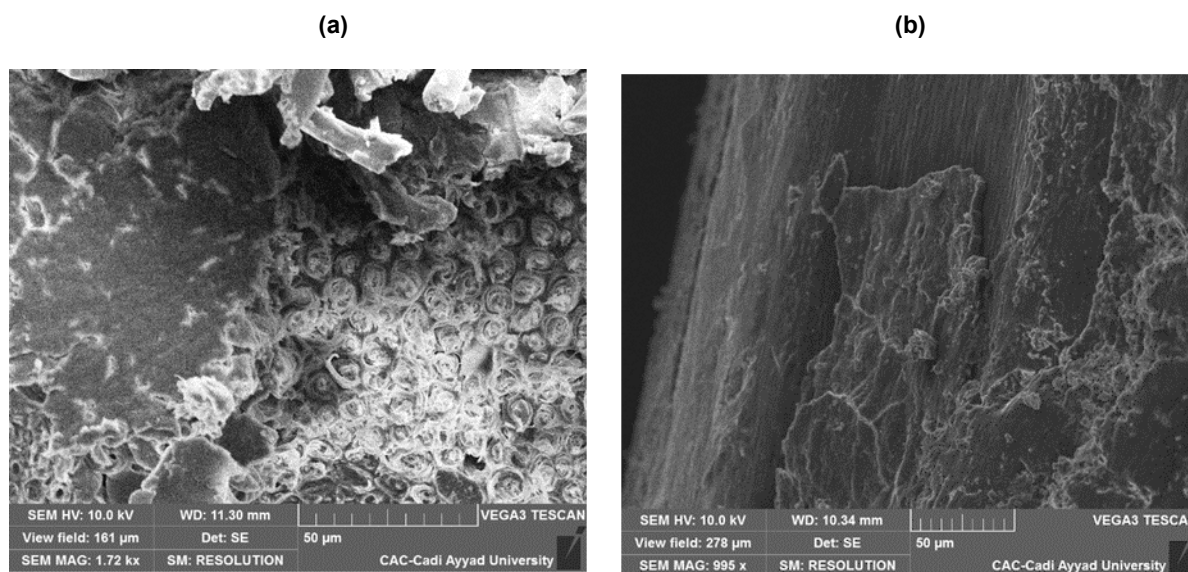


Figure 2. Structure of Alfa fiber :(a) Cross-section (b) External surface

Table 1. Chemical components of Alfa fibers [26], [27]

Cellulose (%)	Hemicellulose (%)	Lignin (%)
39.50	27.60	19.50

Table 2. Properties of Alfa fibers

Density (g/cm <sup>3</sup> )	Young's modulus (GPa)	Stress at break (MPa)	Strain at break (%)
1.40	21.5	247	1.96

Table 3a. Geotechnical characteristics of studied earth.

Grain size distribution	Consistency limits	Methylene Blue Value
Clay <2μm: 23%	Liquid limit, LL=38%	MBV(g/100g)= 3
Silt (2-63 μm):40.3%	The plastic limit, PL=20%	
Fine Sand (0.063-0.2 mm): 36.7%	Plasticity Index, PI=18%	

Table 3b. Physical characteristics of crushed sand

Apparent density	Specific density	Water content (%)	Sand equivalent
1.50	2.60	1.1	85

## 2.2 Sample preparation

Different compositions of adobe prismatic samples were prepared by varying the content and length of the fibers. The adobe sample dimensions of 40x40x160 mm<sup>3</sup> justify the addition of fiber cut up to 3 cm. Additionally, previous research on the critical length and interfacial strength of fibers incorporated into an epoxy matrix also emphasized the importance of acknowledging the influence of fiber length on the interfacial strength and mechanical properties of the composite material [30]. Therefore, it is essential to address the pronounced wall effect and preferential orientation of fibers due to the specific fiber length and mold size, as this can have a substantial impact on the behavior and mechanical performance of the reinforced material. The inclusion of Alfa fibers increased from 1 wt % to 1.5 and 2 wt% (weight percentage), allowing us to compare reinforced to unreinforced specimens.

Samples were manufactured using various mix compositions, as summarized in Table 4, by first mixing the dry fibers and sand manually. The composite was then mixed with slowly added earth until a homogeneous mixture was obtained. This process allowed for a homogenous dispersion of fibers in the mixture. After mixing all the ingredients, the mixture was manually compacted in a wooden mold, as shown in Fig. 3a. This mold was first scattered inside with sand and wet with water to facilitate the removal of specimens. The moist soil was compacted into four layers and discharged when they started to gain consistency. The drying of the samples took place in normal laboratory conditions at 20 ± 2 °C with a relative humidity of 98% for approximately 28 days until constant weight. The shapes of different samples after demolding are shown in Fig. 3.

Table 4. The proportion of mixtures

Mixture designation	Earth (%)	Sand (%)	Water/Soil weight ratio	fraction	Fiber length (cm)
U (Control Specimen)	60	40	0.20	–	–
R1-1	60	40	0.20	1%	1
R1.5-1	60	40	0.20	1.5%	1
R2-1	60	40	0.20	2%	1
R1-2	60	40	0.20	1%	2
R1.5-2	60	40	0.20	1.5%	2
R2-2	60	40	0.20	2%	2
R1-3	60	40	0.20	1%	3
R1.5-3	60	40	0.20	1.5%	3
R2-3	60	40	0.20	2%	3

a: Fiber weight fraction is evaluated on the total weight of the clay-sand mix.

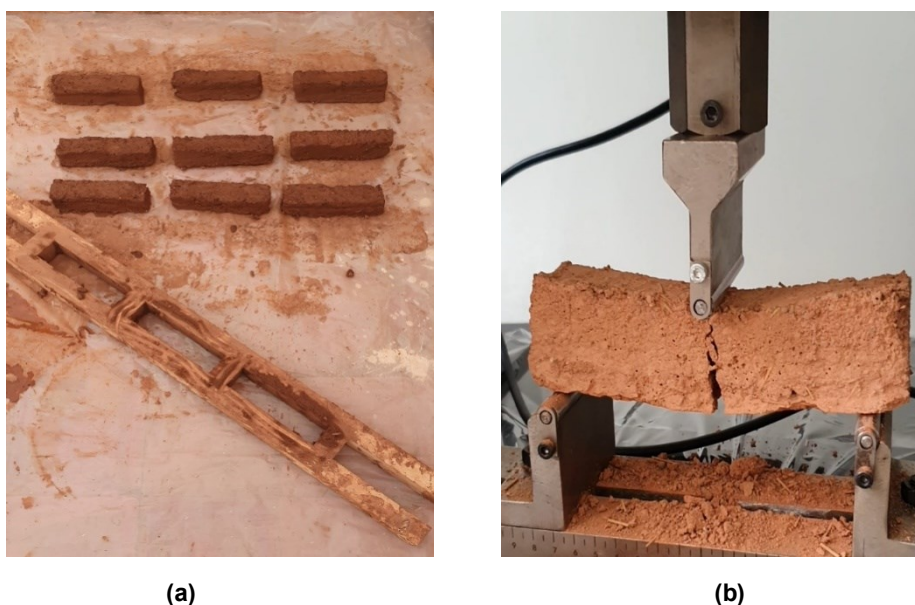


Figure 3. Sample after demolding (a), three-point bending flexural-tests (b)

## 2.3 Experimental testing

### 2.3.1 Tensile strength and water absorption of Alfa fibers

Firstly, to be knowledgeable of certain properties of Alfa fibers and to exploit their highest potential, the fibers were evaluated in terms of tensile strength and water absorption.

The tensile strength of the long fibers was determined experimentally according to ASTM C1557 [31]. This standard test method covers the preparation, mounting, and testing of single fibers obtained either from a fiber bundle or a spool. The fibers were situated straight inside the equipment grips that produced the fiber failure. ASTM C1557 is the standard test method for determining the tensile strength and elastic modulus of fibers at ambient temperature. Therefore, the use of ASTM C1557 for determining the tensile strength of the long fibers is well-established and provides a reliable basis

for the experimental determination of the fiber's tensile strength. Figure 4 presents the equipment used for this purpose. The properties of Alfa fibers are presented in Table 2. Fundamentally, vegetable fibers are characterized by their sensitivity to water [32] because of their chemical composition, as shown below. The water absorption capacity of the fibers under study was established using equation (1).

$$W = \frac{P_h - P_d}{P_d} \quad (1)$$

Where  $P_d$  is the weight of air-dried fibers and  $P_h$  is the weight of soaked fibers in drinking water. The measurement was carried out at 24-hour intervals for 18 days. The average percentages of water absorption for Alfa fibers are given in Fig 5.



Figure 4. Tensile testing of Alfa fiber

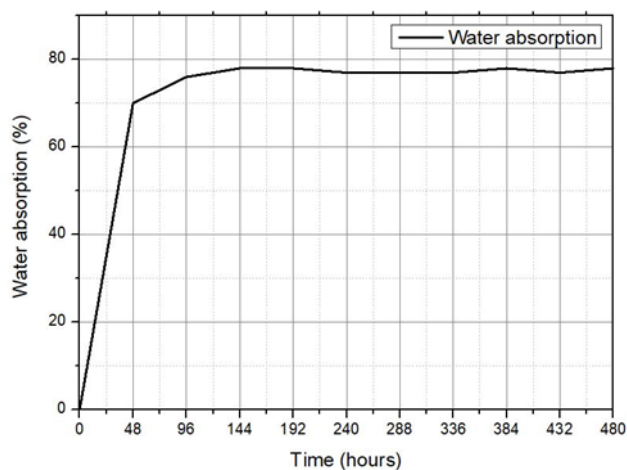


Figure 5. Water absorption of Alfa fiber

### 2.3.2 Unit weight and shrinkage

The next step after the drying process of the samples consisted of measuring the average mass and density as well as the rate of linear shrinkage. Dry density was calculated using the analytical balance. On the other hand, linear drying shrinkage was obtained by decreasing the percentage of the dried sample lengths compared with the initial length of the mold (160 mm). The reduction in the length of the specimen after drying is measured and expressed as a percentage of the original length to give the linear shrinkage, and its value is determined according to equation (2):

$$\text{Percentage of linear shrinkage} = \frac{1 - L_d}{L_o}$$

Where  $L_d$  is the new length of the dry specimen in mm and  $L_o$  is the original length of the specimen in mm.

### 2.3.3 Flexural and compressive strength

The flexural and compressive properties of the hardened specimens were measured after curing, according to the European Standard EN 196-1 [33]. For flexural strength, three specimens from each mix were prepared and tested with three-point bending, as shown in Fig. 3b. All tests were carried out at a controlled rate of 0.4 mm/min with the use of a closed-loop-servo-electric 5 kN tension-compression machine. Flexural strength was calculated by Equation (2):

$$\sigma_f = \frac{1,5 * F_f * L_f}{bd^2} \quad (2)$$

Where:  $\sigma_f$  (MPa) is the strength of the prism at the failure plan,  $F_f$ (N) is the maximum load recorded by the testing machine,  $b$ (mm) is the width of the specimen in the direction transversal to the applied force,  $d$ (mm) is the thickness of the specimen in the direction parallel to the applied force, and  $L_f$  (mm) is the distance between the holders.

The compressive tests have been done on each half specimen obtained after failure with the flexural test and calculated according to Equation (3). Tests were carried out in displacement control at a velocity rate of 4 mm/min

$$R_c = \frac{F_c}{S} \quad (3)$$

Where  $R_c$  (N/mm<sup>2</sup>),  $F_c$  (N), and  $S$  (1600 mm<sup>2</sup>) are the compressive strength, the maximum failure force, and the contact surface between the adobe element and plates used in the test, respectively.

## 3 Results and discussion

### 3.1 Apparent density of dry composite

The apparent density of an adobe brick is considered a fundamental step for building materials and engineering because it impacts material selection, structural design, safety, and serves several important purposes in the construction and building sectors.

The apparent density of an adobe brick holds paramount significance in material selection, structural design, safety, and various aspects of construction and engineering. In Fig. 6, the apparent density of composites, featuring different fiber lengths and addition ratios, is presented. The results show that increasing the fiber percentage results in a

decrease in apparent density. For instance, adding 2% wt of 3 cm Alfa plant cutting reduced the density from 1849 kg/m<sup>3</sup> (unreinforced sample, U) to 1632 kg/m<sup>3</sup> for the R2-3 specimen, indicating a reduction of approximately 12%. This reduction could be attributed to the lower density of fibers compared to soil-sand materials. The increase in fiber quantity leads to a decrease in earth-sand content, consequently lowering the composite's apparent density. The lightening of the adobe brick can also be explained by the fibers' higher water absorption capacity, which in turn increases porosity during the drying process. Hence, the primary advantage of using vegetable fibers is the lightweight nature of the samples, aligning with findings from previous studies [15], [34]–[36]. However, a slight impact of fiber length variation is observed in the results.

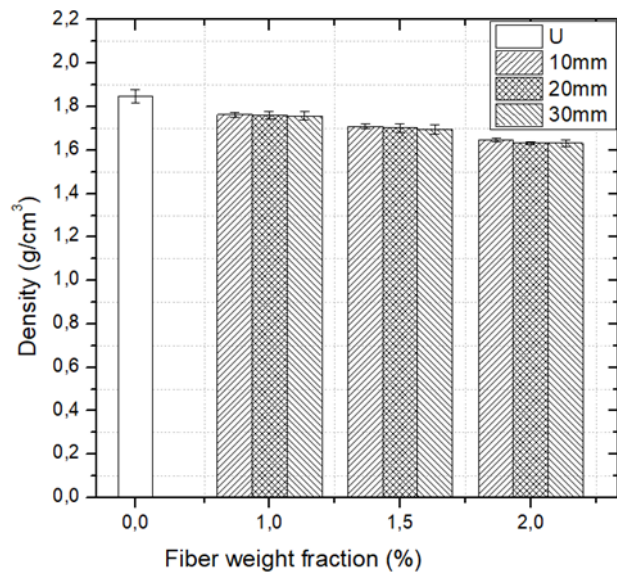


Figure 6. Apparent density of dry composite

### 3.2 Effect of Alfa fiber on linear shrinkage

The dimensional variation of the material due to water evaporation post-manufacture, known as linear shrinkage, was measured for all samples. In Fig. 7, the variation in linear shrinkage with different reinforcement levels is depicted. The results confirm that Alfa fibers effectively reduce shrinkage, with a 2% fiber content leading to a 68% decrease. The unreinforced samples exhibit higher shrinkage, while reinforced soil specimens resist deformation and limit contraction, which is consistent with previous studies [3], [5], and [34]. Additionally, Fig. 7 illustrates the impact of increasing fiber length to 30 mm, showing that the minimum shrinkage rate is associated with the higher fiber content of 30mm length, possibly due to long bonding between the Alfa fiber and the matrix.

The disparity in shrinkage between the reinforced and unreinforced composites can be attributed to the superior water absorption capacity of Alfa fiber and its gradual water-releasing ability. As depicted in Fig. 5, during the initial 48 hours of the drying process, the fibers absorb water and expand. This swelling action displaces the soil, and as the fibers lose humidity towards the end of drying, they contract back to their original size, leaving pores around themselves. This dynamic process during mixing and drying contributes to the observed difference in shrinkage between the reinforced and unreinforced composite materials.

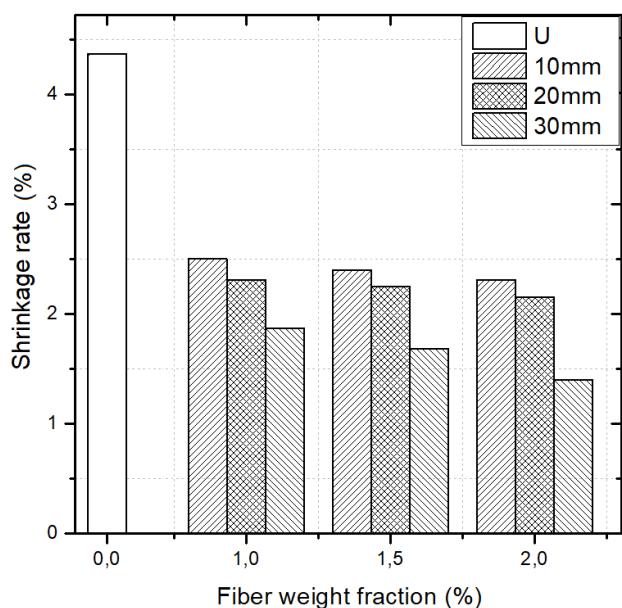


Figure 7. Average value of linear shrinkage for unreinforced and reinforced samples.

### 3.3 Flexural strength

Table 5 provides a summary of flexural strength results at 28 days in relation to fiber content and lengths (10, 20, and 30 mm). The finding indicates that increasing the fiber content up to 2% leads to a notable enhancement in flexural strength, ranging from 25% to 60%, depending on the specific fiber content. Additionally, it is worth mentioning that all reinforced formulations demonstrated higher flexural

strength values compared to unreinforced specimens. Moreover, as illustrated in Fig. 8, it is observed that increasing fiber length from 1 to 2 cm did not significantly increase the flexural strength. However, for the 3 cm fiber length, a slight increase in flexural strength is noticeable between 1% wt and 1.50% wt. The difference becomes more prominent between 1.5% wt and 2% wt fractions, resulting in an approximately 28% increase in flexural strength. This observation indicates that, for each fiber length, higher quantities of Alfa fiber correspond to greater flexural strength. This result affirms that both increasing fiber length and addition rate have a significant impact on flexural strength. The observed findings might be attributed to the substantial contact surface between longer fibers and the matrix, enhancing adhesion forces and subsequently improving load transfer capability. The observed rise in flexural strength with the inclusion of a high fiber fraction, especially with the longest fibers, aligns with findings reported by other researchers [5], [24], and [37].

In the flexural tests, fibrous and nonfibrous samples display distinct mechanical behavior. In unreinforced samples, when a crack initiates, the fracture rapidly extends towards the upper part of the prismatic adobe, resulting in the splitting of the sample into two halves. Contrastingly, a bridging phenomenon was noted in the reinforced samples, effectively delaying the propagation of cracks. Fig. 9 illustrates the U-sample compared to the R2-3 specimen after failure, showcasing the impact of this bridging effect. It can be observed that the introduction of Alfa fibers allows better control of crack propagation, which delays the rupture phase. This behavior of the incorporation of plant fibers in composites has been highlighted by other authors [15], [24], and [38], and it could be explained by the increased toughness and because the fibers at the crack zone bear the tensile stress transferred from the ruptured section.

Table 5. Results of the mechanical properties testing.  
\* In italics the standard deviation

Material mix	Fibre content	Length (cm)	Density (g/cm <sup>3</sup> )*	Compressive strength (MPa)*	Flexural strength (MPa)*	Ultimate deflection (mm)
U	0%	–	1,849 (0.03)	2.012 (0.0221)	0.305 (0.0032)	1.719 (0.021)
R1-1	1%	1	1.763 (0.01)	2.051 (0.017)	0.341 (0.005)	3.025 (0.050)
R1-2		2	1.761 (0.017)	2.102 (0.0231)	0.352 (0.0052)	3.005 (0.042)
R1-3		3	1.757 (0.013)	2.808 (0.0271)	0.361 (0.0032)	3.186 (0.023)
R1.5-1	1.5%	1	1.709 (0.011)	2.106 (0.0143)	0.372 (0.0057)	3.252 (0.031)
R1.5-2		2	1.703 (0.019)	2.304 (0.0278)	0.369 (0.0082)	3.205 (0.024)
R1.5-3		3	1.696 (0.021)	2.900 (0.022)	0.371 (0.0037)	3.365 (0.055)
R2-1	2%	1	1.647 (0.007)	2.250 (0.0381)	0.388 (0.002)	3.687 (0.072)
R2-2		2	1.633 (0.007)	2.300 (0.0157)	0.381 (0.0031)	3.438 (0.024)
R2-3		3	1.632 (0.014)	3.250 (0.0413)	0.488 (0.0021)	4.347 (0.031)

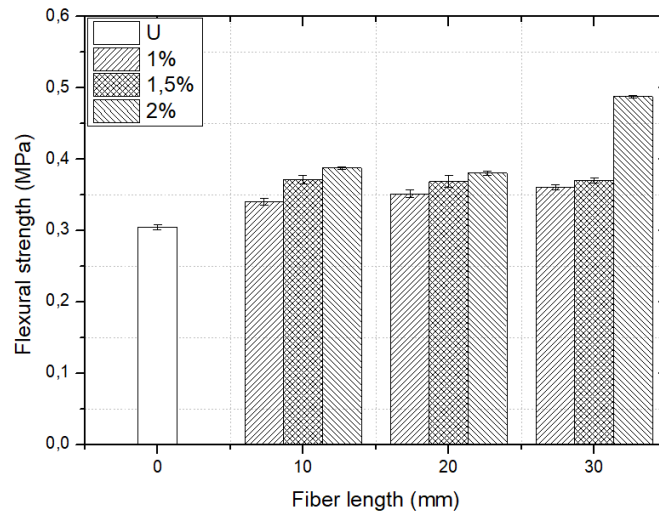


Figure 8. Flexural strength of reinforced samples with cut fibers at 28 days of curing in a laboratory environment



Figure 9. From left to right, unreinforced and reinforced sample after breaking

### 3.4 Compressive Strength

The effect of Alfa fiber length and quantities on the compressive strength of composites is given in Table 5. It is immediately possible to note that the highest value of compressive strength belongs to the R2-3 mixture that reached 3.25 MPa, coinciding with the mix exhibiting the highest flexural strength and the lowest shrinkage rate, thus confirming that the optimal formulation is related to 2 % wt of fiber of 3 cm length. The unreinforced samples exhibited the lowest compressive strength, barely reaching 2.012 MPa. It is noteworthy that this value aligns well with recommenda-

tions by Houben and Guillaud [39] or Binici et al. [6], which suggest a target compressive strength superior to or equal to 2 MPa. However, it is noted that all samples tested in the present study are much higher, namely 2-3.25 MPa. On the contrary, as depicted in Fig.10, it can be observed that the lengths of 10mm and 20mm did not strongly influence the compressive strength, regardless of fiber content. Nevertheless, for 3 cm of length, R1-3, R1.5-3, and R2-3 exhibit compressive strengths of 2.80 MPa, 2.90 MPa, and 3.25 MPa, respectively. These values represent higher strengths compared to other lengths by approximately 30%. This increase in compressive strength with the incorporation

of plant fibers has been previously reported by other authors [6], [9], and [35].

In the case of U-samples (control specimens), the final failure occurs almost immediately after reaching the ultimate load, demonstrating a brittle behavior with large cracks, as expected. However, the presence of Alfa fiber allows for plastic deformation, which characterizes the enhancement of composite elasticity. Breaking manners were similar for all fibrous mixtures, so they do not seem to depend on fiber length and fraction. It's important to highlight that the addition of fibers results in an increase in the ultimate deflection of the material. At maximum load, the deflection ranged from 1.719 mm for the control specimen to 4.347 mm for composite materials with a higher fiber content of 2% wt of 30mm length, as indicated in Table 5.

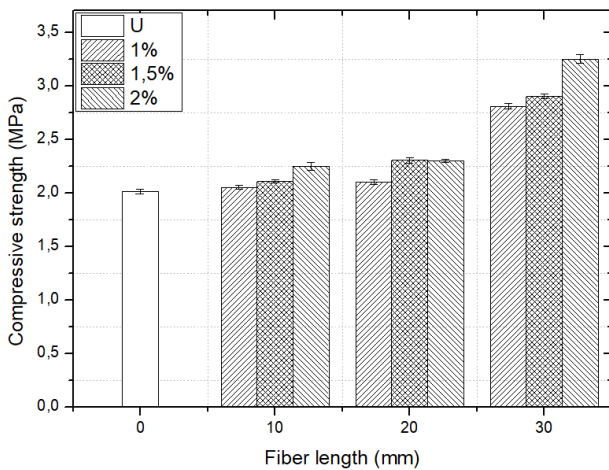


Figure 10. Compressive strength of reinforced samples with cut fibers at 28 days of curing in a laboratory environment

### 3.5 SEM micrographs

Fig. 11 illustrates the microscope observation of the fractured surfaces of the unreinforced composite (U). It can be observed as a heterogeneous composite, less

compacted, with some apparent cracks and large voids. The structure's lower compactness might be the cause of the presence of large pores. Likewise, the interfacial zone between Alfa fiber and matrix of a higher content 2% wt of 3 cm length fibers is shown in Fig. 12. As was expected in terms of bonding, the microscope observation indicated insufficient fiber/matrix adhesion. As observed in Fig. 2, the external surface of Alfa fiber is characterized by a thick layer of dust. This finding could be attributed to the non-treatment of fibers before their addition to the mixture. Alvarez and Vázquez [40] showed that a 1 h acetylation reaction leads to better fiber/matrix adhesion. According to the authors, this better adhesion is due to the change in the morphology of fibers and the production of fibrillation. Conversely, alternative treatments, such as immersion in boiling water, decrease adhesion due to the removal of spine fibers. Moreover, these modification methods could increase the risk of chain degradation and increase production costs [15] and [41].

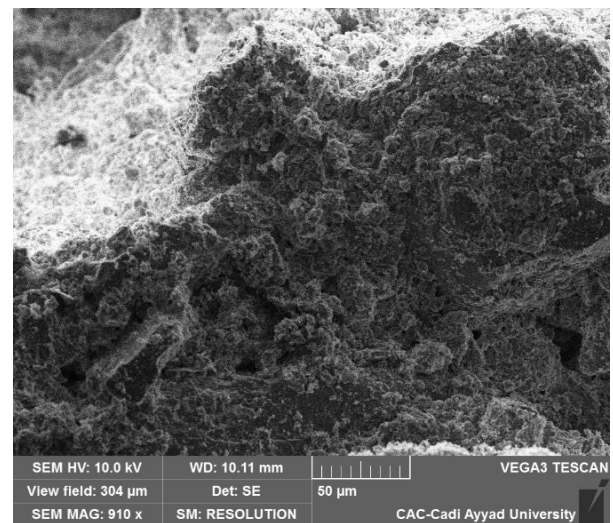


Figure 11. Microscope observation of the reference material (U)

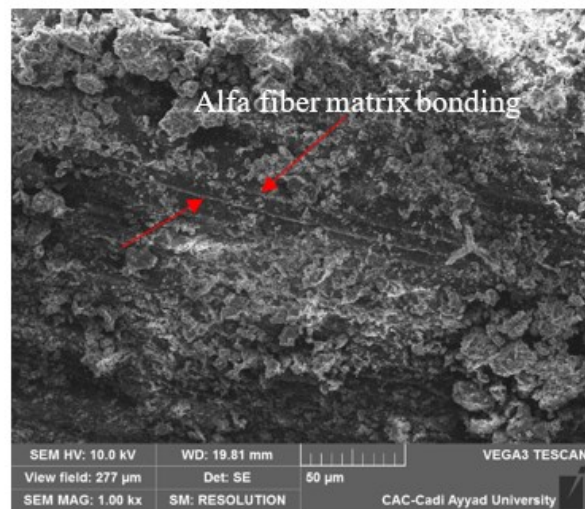
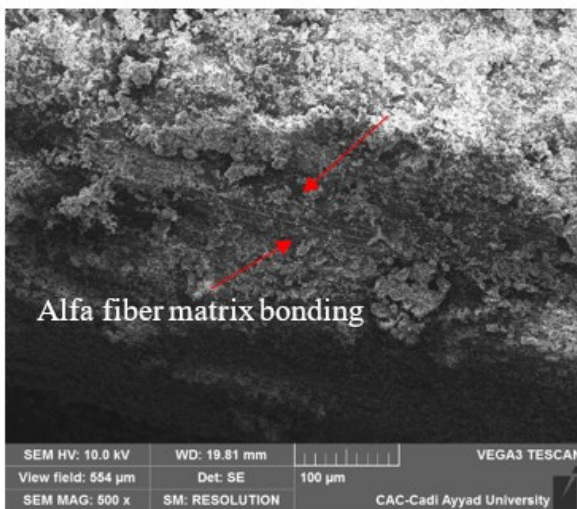


Figure 12. Microscope observation of the composite material with 2% wt Alfa fibers and length of 3 cm (R2-3)

## 4 Conclusion

In conclusion, this comprehensive experimental investigation has demonstrated the potential of Alfa fibers to significantly enhance the mechanical properties and crack resistance of earth-sand building materials. The incorporation of Alfa fibers, derived from the Alfa plant, into the earth-sand composite proved effective in addressing the inherent challenges associated with the mechanical performance and susceptibility to cracking of traditional earth-based construction materials. Based on the results of this experimental study, the following conclusions could be drawn:

- The study demonstrated the potential of Alfa fibers to enhance the mechanical properties and crack resistance of earth-sand building materials.
- The addition of 2% wt of Alfa fibers led to a reduction in unit weight and superior mechanical behavior compared to unreinforced adobe specimens.
- The research findings highlighted the role of Alfa fibers in preventing and delaying crack propagation, underscoring the importance of fiber length and content in attenuating cracks.
- Microstructural observations indicated poor fiber/matrix adhesion, adversely affecting the compactness of the adobe specimens.
- Further research is needed to optimize fiber-matrix adhesion and enhance the overall performance of earth-sand building composites.
- The identified optimal conditions for mechanical behavior and crack resistance pave the way for future advancements in the utilization of Alfa fibers to create environmentally friendly, resilient, and structurally sound construction materials.

## Acknowledgments

The authors gratefully acknowledge Cadi Ayyad University for its support of this thesis research program.

## Conflicts of interest

The authors declare no conflicts of interest.

## Author contributions

Reda Sadouri: Conceptualization, Investigation, Visualisation, Methodology, Testing, Writing original draft, Writing- Review and editing.

Mustafa Benyoucef: Conceptualization, Methodology, Supervision, Validation, Writing – Review and Editing.

Hocine Kebir: Conceptualization, Methodology, Investigation, Writing – Review and Editing.

## References

- [1] D. E. Montgomery, « Dynamically-compacted cement stabilised soil blocks for low-cost walling », PhD Thesis, University of Warwick, 2002.
- [2] Y. Millogo, J.-C. Morel, J.-E. Aubert, et K. Ghavami, « Experimental analysis of Pressed Adobe Blocks reinforced with Hibiscus cannabinus fibers », *Constr. Build. Mater.*, vol. 52, p. 71-78, 2014.
- [3] K. Ghavami, R. D. Toledo Filho, et N. P. Barbosa, « Behaviour of composite soil reinforced with natural fibres », *Cem. Concr. Compos.*, vol. 21, n° 1, p. 39-48, 1999.
- [4] I. Boucheфра, F. Z. E. Bichri, H. Chehouani, et B. Benhamou, « Mechanical and thermophysical properties of compressed earth brick reinforced by raw and treated doum fibers », *Constr. Build. Mater.*, vol. 318, p. 126031, 2022.
- [5] M. Bouhicha, F. Aouissi, et S. Kenai, « Performance of composite soil reinforced with barley straw », *Cem. Concr. Compos.*, vol. 27, n° 5, p. 617-621, 2005.
- [6] H. Binici, O. Aksogan, et T. Shah, « Investigation of fibre reinforced mud brick as a building material », *Constr. Build. Mater.*, vol. 19, n° 4, p. 313-318, 2005.
- [7] S. M. Hejazi, M. Sheikhzadeh, S. M. Abtahi, et A. Zadhoush, « A simple review of soil reinforcement by using natural and synthetic fibers », *Constr. Build. Mater.*, vol. 30, p. 100-116, 2012.
- [8] N. Kouta, J. Saliba, et N. Saiyouri, « Effect of flax fibers on early age shrinkage and cracking of earth concrete », *Constr. Build. Mater.*, vol. 254, p. 119315, 2020.
- [9] C. Galán-Marín, C. Rivera-Gómez, et J. Petric, « Clay-based composite stabilized with natural polymer and fibre », *Constr. Build. Mater.*, vol. 24, n° 8, p. 1462-1468, 2010.
- [10] A. Schicker et S. Gier, « Optimizing the mechanical strength of adobe bricks », *Clays Clay Miner.*, vol. 57, n° 4, p. 494-501, 2009.
- [11] S. Z. Salleh *et al.*, « Recycling food, agricultural, and industrial wastes as pore-forming agents for sustainable porous ceramic production: A review », *J. Clean. Prod.*, vol. 306, p. 127264, 2021.
- [12] A. Mesbah, J. Morel, P. Walker, et K. Ghavami, « Development of a direct tensile test for compacted earth blocks reinforced with natural fibers », *J. Mater. Civ. Eng.*, vol. 16, n° 1, p. 95-98, 2004.
- [13] C. Juárez, B. Guevara, P. Valdez, et A. Durán-Herrera, « Mechanical properties of natural fibers reinforced sustainable masonry », *Constr. Build. Mater.*, vol. 24, n° 8, p. 1536-1541, 2010.
- [14] S. Ismail et Z. Yaacob, « Properties of laterite brick reinforced with oil palm empty fruit bunch fibres », *Pertanika J. Sci. Technol.*, vol. 19, n° 1, p. 33-43, 2011.
- [15] H. Omrani, L. Hassini, A. Benazzouk, H. Beji, et A. ELcafsi, « Elaboration and characterization of clay-sand composite based on Juncus acutus fibers », *Constr. Build. Mater.*, vol. 238, p. 117712, 2020.
- [16] J. C. Morel, K. Ghavami, et A. Mesbah, « Theoretical and experimental analysis of composite soil blocks reinforced with sisal fibres subjected to shear », *Mason. Int.*, vol. 13, n° 2, p. 54-62, 2000.
- [17] C. Kouakou et J. Morel, « Mechanical performance of nonindustrial building materials manufactured with clay as a natural binder », *Submitt. Appl. Clay Sci.*, 2008.
- [18] J.-C. Morel et J.-P. Gourc, « Mechanical behavior of sand reinforced with mesh elements », *Geosynth. Int.*, vol. 4, n° 5, p. 481-508, 1997.
- [19] I. Falorca et M. Pinto, « Effect of short, randomly distributed polypropylene microfibrils on shear strength behaviour of soils », *Geosynth. Int.*, vol. 18, n° 1, p. 2-11, 2011.
- [20] I. Hosseinpour, S. Mirmoradi, A. Barari, et M. Omidvar, « Numerical evaluation of sample size effect on the stress-strain behavior of geotextile-reinforced sand », *J. Zhejiang Univ.-Sci. A*, vol. 11, p. 555-562, 2010.

- [21] Y. Xu *et al.*, « The effects of fiber inclusion on the evolution of desiccation cracking in soil-cement », *Materials*, vol. 14, n° 17, p. 4974, 2021.
- [22] C.-S. Tang, B. Shi, Y.-J. Cui, C. Liu, et K. Gu, « Desiccation cracking behavior of polypropylene fiber-reinforced clayey soil », *Can. Geotech. J.*, vol. 49, n° 9, p. 1088-1101, 2012.
- [23] K. Mustapha, S. T. Azeko, E. Annan, M. G. Zebaze Kana, L. Daniel, et W. O. Soboyejo, « Pull-out behavior of natural fiber from earth-based matrix », *J. Compos. Mater.*, vol. 50, n° 25, p. 3539-3550, 2016.
- [24] F. Aymerich, L. Fenu, et P. Meloni, « Effect of reinforcing wool fibres on fracture and energy absorption properties of an earthen material », *Constr. Build. Mater.*, vol. 27, n° 1, p. 66-72, 2012.
- [25] F. Aymerich, L. Fenu, L. Francesconi, et P. Meloni, « Fracture behaviour of a fibre reinforced earthen material under static and impact flexural loading », *Constr. Build. Mater.*, vol. 109, p. 109-119, 2016.
- [26] S. Ajouguim, K. Abdelouahdi, M. Waqif, M. Stefanidou, et L. Saâdi, « Modifications of Alfa fibers by alkali and hydrothermal treatment », *Cellulose*, vol. 26, p. 1503-1516, 2019.
- [27] A. B. Mabrouk, H. Kaddami, S. Boufi, F. Erchiqui, et A. Dufresne, « Cellulosic nanoparticles from alfa fibers (*Stipa tenacissima*): extraction procedures and reinforcement potential in polymer nanocomposites », *Cellulose*, vol. 19, p. 843-853, 2012.
- [28] D. Astm, « 698; Standard Test Methods for Laboratory Compaction Characteristics of Soil Using Standard Effort », *ASTM Int. West Conshohocken PA USA*, n° 19428-2959, 2007.
- [29] B. Astm, « 117, Standard Practice for Operating Salt Spray (Fog) Apparatus », *ASTM Int. 1997 Ed.*, 2011.
- [30] L. de M. Neuba *et al.*, « Mechanical properties, critical length, and interfacial strength of seven-islands-sedge fibers (*Cyperus malaccensis*) for possible epoxy matrix reinforcement », *Polymers*, vol. 14, n° 18, p. 3807, 2022.
- [31] C. ASTM, « 1557-03. », *Stand Test Method Tensile Strength Young's Modul Fibers* ASTM Int, 2003.
- [32] T. L. Piani *et al.*, « Dynamic behaviour of adobe bricks in compression: The role of fibres and water content at various loading rates », *Constr. Build. Mater.*, vol. 230, p. 117038, 2020.
- [33] E. Standard et others, « Methods of testing cement-Part 1: Determination of strength », *Turk. Stand. Inst. Ank. Turk.*, 2009.
- [34] A. E. M. K. Mohamed, « Improvement of swelling clay properties using hay fibers », *Constr. Build. Mater.*, vol. 38, p. 242-247, 2013.
- [35] I. Demir, « An investigation on the production of construction brick with processed waste tea », *Build. Environ.*, vol. 41, n° 9, p. 1274-1278, 2006.
- [36] H. M. Algin et P. Turgut, « Cotton and limestone powder wastes as brick material », *Constr. Build. Mater.*, vol. 22, n° 6, p. 1074-1080, 2008.
- [37] J. Page, F. Khadraoui, M. Boutouil, et M. Gomina, « Multi-physical properties of a structural concrete incorporating short flax fibers », *Constr. Build. Mater.*, vol. 140, p. 344-353, 2017.
- [38] M. Aziz, P. Paramasivam, et S. Lee, « Concrete Reinforced with Natural Fibres-New Reinforced Concretes (ed.) RN Swamy (Surrey) ». Surrey University Press, 1984.
- [39] H. Houben, H. Guillaud, et others, *Traité de construction en terre*. 1989.
- [40] V. A. Alvarez et A. Vázquez, « Influence of fiber chemical modification procedure on the mechanical properties and water absorption of MaterBi-Y/sisal fiber composites », *Compos. Part Appl. Sci. Manuf.*, vol. 37, n° 10, p. 1672-1680, 2006.
- [41] J. Pandey, V. Nagarajan, A. Mohanty, et M. Misra, « Commercial potential and competitiveness of natural fiber composites », in *Biocomposites*, Elsevier, 2015, p. 1-15.





Original scientific paper

## Experimental investigation of buried flexible HDPE pipe

Rajkumar Ratnaraju\*<sup>1)</sup><sup>5)</sup> Associate Professor (Senior Grade), Department of Civil Engineering, Sri Sivasubramaniya Nadar College of Engineering (Autonomous), Kalavakkam – 603110, Tamil Nadu, India

### Article history

Received: 06 September 2023

Received in revised form:

27 December 2023

Accepted: 29 December 2023

Available online: 26 February 2024

### Keywords

Buried pipe,  
HDPE,  
Deflection,  
Geogrid,  
static loading

### ABSTRACT

Buried pipes are used mainly for water supply and drainage, among many other applications such as oil, liquefied natural gas, coal slurries, and mine tailings. The pipes used may be rigid (reinforced concrete, vitrified clay, and ductile iron) or flexible (steel, UPVC, aluminum, fiberglass, and high-density polyethylene), although the distinction between them is blurring. Deflection or buckling determines the design of flexible pipes. HDPE pipes are preferred due to their light weight, long term chemical stability and cost efficiency. This project aims to design and fabricate an experimental setup of the model trench as a steel tank filled with the desired type of soil and flexible pipe with the required depth and loading provisions to simulate uniform loading and record the behavior, i.e., deflection of the flexible plastic pipe, compare the observation with the theoretical results, and infer the findings. The deflection characteristics were to be measured with the help of a dial gauge fixed inside the pipe. Additionally, the objective is to study the load deformation behavior of the buried pipe and stress variation across the cross section of the pipe under static loading, along with the influence of depth of embedment and density of backfill on the deformation and stresses in the pipe and the deformation behavior of the buried pipe when soil is reinforced with geogrid reinforcement, and evaluate the structural performance of the pipe. Based on the conclusions, various recommendations can be made in terms of the application of buried flexible HDPE pipes in place of conventional pipes and thereby reducing the risk of leakage and damage and also compensating the cost of pipe systems economically.

## 1 Introduction

Pipes are used widely in different walks of life. They are mostly used as service conduits for the transport of natural gas, petroleum, chemicals, and many other fluids. The pipes may be installed above the ground, such as in building service systems, or may be buried underground. For thousands of years, pipelines have been constructed in various parts of the world to convey water for drinking and irrigation. This includes the ancient use in China of pipes made of hollow bamboo and the use of aqueducts by the Romans and Persians. The Chinese even used bamboo pipes to transmit natural gas to light their capital, Peking, as early as 400 B.C.

A significant improvement in pipeline technology took place in the 18th century, when cast-iron pipes were used commercially. Another major milestone was the advent of steel pipe in the 19th century, which greatly increased the strength of pipes of all sizes. The development of high-strength steel pipes made it possible to transport natural gas and oil over long distances. Initially, all steel pipes had to be threaded together. This was difficult to do for large pipes, and they were apt to leak under high pressure [1].

The application of welding to join pipes in the 1920s made it possible to construct leak-proof, high-pressure, large-diameter pipelines. Today, most high-pressure piping consists of steel pipe with welded joints.

Major innovations since 1950 include the introduction of ductile iron, the use of high-density polyethylene (HDPE) pipe for sewers, and many more. These plastic pipes offer a wide range of benefits over conventional steel and cast-iron pipes. Plastic pipes offer a tremendous weight advantage over alternative piping materials. Less weight also means cheaper transport and, ultimately, a lower transportation cost. This also enables larger payloads (more pipes) to be loaded. Plastic pipe's resistance to fracture is an extremely important performance advantage. While plastic pipes are made from rigid PVC compound, these pipes themselves have the ability to yield under loading without fracturing and can successfully be used where the surface will be subject to external loading, such as road traffic.

A major requirement for all piping applications is joint tightness. Plastic pipes are available with deep-insertion, push-together gasketed, or solvent-cement joints. These

\* Corresponding author:

E-mail address: [rajkumarr@ssn.edu.in](mailto:rajkumarr@ssn.edu.in)

pipes provide smoother wall surfaces that reduce fluid friction and resistance to flow. This hydraulic smoothness inhibits slime buildup in sewers and virtually eliminates tuberculation and encrustation in water distribution mains. The end results are significantly lower maintenance costs, more efficient initial pipeline design, and superior performance over the lifetime.

### 1.1 Greenwood and Lang classical theory

Greenwood and Lang [2] found out that the non-uniformity of earth pressure is a function of soil type, degree of compaction, depth of embedment, and pipe stiffness. Greenwood and Lang also presented a modified formula that is more complete than the original formula of Watkins. The modified formula includes the work of Leonhardt (1972-79) [3], who developed a factor to consider the soil resistance of the native soil. The factor that is used to find the soil resistance in Watkins' modified Iowa formula is based on the ratio of the trench width to the pipe diameter and the modulus of the backfill soil around the pipe to the modulus of the native soil. A pipe-soil interaction coefficient, which is an empirical factor, is added to the soil resistance term to reflect the behavior of flexible pipes in the field. The modified formula of Greenwood and Lang [2] is as follows:

$$\Delta X = \frac{K \cdot \gamma \cdot H}{\frac{EI}{r^3} + 0.061 \zeta C_1 E'} - \delta V_0 \quad (1)$$

- $\Delta X$  – horizontal deformation
- $K$  - bedding factor
- $\gamma$  - unit weight of the backfill
- $H$  - height of the backfill above the pipe
- $\delta V_0$  - elongation due to compaction of the side fills
- $E$  – modulus of elasticity of pipe material
- $I$  – moment of inertia of the pipe wall per unit length of pipe
- $r$  – mean radius of pipe
- $\zeta$  – Leonhardt relationship
- $C_1$  – Pipe soil interaction coefficient defined by Greenwood and Lang
- $E'$  – watkins modulus of soil reaction

### 1.2 Failures in pipes

Performance limits and potential failures must be identified for buried pipe design. Chief among those are excessive deformations of the pipe, wall buckling, and collapse. Maximum allowable pipe deflection is usually not determined by structural failure but by conditions such as clearance for pipe-cleaning equipment, special sections, and pipe appurtenances (attachments).

Pipeline designers classify pipes as “flexible” or “rigid,” depending on how they perform after installation. Flexible pipe can move, or deflect, under loads without structural damage, while rigid pipe cannot deflect significantly without structural distress, such as cracking. In 1930, Marston classified pipes according to their rigidity [4].

In reality, the behavior of a buried pipeline will depend on how its stiffness compares with the stiffness of the soil in which it is to be buried. The soil-pipe system is statistically indeterminate. As a result, using statics alone is not capable of calculating the interface pressure between the soil and pipe.

As soil and surface loads are placed over a buried pipe, the ring tends to deflect, primarily into an ellipse with a decrease in vertical diameter and an almost equal (slightly less) increase in horizontal diameter, leading to collapse as shown in Figure 1. The increase in horizontal diameter develops lateral soil support, which increases the load-carrying capacity of the pipe. The decrease in vertical diameter partially relieves the ring of load since the soil above the pipe takes more of the load in arching action over the pipe.



Figure 1. Failure due to deflection

### 1.3 Scope of study

In the future, flexible pipes will almost entirely take the place of concrete and clay pipes in buried piping systems that are already in use. This is due to the cheaper costs of flexible plastic pipes and their favorable characteristics, such as ease of replacement, high deflection capacity, etc. Therefore, to predict the behavior and performance of the buried flexible plastic pipes that would be widely used in underground piping systems and to prevent failures of these pipes, this study becomes essential and of prime importance.

## 2 Objectives

- To study the performance of flexible HDPE pipe buried in a M-Sand backfill subjected to static load.
- The response of the pipes is studied for the influence of deflection on the pipe material.
- To study the performance of flexible HDPE pipe when soil is reinforced with geogrid reinforcement.
- To compare the deflection characteristics with the classical theory devised by Greenwood and Lang.
- However, this study is limited to the pipe material, depth of embedment, pipe without flow, and static loading conditions.

## 3 Literature review

Arokiaswamy et al. [5] performed a field test subjecting high-density polyethylene (HDPE), PVC, and metal large-diameter pipes to a design truck loading. The finite element method was used to determine how the pipe soil system responded to live load application. The above results were taken for comparison. Good performance was demonstrated by using buried flexible pipes embedded with highly compacted graded sand and silt. Under shallow burial conditions, the specified deflection limit for the installation of flexible pipes was found to be 5%, and for vertical deflection, was found to be 2%, according to the AASHTO specification.

Mohammed Hoosseini and Moghaddas Tafreshi [6] studied the behavior of buried pipes under cyclic loading

conditions experimentally; a physical model of the buried pipe trench condition was developed. The steel flexible model pipes were placed inside a soil trench of medium silica sand. The trench was prepared by the raining technique at three different relative densities inside the testing tank. The depth of the pipes in the trench was changed, and cyclic loads with different amplitudes were applied to the trench surface centrally and eccentrically. From the experimental investigation, the deflection and the failure condition were determined.

Neelam and Vipulanandan [7] investigated the behavior of flexible PVC pipes with sand and controlled low-strength materials (CLSM) as backfill materials in the soil box. Pipe deflections were compared against the modified Iowa formula, and an appropriate modification factor was introduced in the modified Iowa formula to better represent the test data.

Babu et al. [8] presented a critical appraisal of the mechanical behavior of buried flexible pipes and proposed a design methodology for the prediction of the performance of buried flexible pipes using finite element analysis for simple loading and boundary conditions.

Suleiman et al. [9] modeled the pipe-soil system using ANSYS. Small and larger deflection theories of ANSYS were used in the analysis, and the results were compared with CANDE, one of the most commonly used programs for buried pipe analysis, and found to be satisfactory.

Zhan and Rajani [10] carried out a non-linear finite element analysis to assess the effects of different trench backfill materials, pipe burial depths, and pipe materials on the amount of traffic load transferred to buried pipe and found that the results were in good agreement with those obtained from field truck load tests.

#### 4 Materials

##### 4.1 M-sand

The M-sand as shown in Figure 2 used for this particular project is homogenous in nature. The sand is made to attain a density of around 18 kN/m<sup>3</sup> by means of controlled tamping using a plunger for preparing the dense sand bed. The sand above the bedding is of ordinary loose density, around 13.5 kN/m<sup>3</sup> and the properties of used M-Sand are given in Table 1.



Figure 2. M-Sand

Table 1. Properties of M-sand

Parameter	Value
Density of dense bed (kN/m <sup>3</sup> )	18.036
Density of loose backfill (kN/m <sup>3</sup> )	13.5
Specific gravity [11]	2.730
Angle of internal friction [12]	29.89°

##### 4.2 HDPE Pipe:

HDPE pipes of 200 mm outer diameter and 6 mm thickness as shown in Figure 3, were used in the study. The pipes used conform to the Indian standard IS 14333 (1996) [11] and are characterized by a black color. The specifications of the pipe are listed below in Table 2.



Figure 3. HDPE pipe

Table 2. Properties of HDPE pipes

Properties	Values
Diameter	200.00 mm
Young's modulus	800.00 MPa
Thickness	6.00 mm
Moment of inertia	18.00 mm <sup>3</sup>
D/T ratio	33.33
EI	14400.00 N.mm

##### 4.3 Geogrid

The geogrid, as shown in Figure 4, is used to effectively reduce the stress on the pipes. These geogrids are black in color. The properties of the geogrid obtained from the manufacturer are listed below in Table 3.



Figure 4. Geogrid

Table 3. Properties of geogrid

Properties	Values
Ultimate tensile strength	30 kN/m
Aperture dimension	40 mm
Rib thickness	1.5 mm
Rib width	2.3 mm
Junction efficiency	95%
Resistance to UV degradation	100%

#### 4.4 Specially fabricated tank

The steel tank of dimension 600 mm x 800 mm x 1200 mm shown in Figure 5 was fabricated with side plates consisting of holes of diameter 200mm with suitable tolerance for the pipe to fit. The steel tank is fabricated with a manual loading arrangement that produces a uniform load on the soil, which is dispersed to the pipe, which in turn gives the deflection reading.



Figure 5. Front and side view of tank

reference in the fabrication process is shown below in Figure 7.



Figure 6. Proving Ring

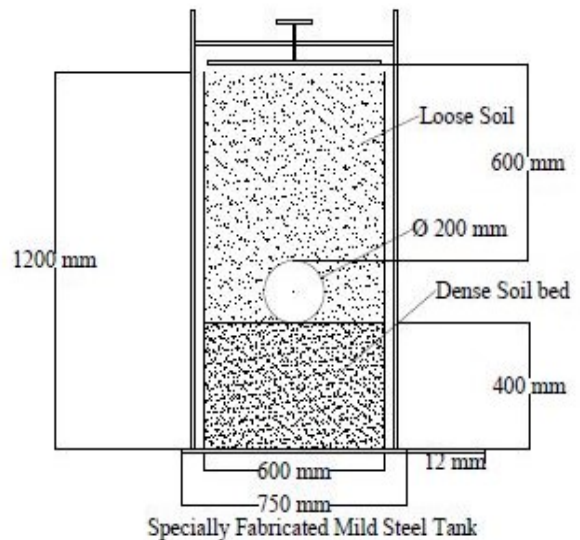


Figure 7. Line diagram of steel tank

#### 4.5 Dial Gauge

The dial gauges are used to record the amount of deflection which are placed both in crown and spring line direction at 300 mm from the center on either side.

#### 4.6 Proving Ring

The proving arrangement shown in Figure 6 is facilitated to find the amount of load applied on the soil.

The line diagram of the proposed steel tank with appropriate dimensions to be specially fabricated, used as a

### 5 Experimental Procedure

The basic concept behind the experiment involves measuring the deflection values of the pipe for different loads in the presence and absence of geogrids. The sequence and process to be followed are explained below:

- The steel tank with loading arrangement and the pipe hole were fabricated. The dimensions of the tank are 600 mm x 800 mm x 1200 mm.
- A dense bed with M-Sand was prepared up to 400 mm (the height of the fixed plates), and thereby the bulk density was maintained to a dense level by suitable compaction.

- The HDPE pipe of diameter 200 mm was fitted with two dial gauges, one for the crown deflection and the other for the springing line deflection.
- The HDPE pipe was inserted through the sand test tank through the plates with the hole.
- The loose backfill was prepared by pouring M-Sand by raining technique into the tank without any alterations. This backfill was prepared up to the height of the hollow plates.
- The deflection in the crown was recorded for every increment of 15 kg of load above the crown level of the HDPE pipe.
- The side plates were then placed, and the loose backfill was filled simultaneously, taking the readings of deflection for the corresponding sand load. Thus, values for the plot load vs. deflection graph for the self-weight condition were obtained.
- The tension-proving ring, along with the magnetic base, was attached to the loading frame in order to determine the load corresponding to the downward movement of the loading plate.
- The lever arm was rotated to provide loading for the loose bed. As the lever turned, the loading plate moved downwards by a thread rod mechanism, and loading was applied to the loose backfill.
- The load value was determined from the proving ring dial gauge, and the deflection value both for the springing line and the crown was determined using the deflection dial gauge.
- The values were tabulated in order to obtain the load vs. deflection graph without a geogrid reinforcement case.
- The same procedure was repeated after placing the geogrid, and the deflection readings were observed for the reinforcement case as well.
- The values are tabulated, and graphical results are plotted.
- The experimental values were correlated with the theoretical reviews, and thereby a comparison study was obtained.

## 6 Preparation of a dense bed

- The sand was filled in layers and compacted using the rammers to a depth of 400 mm, as shown in figure 8.
- The density of the dense bed is maintained within the range of 17 kN/m<sup>3</sup> to 20 kN/m<sup>3</sup>.



Figure 8. Compacted a dense M-Sand bed

Observation:

Volume of sand used = 0.192 m<sup>3</sup>

Mass of the sand = 353 kg

Achieved density =  $\frac{353 \times 10^{-3} \times 9.81}{0.192} = 18.036 \text{ kN/m}^3$

## 7 Preparation of loose backfill

The sand was filled in a loose condition using the raining technique to a depth of 800 mm, including the pipe material, as shown in Figure 9.

The density of the loose soil is maintained within the range of 12 kN/m<sup>3</sup> to 15 kN/m<sup>3</sup>

Observation:

Volume of sand = 0.359 m<sup>3</sup>

Mass of sand = 495 kg

Achieved density =  $\frac{495 \times 10^{-3} \times 9.81}{0.359} = 13.5 \text{ kN/m}^3$



Figure 9. Filling of loose M-Sand bed

## 8 Orientation of HDPE pipe

The geogrid is placed in a parabolic shape above the circumference of the pipe, extending along the spring line as shown in Figure 10.

This orientation of the geogrid facilitates the pipe's ability to transfer the load along the spring line and increases its ability to resist deflection.

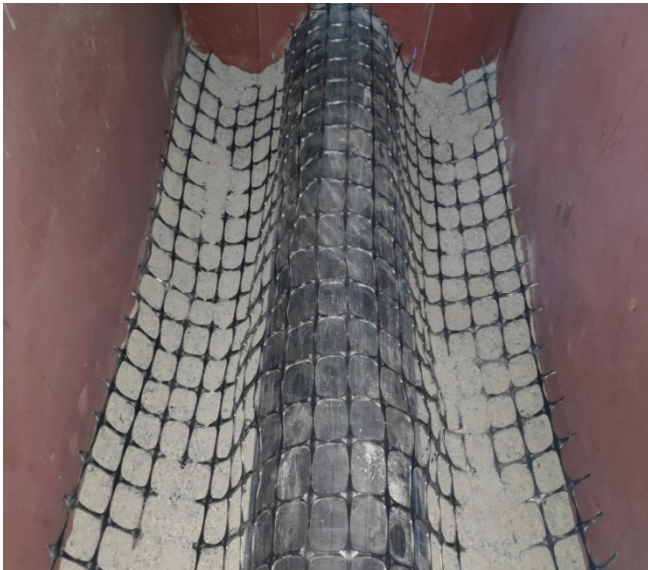


Figure 10. Orientation and placement of geo-grid over HDPE Pipe

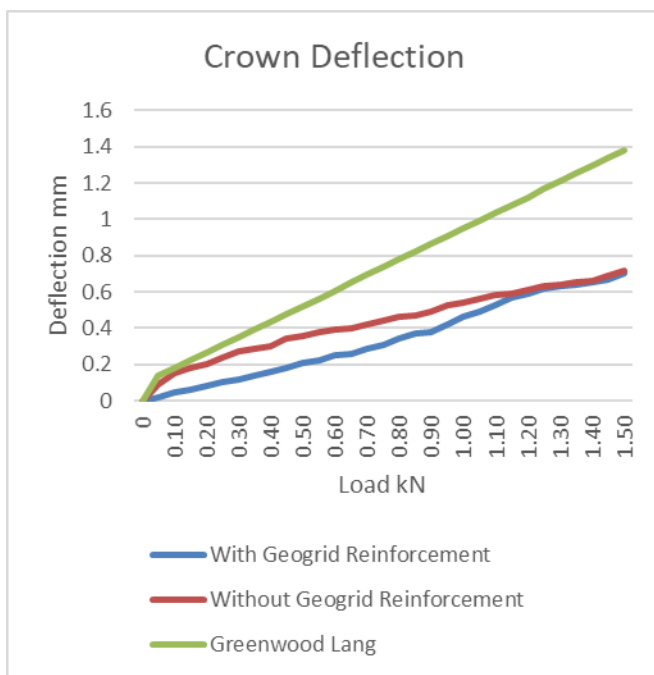


Figure 11. Load vs Crown Deflection Comparison

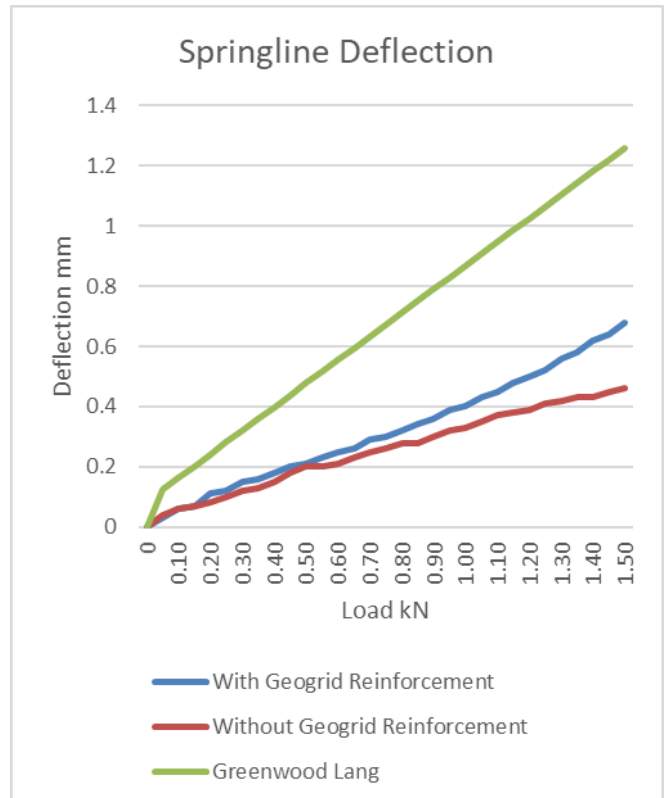


Figure 12. Load vs spring line deflection comparison

## 9 Results and discussion

- The deflections obtained at the crown and spring lines of the pipe with and without the presence of geogrid reinforcement are presented graphically in figures 11 and 12, respectively, and the following results are discussed.
- The deflection of the pipe due to the filling of M-sand up to the crown of the pipe was found to be insignificant, and therefore, the values were neglected.
- The M-sand was filled above the crown level of the pipe in increasing amounts of 15 kg, the deflection readings were recorded for each increment of sand filling.
- In the case of pipe without geogrid reinforcement, the deflection due to self-weight was found to be 1.18 mm.
- In the case of pipe with geogrid reinforcement, the deflection due to self-weight was found to be 0.50 mm.
- In the case of pipe without geogrid reinforcement, the applied uniform load of 1.50 kN yielded a crown deflection of 0.72 mm and a spring-line deflection of 0.46 mm.
- In the case of pipe with geogrid reinforcement, the applied uniform load of 1.50 kN yielded a crown deflection of 0.70 mm and a spring-line deflection of 0.68 mm.
- The load-versus-deflection characteristics of the HDPE pipe were computed using the theoretical equation derived by Greenwood and Lang.
- In the case of theoretical computation, the application of a uniform load of 1.50 kN yielded a crown deflection of 1.38 mm and a spring-line deflection of 1.26 mm.

## 10 Conclusion

- The introduction of Geogrid Reinforcement exhibited an improvement in the characteristics of HDPE pipe in loose M-sand backfill, i.e., the deflection due to the load imposed by the self-weight of M-sand applied to the pipe was considerably reduced by 0.68 mm, i.e., a 58 % decrease.

- Similarly, the crown deflection due to the application of a uniform load was reduced by 35 % due to the introduction of Geogrid reinforcement.

- The spring line deflection characteristics did not show satisfactory behavior, which suggests that this specific orientation of geogrid reinforcement is not suitable for reducing of spring-line deflection.

- The Greenwood and Lang theoretical computation of the load vs deflection characteristics of HDPE pipe in loose M-sand backfill under uniform load overestimates the experimental findings.

- Therefore, the results suggest that this orientation of geogrid reinforcement is best suited for reducing the crown deflection of HDPE pipe in loose M-sand backfill under uniform loading and self-weight.

## Acknowledgement

I sincerely thank the management of Sri Sivasubramaniya Nadar College of Engineering for providing the necessary facilities and support to complete the proposed work. I also thank the Department of Civil Engineering for the motivation and encouragement rendered towards the successful completion of the experimental work in the laboratory.

## References

- [1] A.P. Moser, Buried Pipe Design, McGraw Hill Publications, New York. 1990.
- [2] M.E. Greenwood and D.C Lang, Vertical deflection of buried flexible pipes, Buried Plastic Pipe Technology, ASTM STP 1093, Philadelphia, 1990.
- [3] G. Leonhardt, Einflub der Bettungsstefigkiet anf die Trafahigkeit ond die verformungen von Flexiben rohren, Strasse Bruccke Tunnel, Vol.3, 1972.
- [4] A. Marston, The theory of loads on pipes in Ditches and tests of cement and clay drain tile and sewer pipe, Iowa state college Bulletin, No.31, Vol XI, (1930).
- [5] M. Arockiasamy, O. Chaallal and T. Limpeteeprakam, Full-Scale field tests on flexible pipes under live load application, Journal of Performance of Constructed Facilities, American Society of Civil Engineers, Vol. 20, Issue 1 (2006), pp. 21- 27.
- [6] S.M. Mir Mohammed Hosseini and S.N. Moghaddas Tafreshi, A new physical model to study the behaviour of buried pipes under cyclic loading conditions, International Journal of Engineering, Vol. 15, (2000) No. 2 pp. 117-124.
- [7] M.K. Neelam and C. Vipulanadan (1998), Flexible PVC Pipe–Backfill Interaction Study, <[http://cigmat.uh.edu/content/conf\\_exhib/00\\_Poster/8.htm](http://cigmat.uh.edu/content/conf_exhib/00_Poster/8.htm)>.
- [8] S. Babu, V.K. Ranjith, R. Seshagiri Rao and B.R. Srinivasa Murthy, Finite element analysis of Buried Flexible pipes Indian Geotechnical journal, Vol.33(2) (2003), pp 125-142.
- [9] M.T. Suleiman., R.A. Lohnes, T.J. Wipf and F.W. Khaliber, Analysis of Deeply Buried Flexible Pipes, Transportation Research Board Annual Meeting, 2002.
- [10] C. Zhan and B. Rajani, Load transfer analysis of buried pipe in different backfills, Journal of Transportation Engineering, Vol.123, No.6 (1997), pp 447-453.
- [11] IS 14333 (1996) High density polyethylene pipes for sewerage – specifications.





Original scientific paper

## Concrete crack analysis using a deep belief convolutional neural network

Geetha Ramalingam<sup>1)</sup>, Vijayalakshmi Ramalingam<sup>\*2)</sup>, Prakash Ramaiah<sup>3)</sup>, Sathia Ramalinam<sup>4)</sup><sup>6)</sup> Department of Biomedical Engineering, Saveetha School of Engineering, SIMATS, Chennai, India<sup>7)</sup> Associate Professor, Department of Civil Engineering, Sri Sivasubramaniya Nadar College of Engineering- India<sup>8)</sup> Associate Professor, Department of Civil Engineering, Government College of Engineering, Tirunelveli- India<sup>9)</sup> Associate Professor, Department of Civil Engineering Sri Venkateswara College of Engineering, India

### Article history

Received: 02 January 2024

Received in revised form:

19 February 2024

Accepted: 04 March 2024

Available online: 22 March 2024

### Keywords

Machine Learning,  
Convolutional Neural Network,  
Concrete structure,  
cracks,  
Deep Neural Network,  
Unsupervised Learning

### ABSTRACT

The assessment of surface cracks in concrete structures plays a pivotal role in determining structural integrity. However, current diagnostic technologies suffer from drawbacks such as being time-consuming, subjective, and reliant on inspectors' experience, resulting in low detection accuracy. This paper seeks to address these issues by proposing an automated, vision-based method for identifying the surface condition of concrete structures. The method integrates advanced pre-trained convolutional neural networks (CNNs), transfer learning, and decision-level image fusion. To develop and validate this approach, a total of 6,500 image patches from diverse concrete surfaces were generated. Each pre-trained CNN establishes a predictive model for the initial diagnosis of surface conditions through transfer learning. Given the potential for conflicting results among different CNNs due to architectural differences, a modified Deep Belief CNN algorithm is crafted, thereby enhancing crack detection accuracy. The effectiveness of the proposed method is confirmed through a comparison with other CNN models. Robustness is tested by subjecting the method to images with various types and intensities of noise, yielding satisfactory outcomes. In practical scenarios, the hybridised approach is applied to analyse field-captured images of concrete structures using an exhaustive search-based scanning window. Results showcase the method's capacity to accurately identify crack profiles, with minimal areas of incorrect predictions underscoring its potential for practical applications.

## 1 Introduction

Cracks in concrete are a common phenomenon that may occur due to moisture movement, temperature variation, elastic deformation, creep, chemical reactions, foundation movement, and the settlement of soil. But unforeseen cracks may affect the durability and serviceability of the structure which in turn may affect its service life. Cracks in concrete occur when the strain exceeds the tensile strain capacity of the concrete [1]. For flexural members, the crack occurs on the top and bottom surfaces of the flexural member. The cracks start from the tension face and propagate to the compression zone perpendicular to the axis of the member. Widening of cracks may lead to corrosion of the reinforcement and ultimately lead to the failure of the structure [2]. Various parameters that influence the width of cracks are tensile stress in the longitudinal bars, thickness of the concrete cover, diameter and spacing of the longitudinal bars, depth of the member and location of the neutral axis, bond strength, and tensile strength of the concrete [3]. The crack width in a structural member is calculated to satisfy the limit state of serviceability. Different patterns of cracks

developed in beams and columns are shown in Figures 1 and 2 respectively. Adding fibres to the concrete helps to increase the tensile strength, impact strength, strain capacity, and crack width and shrinkage. Previous research has demonstrated that adding fibres to concrete helps improve the properties of concrete in the post-cracking behaviour [4]. Fibres added to the concrete matrix improve the fracture energy, post-cracking stiffness, and ductility of the concrete rather than its strength. The tensile strength of fibres contributes mainly to improving the crack arresting mechanism of concrete in pre-cracking as well as in the post-peak region [5]. Once cracks develop in concrete, the fibres share the stress and distribute the stress across the cross section, which reduces the stress concentration and prevents the formation of wider Cracks, as shown in Figure 3. The strain redistribution across the cracks in plain concrete is achieved through bridging actions in the form of aggregate interlock. In FRC, the fibre stretching and pull-out help with crack bridging in addition to the aggregate interlock [6]. An experimentally tested specimen showing the crack width behaviours for plain concrete and fibre-reinforced concrete is shown in Figure. 4.

<sup>\*</sup> Corresponding author:E-mail address: [VijayalakshmiR@ssn.edu.in](mailto:VijayalakshmiR@ssn.edu.in)

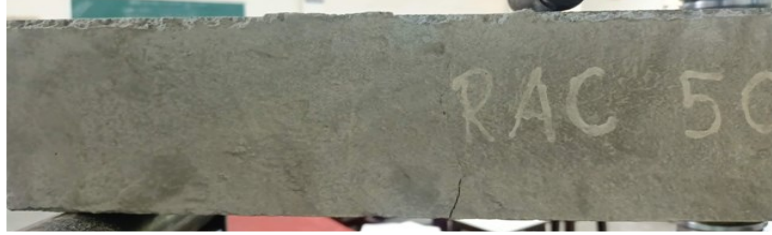


Figure 1. Cracks in structural beam member with flexural shear crack



Figure 2. Cracks in column members(a) Diagonal Cracks (b) Splitting Cracks



Figure 3. Crack pattern in masonry unit without fibre and with natural fibre

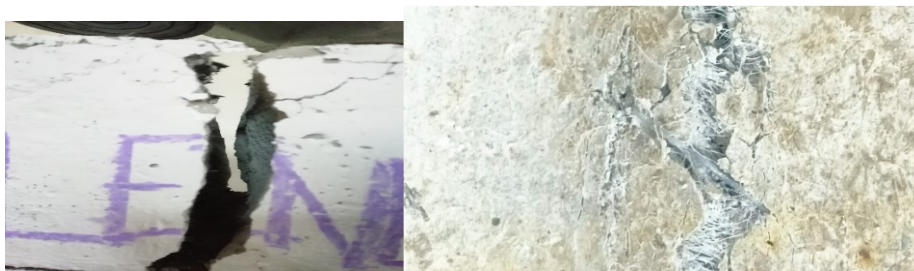


Figure 4. Crack width of concrete (a) without fibres and (b) bridging of crack in fibre-reinforced concrete

Empirical formulas and equations were suggested by many codal standards, such as IS 456-2000 (equation 1-4), BS-Euro code - BS EN1992-1-1-2004 (equation 5-9), Egyptian code (equation 10-13) and American Concrete Institute ACI-code (equation 14-16). In addition, many researchers have developed an empirical model to calculate the crack width in concrete. The formulas suggested by different codes are given below.

The crack width ( $W_{cr}$ ) formula suggested by IS 456-2000:

$$W_{cr} = \frac{3a_{cr}\varepsilon_m}{1 + \frac{2(a_{cr}-c_{min})}{h-x}} \quad (1)$$

$$\varepsilon_m = \varepsilon_1 \frac{b(h-x)(a-x)}{3E_s A_s (d-x)} \quad (2)$$

$$\varepsilon_1 = \frac{Mx}{I_c(0.5E_c)} \quad (3)$$

$$I = \frac{bx}{3} + (mA_{st}(d-x)^2) \quad (4)$$

The equation for crack width as per EURO code:

$$w_k = S_{r,max}(\varepsilon_{sm} - \varepsilon_{cm}) \quad (5)$$

$$(\varepsilon_{sm} - \varepsilon_{cm}) = \frac{(f_s - k_t \left( \frac{ct, eff(1 + n\rho_{eff})}{\rho_{eff}} \right))}{E_s} \geq 0.6 \frac{f_s}{E_s} \quad (6)$$

$$n = \frac{E_s}{E_c} \quad (7)$$

$$\rho = \frac{A_s}{A_{c,eff}} \quad (8)$$

$$S_{r,max} = 3.4C + \frac{0.425k_1k_2\phi}{\rho_{eff}} \quad (9)$$

The equation of crack width as per Egyptian code:

$$W_k = \beta \varepsilon_{sm} S_{rm} \quad (10)$$

$$\varepsilon_{sm} = \frac{f_s}{E_s} (1 - \beta_1 \beta_2 \left( \frac{f_{scr}}{f_s} \right)^2) \quad (11)$$

$$S_{rm} = 50 + 0.25k_1k_2\phi\rho_{eff} \quad (12)$$

$$f_{scr} = \frac{mMd_c}{I_{cr}} \quad (13)$$

The equation suggested by ACI 318-95 code:

$$W_{max} = 0.011\beta f_s \sqrt[3]{d_c A_o} 10^{-3} mm \quad (14)$$

$$A_o = \frac{2d_c b}{3} \quad (15)$$

$$\beta = \frac{h-x}{d-x} \quad (16)$$

In addressing the importance of identifying structural surface cracks and recognising the limitations of existing inspection methods, both academia and industry are actively pursuing the automation of crack diagnosis with high accuracy and real-time capability. The rapid advancement of computer vision and machine learning (ML) technologies in recent years has led to the proposal of numerous automatic approaches as powerful tools to tackle the challenges of crack detection in practical applications [7]. Early research in vision-based automated crack detection primarily focused on developing algorithms for crack edge detection using image processing methods. For example, Abdel-Qader et al. conducted a performance comparison of four edge detection filters—fast Fourier transform, fast Haar transform, Canny, and Sobel—for crack detection, with results based on fifty images of a concrete bridge showing that the fast Haar transform outperformed the other three filters, demonstrating the highest accuracy in crack detection. Kim et al. investigated the parameter optimization of current binarization methods for crack detection by reducing errors

between real crack widths and estimated ones [8]. Rabah et al. proposed a three-step approach, involving shade rectification, crack detection, and mapping, for detecting and mapping cracks based on terrestrial laser scanning (TLS) point cloud data [9]. In another study, Yamaguchi et al. introduced a novel percolation model to extract concrete surface cracks by considering percolated area shape and brightness connectivity [10]. The primary limitation of existing image processing-based approaches is their tendency to emphasise local patterns more than global features, despite cracks being global properties of the image. Some cracks in an image may be neglected when more attention is given to local patterns. To address this issue, several studies have started integrating image processing methods with ML technologies to enhance detection accuracy. Lee et al. initiated the utilisation of artificial neural networks to identify the length, width, and orientation of concrete surface cracks [11]. Li et al. created a new way to find concrete that uses an active contour model along with the Canny filter and support vector machine (SVM) [12]. Jahanshahi et al. utilised linear discriminant analysis (LDA) to extract features sensitive to cracks, which were then used as inputs to train three classifiers, including SVM, ANN, and nearest-neighbour [13]. In [14,15] CNN model is trained to discern the crack patterns, allowing it to forecast stress-crack correlations. Initially tailored to specific air-void configurations, it possesses the flexibility to accommodate a wider array of microstructures, thereby incorporating a broader spectrum of pore-related data. Although the combination of ML and image processing-based feature extraction has demonstrated the ability to improve crack detection accuracy, it may still encounter challenges in identifying cracks in images with complex background characteristics and noise. The main reason for this issue is that crack feature extraction is typically performed manually. While hand-crafted crack features may offer an optimal solution for a specific dataset, they may struggle to consistently perform well on a set of new crack images captured in a more intricate environment.

## 2 Literature review

In recent years, deep learning (DL), as a subset of machine learning (ML), has experienced rapid development, leveraging the advantage of seamlessly integrating automatic feature extraction and nonlinear classification [16]. A plethora of predictive models featuring deeper network architectures have emerged for the purpose of concrete surface crack detection. For instance, Xu et al. introduced a deep learning model comprising multiple layers of restricted Boltzmann machines for abstract feature learning, effectively identifying fatigue cracks within images featuring complex backgrounds [17]. Modarres et al. applied convolutional neural networks (CNN) to classify structural surface cracks of varying shapes and sizes, demonstrating that the performance of the trained model remains robust across different locations and pixel resolutions in images [18]. Additionally, Jo and Jadidi devised an autonomous crack classification system based on a deep belief network, trained using 15,000 infrared and RGB images with and without cracks [19]. Li and Zhao modified AlexNet to create a deep CNN model tailored for concrete crack detection, successfully incorporating it into a smartphone for practical applications [20]. Chen and Jahanshahi fused CNN with a data fusion algorithm to analyse video frames for crack detection. The proposed fusion framework aggregates features from each frame, enhancing the robustness and accuracy of the system [21]. Similar endeavours are

documented in Ref. [22], where a hybrid model comprising fully connected CNN and naive Bayes fusion was employed to recognise cracks in a concrete bridge.

In general, image-based deep learning (DL) approaches for crack identification can be classified into three groups: **Region-Based Detection:** Focuses on localising cracks within an image by generating image patches and determining whether each patch contains a crack. Preferred for automatically diagnosing the localised crack area on the surface of concrete structures. **Object Detection:** Aims to distinguish cracks from other objects using DL-based detectors. **Segmentation Methods:** Conducts pixel-level crack detection by classifying whether each pixel contains a crack or not. Each category of method has its own advantages and drawbacks. For example, while crack segmentation methods require significant computational power, region-based methods are preferred for localising crack areas on concrete structures for automatic diagnosis. Current approaches for crack region detection often utilise convolutional neural networks (CNNs) to handle image patches with pixel resolutions of  $512 \times 512$  or  $256 \times 256$ , detecting cracks in images with larger pixel sizes. However, a limitation of this method is that the developed CNNs can only detect cracks of similar sizes as the patches. In cases where a crack has a pixel size of  $32 \times 32$  in an image with a pixel size of  $256 \times 256$ , the trained model will consider the entire patch containing the crack, resulting in a coarse detection result. Consequently, these CNN models need to be retrained based on many image patches with smaller pixel sizes, which is computationally expensive. Figure 5 depicts the architecture of a basic CNN model.

To overcome the challenges outlined above, this research proposes an integrated method for detecting surface cracks in concrete structures with greater precision. This approach incorporates a sliding window based on an exhaustive search, pre-trained Convolutional Neural Networks (CNNs) with more complex architectures, transfer learning, and data fusion techniques. Initially, a sliding window is applied to divide the original image into smaller patches with reduced pixel resolution for crack detection. Subsequently, CNN-based classification models are established to determine whether each crack contains the defect or not. It is well recognised that the efficacy of the developed model is contingent on the quality and quantity of the training data. However, obtaining a large number of image samples with diverse crack patterns for training a deep network architecture is impractical in real-world scenarios. Alternatively, models for crack patch detection can be derived by retraining CNN models originally developed for distinct but related tasks using transfer

learning. In this context, 15 pre-trained CNNs initially designed for classifying images into 1000 object categories are repurposed as models for crack patch detection. As these pre-trained CNNs exhibit varying performances due to distinct network architectures, the predictive outcomes from different models may conflict, making it challenging for the system to reach a final decision. To address this issue, a new Deep Belief CNN algorithm is devised to amalgamate the detection results from various CNN models, yielding a comprehensive assessment of the surface condition of concrete structures.

The capacity of CNNs to generalise effectively is widely acknowledged, primarily contingent on having a substantial volume of training data, especially data with clear labels. When there's a reduction in the quantity of training data, the ensuing decline in classification accuracy can lead to the challenge of overfitting. The exceptional performance of CNNs in image recognition is fundamentally linked to their training on extensive datasets. However, researchers in the engineering domain often encounter difficulties in acquiring a satisfactory amount of meaningful data. In response to this challenge, transfer learning (TL) has emerged as a robust technique. It not only diminishes the dependence of networks on the magnitude of training data but also maximises the utilisation of existing data. In contrast to conventional machine learning methods, TL categorises the dataset into source and target domains. The central tenet of TL involves applying knowledge gleaned from the source domain to address pertinent tasks in the target domain, effectively resolving issues specific to the target [23].

### 3 Proposed method

A Deep Belief Network (DBN) is proposed in this work, shown in Figure 6. It is a type of artificial neural network architecture. DBN consists of multiple layers of stochastic, latent variables. It belongs to the broader family of deep learning models and is particularly associated with unsupervised learning tasks. DBNs are notable for their ability to learn hierarchical representations of data and have been used in various applications, including feature learning, dimensionality reduction, and generative modelling. A typical DBN is structured as a stack of Restricted Boltzmann Machines (RBMs). An RBM is a type of probabilistic graphical model with two layers: a visible layer representing the input data and a hidden layer capturing learned features. Training a DBN involves a two-step process: pre-training and fine-tuning. Pre-training: Each RBM in the stack is trained in an unsupervised manner to capture hierarchical features.

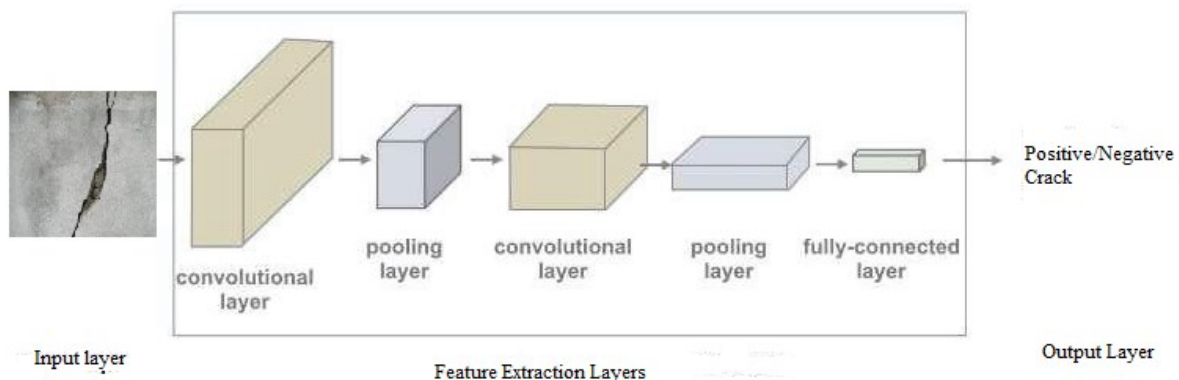


Figure 5. Architecture of a basic Convolutional Neural Network

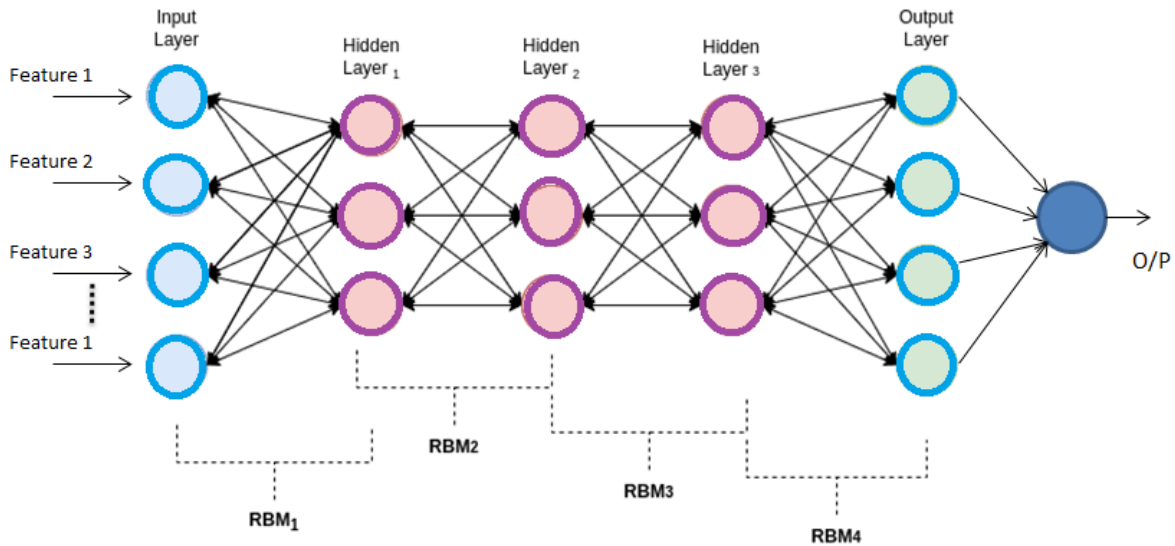


Figure 6. Deep Belief Network

This layer-wise pre-training initialises the weights of the network. Fine-tuning: The entire network is fine-tuned using supervised learning, typically using back propagation and gradient descent. DBNs can be used as generative models, capable of generating new samples similar to the training data. The RBM's capacity to learn a probability distribution over the input data facilitates this. Lower layers capture simple and local features, while higher layers represent more complex and global features, thanks to the hierarchical representation that DBNs learn. Dimensionality Reduction: DBNs can be used to reduce the dimensionality of data while retaining important features. Feature Extraction: Extracting meaningful features from raw data in an unsupervised manner. Generative Tasks: Generating new samples like the training data. Training deep networks can be computationally intensive, and fine-tuning requires labelled data for supervised learning. DBNs share similarities with deep autoencoders and deep neural networks. However, the layer-wise training of RBMs distinguishes them from some other deep learning architectures. It is important to note that while DBNs have been influential, more recent advancements in deep learning, such as deep neural

networks (DNNs) and convolutional neural networks (CNNs), have gained more prominence due to their scalability and performance on a wide range of tasks. The dataset, comprising images of cracks along with their associated depth information, is inputted into a Convolutional Neural Network (CNN). Within the CNN model, the feature extraction layer processes the images, extracting pertinent features. Subsequently, these extracted features serve as input for training and testing the regression models. The integrated CNN model is employed to predict the depth of the cracks. Figure 7. depicts the flow of the developed CNN model to predict the cracks.

### 3.1 Boundary

DBNs are generative models and can generate new samples from the learned probability distribution. This property allows them to be used for tasks such as generating synthetic data or filling in missing values. DBNs are adept at learning hierarchical representations of the input data, capturing both low-level and high-level features in a distributed manner across the layers.

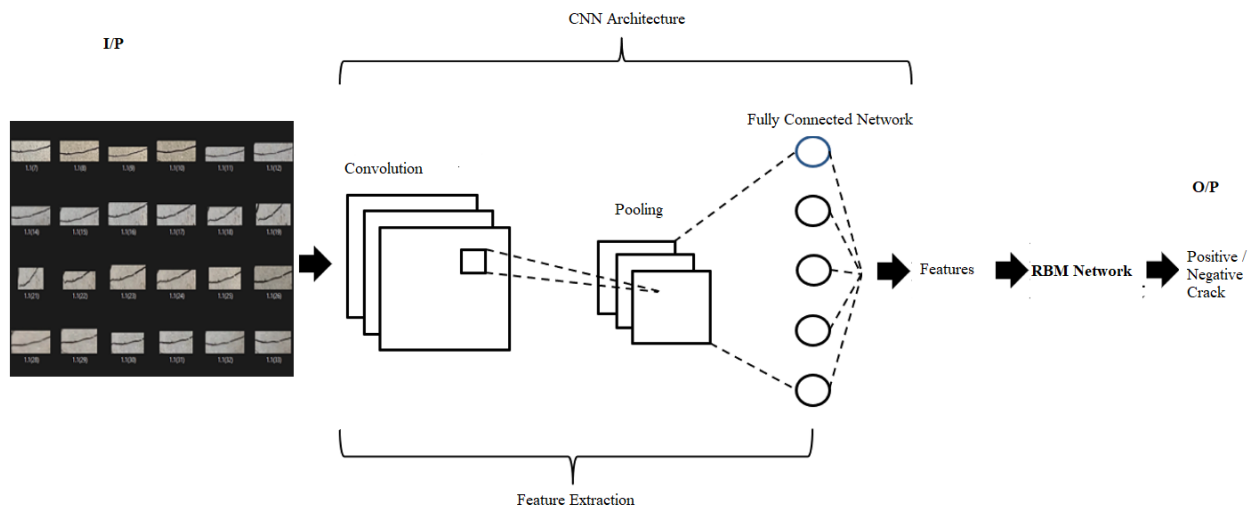


Figure 7. Integrated CNN model for crack prediction

3.2 Assumptions

DBN assumes that the hidden units within each layer are conditionally independent of the visible units. This assumption simplifies the modelling and learning process. DBN assumes the statistical properties of the data, and they remain constant across the layers. The assumptions may not always hold true, but even then, they simplify the learning process and enable effective feature learning.

Mathematically, the key equations governing the behaviour of a DBN involve the energy function and the conditional probabilities associated with each layer in an RBM. The joint probability distribution over visible units ( $v$ ) and hidden units ( $h$ ) is given by:

$$P(v, h) = \frac{1}{Z} e^{-E(v,h)}$$

where,  $Z$  is the normalisation constant

$E(v, h)$  is the energy function defined as  $-v^T W a - b^T v - c^T h$ , where  $W$  is the weight matrix connecting visible and hidden units,  $a$ ,  $b$ , and  $c$  are the biases for visible units, visible-to-hidden connections, and hidden units respectively.

The conditional probabilities are then calculated as:

$$P(h|v) = \frac{1}{1 + e^{-(Wv+c)}}$$

$$P(v|h) = \frac{1}{1 + e^{(W^T h+c)}}$$

These equations govern the learning and inference processes in DBN.

Initially, the concrete surface images undergo segmentation, with each original image sliced into smaller patches using a sliding window. These patches, characterised by reduced pixel sizes, are then classified based on the actual surface conditions, distinguishing between intact and cracked areas. Following this, training and validation samples are randomly drawn from these categorised patches. These samples are then inputted into various CNN models, including AlexNet, DarkNet-19, DarkNet-53, DenseNet-201, EfficientNet-b0, GoogLeNet, Inception-v3, MobileNet-v2, ResNet-18, ResNet-50, ResNet-101, ShuffleNet, SqueezeNet, VGG-16, and VGG-19, for the initial recognition of surface conditions. These chosen CNNs are pretrained on the ImageNet dataset, which contains over a million images used for classifying a thousand objects. The Kaggle images [24] used in this experiment relate to structural engineering elements such as buildings, bridges, beams, columns, and walls, specifically focused on concrete crack images. Then, these CNNs that have already been trained on different deeper architectures are fine-tuned on new concrete surface image patches to turn them into models for finding crack patches.

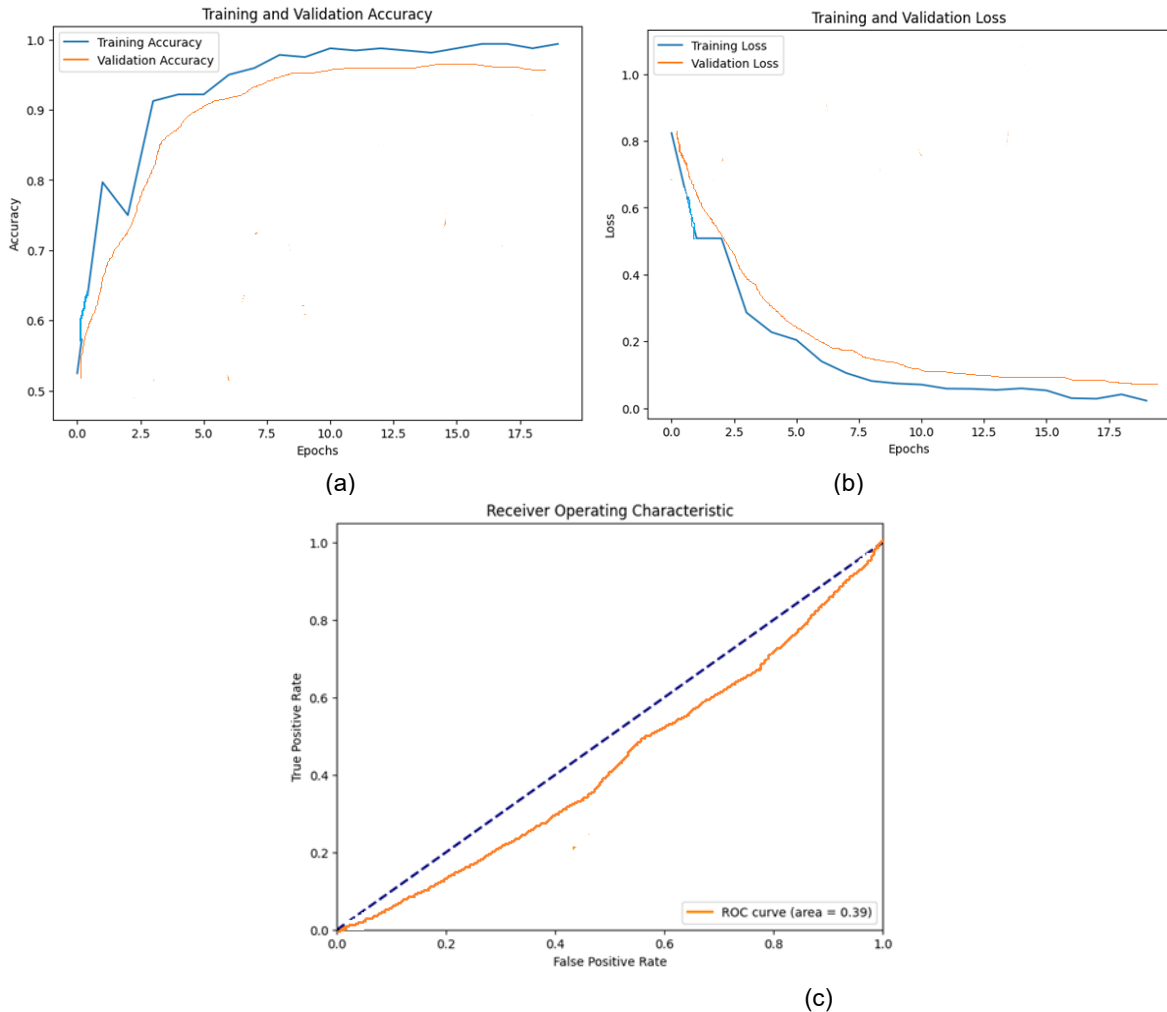


Figure 8. a) Training and validation accuracy b) Training and validation loss c) ROC curve

Differing from traditional networks that provide hard decisions, the CNNs in this study generate soft decisions, presenting probability values for all potential categories. As different network architectures exhibit varying capabilities for diagnosing concrete cracks, results from different CNN models may present conflicts. To address this, the proposed framework adopts a hierarchical configuration where the outputs of prior operations serve as inputs for subsequent operations. This approach significantly bolsters crack detection accuracy with a high level of confidence, leveraging multi-level information processing.

#### 4 Results and discussion

To validate the effectiveness of the concrete crack prediction method utilising the deep belief network in real-world scenarios, a simulation experiment is conducted. The dataset was trained and validated using Python software. The program was executed in Google Colab for faster execution of a huge dataset and a large number of epochs.

Table 1: Number of images used for training and validation

Category	Training	Validation
With crack	3000	800
Without crack	3500	850

This research's primary innovation lies in the integration of deep learning-based Convolutional Neural Networks (CNNs), transfer learning through the deep belief algorithm, creating a hybridised model for predicting surface cracks in concrete structures. This model demonstrates superior predictive capabilities and robustness compared to existing deep learning methods. Additionally, the introduction of decision-level image fusion to concrete crack detection represents a novel aspect. This application significantly elevates the confidence level of prediction results, thereby further improving prediction accuracy. Equation (17-20) is used to measure the performance metrics of the parameters mentioned. Figure 8 depicts the curve for accuracy during training and validation of the dataset, the loss curve and the ROC curve, respectively.

$$\text{Sensitivity} = \frac{TN}{TN + FP} \quad (17)$$

$$\text{Precision} = \frac{TP}{TP + FP} \quad (18)$$

$$\text{NPV} = \frac{TN}{TN + FN} \quad (19)$$

$$\text{Accuracy} = \frac{TP + TN}{TN + TP + FP + FN} \quad (20)$$

Table 2. Comparison of accuracy and Area under curve (AUC) for different CNN models

Model Name	Precision	Accuracy	F1 score	AUC
DarkNet-51	97.55%	97.84%	95.78%	0.9292
ResNet-101	97.20%	97.51%	95.11%	0.9615
ShuffleNet	95.55%	97.82%	95.05%	0.9535
SqueezeNet	97.44%	97.11%	95.15%	0.9182
AlexNet	97.21%	97.57%	95.41%	0.9339
DarkNet-19	97.49%	97.72%	95.55%	0.9647
ResNet-50	97.27%	97.59%	95.47%	0.9311
GoogLeNet	97.57%	97.72%	95.71%	0.919
Inception-v1	97.18%	97.55%	95.19%	0.9063
MobileNet-v2	95.74%	97.41%	95.18%	0.8946
VGG-15	97.48%	97.98%	95.82%	0.9052
VGG-19	97.74%	97.98%	97.01%	0.8913
EfficientNet-b0	95.11%	98.05%	95.12%	0.9447
DenseNet-201	97.91%	97.41%	95.75%	0.9714
ResNet-18	95.70%	98.05%	95.10%	0.9734
<b>Proposed</b>	<b>98.29%</b>	<b>98.05%</b>	<b>97.51%</b>	<b>0.9796</b>

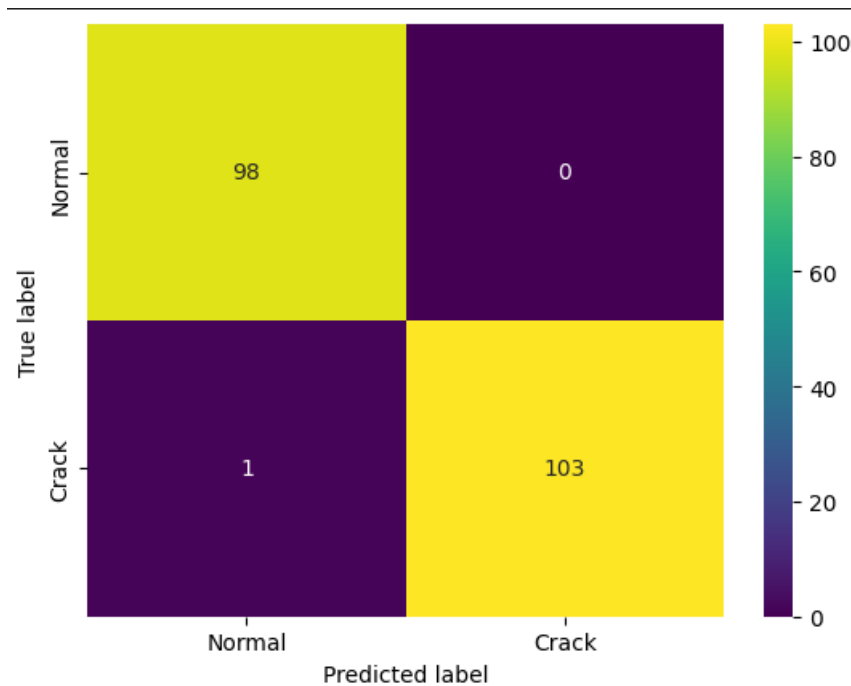


Figure 9. Confusion matrix for the proposed method

The proposed method has the highest values of metrics precision (98.29%), accuracy (98.05%), F1 score (97.51%), and AUC (0.9796). Figure 9 shows the confusion matrix.

#### 4.1 Effects of Noise

In practical scenarios, images captured from the surfaces of concrete structures inevitably encounter various forms of contamination due to factors such as transmission channels and environmental conditions during acquisition and transmission. This results in the introduction of diverse noises, leading to information loss and distortion in the images. It is imperative to assess the resilience of the proposed method concerning crack patch detection in the presence of different types of noise. In pursuit of this objective, the study focuses on evaluating the robustness of the proposed method against two prevalent types of image noise: Salt and Pepper (SP) noise and Motion Blur (MB) noise. SP noise typically arises from improper ISO settings, while MB noise is a consequence of relative movement between the focal location and the camera. The evaluation indices of all the models are calculated after the test images undergo a noise removal process.

The study employed MATLAB software version 2021 installed on a PC with 16GB of RAM and 1TB of storage to incorporate noise effects into the concrete images. MATLAB is a widely used tool in the field of image processing due to its versatility and comprehensive set of functions tailored for handling and manipulating images.

## 5 Conclusion

The hybrid patch-based crack detection approach proposed in this study achieves an impressive identification accuracy of up to 97.7%. This notably outperforms both individual CNN models and the region-based crack detection method outlined in [25-27], which attains an optimal accuracy

of 96%. So, the proposed method effectively fixes the problem of current crack detection models wrongly identifying cracks, which stops wrong estimates of the structure's remaining strength. The results presented in Figure 8, Figure 9, and Table 2 adequately demonstrate the effectiveness of the proposed hybridised method in concrete crack patch detection. The accuracy value and precision are almost 98% for the proposed DBN model. It rarely predicts a normal image as a concrete crack image, which is evident in the confusion matrix. Furthermore, this method is versatile; in addition to detecting surface cracks, it can also be employed to identify other types of structural defects, such as spalling, rebar exposure, corrosion, etc., provided corresponding images of structural defects are available for training. Even then, it is essential to note a significant drawback of the proposed method, which involves the rough estimation of crack area. This assumption is based on considering the size of the crack to be the same as the patch size.

The present study is subject to certain limitations. The models were specifically trained to identify and predict crack depths because of monotonic loading. There is a need for further investigations to validate the model's performance when confronted with cracks induced by different types of loading, such as cyclic loading. In addition to that, the models underwent training and testing using an image dataset characterised by a limited number of images. These images were captured under favourable lighting conditions, with efforts made to eliminate background noise. Future studies are encouraged to explore a broader range of illumination conditions and consider scenarios where background noise is present. It is worth noting that, in this study, the maximum crack depth was assumed to be uniform along the length of the crack. To address this simplification, further investigations are warranted to explore the actual variation in crack depth along the length of the crack. These refinements will contribute to a more comprehensive understanding of the model's applicability and performance across diverse conditions.

**CRedit authorship contribution statement**

Geetha R: Conceptualization, Methodology, Formal analysis,  
 Vijayalakshmi R: Investigation, Formal analysis, Writing – original draft.  
 Prakash R: Formal Analysis  
 Sathia R, Writing – original draft.

**Declaration of Competing Interest**

The authors declare that they have no known competing financial interests or personal relationships that could have appeared to influence the work reported in this paper.

**Nomenclature**

$W_{cr}$ - Crack width as per IS 456-2000  
 $a_{cr}$  - Distance considered from the point of the surface to the nearest longitudinal bar  
 $\varepsilon_m$  - Average steel strain  
 $C_{min}$  - Minimum cover of the longitudinal bar  
 $h(or)D$  - Overall depth of the member  
 $x$  - Depth of the neutral axis  
 $a$  -Distance from the compression face to point at which crack width is estimated  
 $E_s$ - Modulus of elasticity of steel  
 $A_s(or)A_{st}$ - Area of tension reinforcement  
 $\varepsilon_1$  - Strain at the level considered, calculation by ignoring concrete in the tension zone  
 $b$  - Breadth of beam  
 $d$  - Effective depth  
 $m, n$  - Modular ratio  
 $W_k$  - Design crack width as per BS EN1992-1-1-2004  
 $\varepsilon_{sm}$  - Mean steel strain mostly under the effect of tension stiffening or shrinkage 0  
 $\varepsilon_{cm}$  - Mean strain in concrete  
 $f_s$  - Stress in tension reinforcement  
 $k_t$  - Factor that expresses the duration of loading  
 $f_{ct, eff}$  - Mean value of tensile strength of the concrete  
 $A_{c, eff}$ - Effective tension area  
 $k_1$ - Coefficient which considers the bond properties of bonded reinforcement  
 $k_2$  - Coefficient strain distribution  
 $\Phi$  - Dia of bar  
 $S_{r, max}$  - Average stabilized crack spacing  
 $\rho_{eff}$  - Effective reinforcement ratio  
 $E_s$  - Modulus of elasticity for steel  
 $E_c$  - Modulus of elasticity for concrete  
 $C$  - Cover provided at the longitudinal bar  
 $A_s$  - Area of tension reinforcement  
 $W_k$  - Design crack width as per EGYPTIAN CODE; 203-2007  
 $S_{rm}$  - Average stabilized crack spacing  
 $\beta$ - Coefficient which is related to average crack width  
 $\beta_1$  - Coefficient for bar bond characteristics  
 $\beta_2$  - Coefficient which accounts load duration  
 $f_{scr}$  - Stress in tension longitudinal reinforcement that causes under first crack stress in the tension reinforcement  
 $d_c$  - Effective cover  
 $M$  - Applied movement  
 $I_{cr}$  - Moment of inertia for cracked section  
 $W_{max}$ - Design crack width as per ACI 318-95  
 $h$  - Overall depth  
 $x$  - Depth of neutral axis  
 $\beta$  - Coefficient relating the average crack width to the design value  
 $A_o$ - Area of concrete surrounding each reinforcing bar

## References

- [1] W. Kaufmann, A. Amin, A. Beck, and M. Lee, "Shear transfer across cracks in steel fibre reinforced concrete," *Eng Struct*, 2019; Vol. 186:508–24.
- [2] P. Folino, M. Ripani, H. Xargay, and N. Rocca, "Comprehensive analysis of fiber reinforced concrete beams with conventional reinforcement," *Eng Struct.*, 2020;202:109862.
- [3] A. Bhosale, MA. Rasheed, SS. Prakash, and G. Raju, "A study on the efficiency of steel vs. synthetic vs. hybrid fibers on fracture behaviour of concrete in flexure using acoustic emission," *Constr Build Mater* 2019;199:256–68.
- [4] R. Sathia and R. Vijayalakshmi, "Fresh and mechanical property of caryota-urens fiber reinforced flowable concrete," *J. Mater. Res. Technol.*, vol. 15, pp. 3647–3662, 2021, doi: 10.1016/j.jmrt.2021.09.126.
- [5] R. Vijayalakshmi et al., "Fresh and Hardened Property of Fish Tail Palm Fiber Reinforced concrete - Effect of Fiber Content and Fiber Length," *Eur. J. Environ. Civ. Eng.*, pp. 1–19, 2022, [Online]. Available: <https://doi.org/10.1080/19648189.2022.2086178>.
- [6] B. Bhosale, C. Lakavath, and S. Suriya Prakash, "Multi-linear tensile stress-crack width relationships for hybrid fibre reinforced concrete using inverse analysis and digital image correlation," *Eng. Struct.*, vol. 225, no. February, p. 111275, 2020, doi: 10.1016/j.engstruct.2020.111275.
- [7] S. Mansourdehghan, K.M. Dolatshahi, A.H. Asjodi, Data-driven damage assessment of reinforced concrete shear walls using visual features of damage, *J. Build. Eng.* (2022), 104509.
- [8] H. Kim, E. Ahn, S. Cho, M. Shin, S.H. Sim, Comparative analysis of image binarization methods for crack identification in concrete structures, *Cement Concr. Res.* 99 (2017) 53–61.
- [9] M. Rabah, A. Elhattab, A. Fayad, Automatic concrete cracks detection and mapping of terrestrial laser scan data, *NRIAG J. Astron. Geophys.* 2 (2) (2013) 250–255.
- [10] T. Yamaguchi, S. Nakamura, R. Saegusa, S. Hashimoto, Image-based crack detection for real concrete surfaces, *IEEJ Trans. Electr. Electron. Eng.* 3 (1) (2008) 128–135.
- [11] B.Y. Lee, Y.Y. Kim, S.-T. Yi, J.-K. Kim, Automated image processing technique for detecting and analysing concrete surface cracks, *Struct. Infrastruct. Eng.* 9 (6) (2013) 567–577.
- [12] G. Li, X. Zhao, K. Du, F. Ru, Y. Zhang, Recognition and evaluation of bridge cracks with modified active contour model and greedy search-based support vector machine, *Autom. ConStruct.* 78 (2017) 51–61.
- [13] M.R. Jahanshahi, S.F. Masri, C.W. Padgett, G.S. Sukhatme, An innovative methodology for detection and quantification of cracks through incorporation of depth perception, *Mach. Vis. Appl.* 24 (2) (2013) 227–241.
- [14] C.V. Dung, "Autonomous concrete crack detection using deep fully convolutional neural network," *Autom. Constr.* 2019, 99, 52–58
- [15] Sandeep Sony, Kyle Dunphy, Ayan Sadhu, Miriam Capretz, A systematic review of convolutional neural network-based structural condition assessment techniques, *Engineering Structures*, Volume 226, 2021, 111347, ISSN 0141-0296.
- [16] D. Li, J. Liu, S. Hu, G. Cheng, Y. Li, Y. Cao, B. Dong, Y.F. Chen, A deep learning-based indoor acceptance system for assessment on flatness and verticality quality of concrete surfaces, *J. Build. Eng.* 51 (2022), 104284.
- [17] Y. Xu, S. Li, D. Zhang, Y. Jin, F. Zhang, N. Li, H. Li, Identification framework for cracks on a steel structure surface by a restricted Boltzmann machines algorithm based on consumer-grade camera images, *Struct. Control Health Monit.* 25 (2) (2018), e2075.
- [18] C. Modarres, N. Astorga, E.L. Drogue, V. Meruane, Convolutional neural networks for automated damage recognition and damage type identification, *Struct. Control Health Monit.* 25 (10) (2018), e2230.
- [19] J. Jo, Z. Jadidi, A high precision crack classification system using multi-layered image processing and deep belief learning, *Struct. Infrastruct. Eng.* 16 (2) (2020) 297–305.
- [20] S. Li, X. Zhao, Image-based concrete crack detection using convolutional neural network and exhaustive search technique, *Adv. Civ. Eng.* (2019) 2019.
- [21] F.-C. Chen, M.R. Jahanshahi, NB-CNN, Deep learning-based crack detection using convolutional neural network and Naïve Bayes data fusion, *IEEE Trans. Ind. Electron.* 65 (5) (2017) 4392–4400.
- [22] F. Fang, L. Li, Y. Gu, H. Zhu, J.-H. Lim, A novel hybrid approach for crack detection, *Pattern Recogn.* 107 (2020), 107474.
- [23] A. Krizhevsky, I. Sutskever, G.E. Hinton, Imagenet classification with deep convolutional neural networks, *Adv. Neural Inf. Process. Syst.* 25 (2012) 1097–1105.
- [24] C.F. Ozgenel, (2019), "Concrete Crack Images for Classification", *Mendeley Data*, V2, doi: 10.17632/5y9wdsg2zt.2
- [25] K. Simonyan, A. Zisserman, Very Deep Convolutional Networks for Large-Scale Image Recognition, 2014, p. 1556, arXiv preprint arXiv:1409.
- [26] S.J. Pan, Q. Yang, A survey on transfer learning, *IEEE Trans. Knowl. Data Eng.* 22 (10) (2009) 1345–1359.
- [27] .S. Rao, T. Nguyen, M. Palaniswami, T. Ngo, Vision-based Automated Crack Detection Using Convolutional Neural Networks for Condition Assessment of Infrastructure, *Structural Health Monitoring*, 2020, 1475921720965445.

## IN MEMORIAM – Prof. Mihailo Muravljev, PhD December 19, 1937 – January 11, 2024



Numerous friends, colleagues, former students, and admirers of the honoured Professor Mihailo Muravljev, PhD received with deep sorrow the news that he left us forever on January 11, 2024.

As a retired full professor of the Faculty of Civil Engineering at the University of Belgrade, Professor Mihailo Muravljev left behind an exceptionally rich pedagogical, scientific, and professional legacy, which certainly places him among the true doyens of Serbian engineering.

Professor Mihailo Muravljev was born in Petrovgrad (now Zrenjanin) on December 19, 1937. He finished elementary school and secondary school in his hometown before enrolling at the Faculty of Civil Engineering of the University of Belgrade in 1954. He graduated in 1960 with a thesis on Concrete Bridges under the guidance of the renowned Professor Mijat Trojanović. On the same faculty, he obtained his master's degree in 1968 with the thesis "Contribution to the Calculation of Girder Bridges in the Curve" and then earned his PhD in 1975 with the thesis "Behavior of Open-Profile Thin-Walled Beams Made of Prestressed Concrete under Limited Torsion with Concrete Creep Effects."

After graduation, he worked for construction companies "Tunelogradnja" in Belgrade and "Rudar" in Tuzla, as well as at the Institute for Mining and Chemical-Technological Research in Tuzla. From 1967 to 1981, he was employed at the Institute for Materials Testing of the Republic of Serbia (IMS) as an assistant, research associate, and senior research associate. In the period between 1969 and 1970, he spent six months in Cuba as a technical assistant. In 1975, he spent two months at the University of Berkeley (USA - California), focusing on the issue of the seismic resistance of buildings. In 1981, he joined the Faculty of Civil Engineering of the University of Belgrade as an associate professor, teaching Building Materials. He was promoted to full professor in 1988. In addition to Building Materials, during his academic career, he also held courses such as Building Materials 2, Concrete Technology, Installations and Finishing Works in Civil Engineering, Building Design and Construction 2, and Testing of Structures. He also lectured on the Rheology of Building Materials, Selected Chapters of Concrete Technology and Concrete Structures, and Lightweight Concrete in postgraduate studies. For almost all the above-mentioned courses, students had access to appropriate textbooks authored or co-authored by Professor Muravljev. He also mentored a large number of undergraduate and master's theses, as well as 14 doctoral dissertations.

In addition to actively teaching at his home faculty in Belgrade, Professor Muravljev laid the foundations and held courses for many years in various subjects in the field of building materials and concrete technology at the Faculty of Technical Sciences in Novi Sad, the Faculty of Civil Engineering and Architecture in Niš, the Faculty of Civil Engineering in Podgorica, and at the Faculty of Civil Engineering in Priština (later in Kosovska Mitrovica). At all these institutions of higher education, Professor Muravljev, along with his colleagues, was present practically until personnel capable of independently conducting classes emerged, thanks to his generous help and commitment.

Between 1984 and 1986, Professor Muravljev was the director of the Institute for Materials and Structures (IMK), and in two terms, from 1991 to 1998 and from 2001 to 2003, he was the head of the Department of Materials and Structures, as well as the president of the Department of Structures at the Faculty of Civil Engineering, University of Belgrade.

Throughout more than half a century in his scientific-research and professional activities, Professor Mihailo Muravljev was primarily focused on building materials, concrete technology, as well as civil engineering structure design in the broadest sense of the word (structures of reinforced and prestressed concrete, masonry structures, structural testing, etc.). In addition, he made a significant contribution to the areas of repair, reconstruction, and strengthening of civil engineering structures. In his work, he emphasised the organic connection between materials and structures, as well as the need for combining the analytical and experimental approaches to solving a wide range of civil engineering problems. This particularly applies to his work related to the issues of structure repair and strengthening, using modern materials such as carbon fibres, composite reinforcement, and synthetic resins.

Both in the scientific and professional fields, Professor Muravljev was extremely "socially active." Since 2001, he was a regular member of the Serbian Engineering Academy. As an exceptionally prolific author, he contributed to 28 books, wrote about 250 scientific papers, and participated in about 100 significant projects, along with providing a large number of expert opinions, reviews, and technical solutions. He supervised the implementation of two scientific projects and 12 studies. He was also the long-time president of the Yugoslav Society for Testing and Research of Materials and Structures (JUDIMK) in three terms, and later became the life-long honorary president of that Society. Within JUDIMK, with great enthusiasm and energy, he organised a number of scientific and professional thematic conferences. He received the title of honorary member of the Union of Civil Engineers and Technicians of Serbia and Yugoslavia, as well as the Award for Lifetime Achievement in the field of civil engineering construction from the Society of Civil Engineers of Serbia, along with much other social recognition. In 2018, he received the Award for Lifetime Achievement from the Engineering Chamber of Serbia, holding a "zero licence" as a responsible designer of civil engineering structures for high-rise, low-rise, and hydro-structures. He also received a special plaque on the occasion of the celebration of 175 years since the beginning of education in the field of civil engineering in Serbia.

Professor Muravljev was also a long-time member of the Commission for Vocational Examinations of the Union of Civil Engineers of Serbia, and participated in the work of numerous professional commissions for the preparation of technical regulations, such as rulebooks, standards, by-laws, etc. He was the editor of the journal "Naše građevinarstvo" the chief editor of the "Građevinski kalendar," as well as a member of the editorial boards of many other journals and publications. Additionally, he was a long-time member of the international RILEM association, the European Committee for Concrete, and a member of the UNESCO Commission for Monitoring the Reconstruction of the Old Bridge in Mostar.

From the vast number of works of Professor Mihailo Muravljev in the field of civil engineering construction, only the most significant realised projects are listed here:

- Bridge over the Danube River near Beška (first collaborator of the project designer, academician Branko Žeželj),
- Remediation of the same bridge damaged by bombing by NATO aviation (conceptual solution holder and consultant during project development),
- Pedestrian suspension bridge over the Ibar River in Mataruška Banja,
- Bridge over the Neretva River in Mostar,
- Bridge over the Neretva River in Čapljina,
- Bridge over the Željeznica River in Serbian Sarajevo,
- Several structures in the prefabricated skeleton system IMS,
- Repair of a part of the "Bečići" hotel complex after the earthquake in Montenegro,
- Repair of the "Southern Shore" and "Southern Wharf" structures of the shipyard in Bijela,
- Structural project of the Yugoslav Drama Theatre building in Belgrade,
- Repair of a number of structures within the Oil Refinery in Pančevo,
- Repair of the roof of the JP SRPC "Milan Gale Muškatirović" building in Belgrade,
- Repair of the 150 m high reinforced concrete chimney within blocks A1, A2, and A3 of TENT – Obrenovac.

In all the listed projects, Professor Muravljev was practically involved in all phases of implementation: from conceptual solutions, through the main project, detailed elaboration, field research, execution, and supervision.

In his work with younger associates, Professor Muravljev always showed exceptional care and respect, as an older and more experienced colleague, but at the same time as a teacher and a father figure. Even after his retirement in 2003, although formally he could no longer be a teacher and mentor, he selflessly continued to assist younger colleagues, inspiring topics for new research and actively participating in the implementation of experimental tests. Despite his advanced age and declining health, he visited the faculty almost every day, where he spent a full 43 years. In his office, he devotedly and diligently worked on new and useful publications, followed innovations in the field of materials and structures, was always ready for professional discussions, and provided appropriate suggestions for practical engineering solutions.

It can be freely said that Professor Muravljev devoted the largest part of his energy and effort to education, both for students and accomplished engineers. He had that very rare talent to present difficult and complicated matters in a simple and understandable way. Moreover, he skillfully seasoned theory with interesting examples from practice. In addition, Professor Muravljev was an extremely prolific author of a large number of books (some of which had seen multiple editions), monographs, and other publications. His most significant bibliographic entries include the following titles:

- Building Materials,
- Building Materials 2 (co-authored with D. Jevtić),
- Collection of solved examples from Building materials exams (co-authored with S. Živković),
- Fundamentals of the Theory and Technology of Concrete,
- Collection of solved examples from Concrete technology exams (co-authored with D. Zakić),
- Concrete Technology – Theory and Practice (co-authored with D. Zakić and A. Radević),
- Masonry and Timber Building Structures (co-authored with B. Stevanović),
- Repair of Civil Engineering Structures and Facilities (co-authored with B. Stevanović and D. Ostojić),
- Concrete and Reinforced Concrete according to BAB 87, Volume 1, three chapters in the Handbook,
- Special Mortars and Concretes (author of five chapters and editor of the monograph),
- Civil Engineering Physics and Materials (author of two chapters and editor of the monograph),
- Practical Application of Sika Carbon Straps in Strengthening of Concrete Structures,
- Basic Aspects of Practical Application of Composite GFRP Reinforcement,
- Monograph "135 Years of Higher Education in the Field of Building Materials at the Faculty of Civil Engineering in Belgrade" (co-authored with S. Živković, D. Jevtić, D. Zakić, and A. Savić),
- Methods of Increasing the Bearing Capacity of Concrete Structures with Examples from Practice,
- Basics of Concrete Structure Repair Using Injection Procedures,
- A Brief History of the Development of Building Materials with Examples of Use to the Present Day.

- Based on the above, it is clear that Professor Muravljev was a distinguished educator, lucid engineer, and respected scientist with vast knowledge and experience, who left an indelible mark in the field of civil engineering through his comprehensive and long-standing work. Moreover, throughout his entire career, he was characterised by the highest human, professional, and ethical virtues. The results of his work, both in terms of quantity and quality, can serve as the best example of an outstanding career for future generations of students, teachers, and engineers.

What can be said in the end, when we lose someone who was such a great person, professor, scientist, and engineer, someone who was a top authority in the field of Civil engineering not only in Serbia but also in the wider territory of the former Yugoslavia and the entire Balkans? As a consolation to the family and friends, it remains the fact that Professor Muravljev lived a fulfilled and fruitful life, filled with love and respect from his closest family members as well as his students, colleagues, and friends. Many people adored and respected him.

Although Professor Muravljev is no longer with us, we will often mention him and fondly remember him; his books will continue to teach new generations of students and engineers, while close colleagues and friends will continue to cherish his memory. Mihailo Muravljev was extremely dedicated to his family, his wife Miroslava, his son Nikola, and especially his grandchildren Ružica and Ljubica, whom he loved boundlessly and was particularly proud of. His departure is a painful and irreplaceable loss for all those who knew and respected him, for all who learned from him and socialised with him, and most of all for close family members, to whom we once again express our deepest and most sincere condolences.

In Belgrade, March 2024

Prof. Dragica Jevtić, PhD TE

Prof. Dimitrije Zakić, PhD CE



# Building Materials and Structures

## GUIDE FOR AUTHORS

In the journal *Building Materials and Structures*, the submission and review processes take place electronically. Manuscripts are submitted electronically (online) on the website <https://www.dimk.rs>. The author should register first, then log in and finally submit the manuscript which should be in the form of editable files (e.g. Word) to enable the typesetting process in journal format. All correspondence, including Editor's decision regarding required reviews and acceptance of manuscripts, take place via e-mail.

### TYPES OF ARTICLES

The following types of articles are published in *Building Materials and Structures*:

**Original scientific article.** It is the primary source of scientific information, new ideas and insights as a result of original research using appropriate scientific methods. The results are presented briefly, but in a way to enable readers to assess the results of experimental or theoretical/numerical analyses, so that the research can be repeated and yield with the same or results within the limits of tolerable deviations.

**Review article.** It presents the state of science in particular area as a result of methodically systematized, analyzed and discussed reference data. Only critical review manuscripts will be considered as providing novel perspective and critical evaluation of the topics of interest to broader BMS readership.

**Preliminary report.** Contains the first short notifications of research results without detailed analysis, i.e. it is shorter than original research paper.

**Technical article.** Reports on the application of recognized scientific achievements of relevance to the field of building materials and structures. Contain critical analysis and recommendations for adaption of the research results to practical needs.

**Projects Notes.** Project Notes provide a presentation of a relevant project that has been built or is in the process of construction. The original or novel aspects in design or construction should be clearly indicated.

**Discussions.** Comment on or discussion of a manuscript previously published in *Building Materials and Structures*. It should be received by the Editor-in-Chief within six months of the online publication of the manuscript under discussion. Discussion Papers will be subject to peer review and should also be submitted online. If Discussion Paper is selected for publication the author of the original paper will be invited to respond, and Discussion Paper will be published alongside any response that the author.

Other contributions

**Conference Reports.** Reports on major international and national conferences of particular interest to *Building Materials and Structures*. Selected and/or awarded papers from the ASES Conferences are published in Special issues.

**Book Reviews.** Reviews on new books relevant to the scope of *Building Materials and Structures*.

### PREPRINTS

These are the author's own write-up of research results and analysis that has not been peer reviewed, nor had any other value added to it by a publisher (such as formatting, copy-editing, technical enhancements and the like). Authors can share their preprint anywhere at any time. If accepted for publication, we encourage authors to link from the preprint to their formal publication via its Digital Object Identifier (DOI). Preprints should not be added to or enhanced in any way in order to appear more like, or to substitute for, the final versions of articles.

### MANUSCRIPT STRUCTURE

The manuscript should be typed one-sided on A4 sheets. Page numbers should be included in the manuscript and the text should be single spaced with **consecutive line numbering** - these are essential peer review requirements. The figures and tables included in the single file should be placed next to the relevant text in the manuscript. The corresponding captions should be placed directly below the figure or table. If the manuscript contains Supplementary material, it should also be submitted at the first submission of the manuscript for review purposes.

There are no strict rules regarding the structure of the manuscript, but the basic elements that it should contain are: Title page with the title of the manuscript, information about the authors, abstract and keywords, Introduction, Materials / Methods, Results and Conclusions.

### ***The front page***

The front page contains the title of the manuscript which should be informative and concise; abbreviations and formulas should be avoided.

Information about the authors are below the title; after the author's name, a superscript number is placed indicating his/her affiliation, which is printed below the author's name, and before the abstract. It is obligatory to mark the corresponding author with superscript \*) and provide his/her e-mail address. The affiliation should contain the full name of the institution where the author performed the research and its address.

### ***Abstract***

Abstract should contain 150-200 words. Motivation and objective of the conducted research should be presented; main results and conclusions should be briefly stated as well. References and abbreviations should be avoided.

### ***Keywords***

Keywords (up to 10) should be listed immediately after the abstract; abbreviations should be used only if they are generally accepted and well-known in the field of research.

### ***Division into chapters***

The manuscript should be divided into chapters and sub-chapters, which are hierarchically numbered with Arabic numbers. The headings of chapters and sub-chapters should appear on their own separate lines.

At the end of the manuscript, and before the references, it is obligatory to list the following statements:

### ***CRediT authorship contribution statement***

For transparency, we require corresponding authors to provide co-author contributions to the manuscript using the relevant CRediT roles. The [CRediT taxonomy](#) includes 14 different roles describing each contributor's specific contribution to the research output. The roles are: Conceptualization; Data curation; Formal analysis; Funding acquisition; Investigation; Methodology; Project administration; Resources; Software; Supervision; Validation; Visualization; Roles/Writing - original draft; and Writing - review & editing. Note that not all roles may apply to every manuscript, and authors may have contributed through multiple roles.

### ***Declaration of competing interest***

Corresponding authors, on behalf of all the authors of a submission, must disclose any financial and personal relationships with other people or organizations that could inappropriately influence their work. Examples of potential conflicts of interest include employment, consultancies, stock ownership, honoraria, paid expert testimony, patent applications/registrations, and grants or other funding. All authors, including those *without* competing interests to declare, should provide the relevant information to the corresponding author (which, where relevant, may specify they have nothing to declare).

### ***Declaration of generative AI in scientific writing***

This guidance only refers to the writing process, and not to the use of AI tools to analyze and draw insights from data as part of the research process. Where authors use generative artificial intelligence (AI) and AI-assisted technologies in the writing process, authors should only use these technologies to improve readability and language. Applying the technology should be done with human oversight and control, and authors should carefully review and edit the result, as AI can generate authoritative-sounding output that can be incorrect, incomplete or biased. AI and AI-assisted technologies should not be listed as an author or co-author, or be cited as an author. Authorship implies responsibilities and tasks that can only be attributed to and performed by humans. Authors should disclose in their manuscript the use of AI and AI-assisted technologies in the writing process by following the instructions below. A statement will appear in the published work. Please note that authors are ultimately responsible and accountable for the contents of the work.

### ***Disclosure instructions***

Authors must disclose the use of generative AI and AI-assisted technologies in the writing process by adding a statement at the end of their manuscript in the core manuscript file, before the References list. The statement should be placed in a new section entitled 'Declaration of Generative AI and AI-assisted technologies in the writing process'.

*Statement: During the preparation of this work the author(s) used [NAME TOOL / SERVICE] in order to [REASON]. After using this tool/service, the author(s) reviewed and edited the content as needed and take(s) full responsibility for the content of the publication.*

This declaration does not apply to the use of basic tools for checking grammar, spelling, references etc. If there is nothing to disclose, there is no need to add a statement.

### **Acknowledgments**

State the institutions and persons who financially or in some other way helped the presented research. If the research was not supported by others, it should also be stated in this part of the manuscript.

### **Appendices**

The manuscript may have appendices. If there is more than one appendix, they are denoted by A, B, etc. Labels of figures, tables and formulas in appendices should contain the label of the appendix, for example Table A.1, Figure A.1, etc.

### **ABBREVIATIONS**

All abbreviations should be defined where they first appear. Consistency of abbreviations used throughout the text should be ensured.

### **MATH FORMULAE**

Formulae should be in the form of editable text (not in the format of figures) and marked with numbers, in the order in which they appear in the text. The formulae and equations should be written carefully taking into account the indices and exponents. Symbols in formulae should be defined in the order they appear, right below the formulae.

### **FIGURES**

- figures should be made so that they are as uniform in size as possible and of appropriate quality for reproduction;
- the dimensions of the figures should correspond to the format of the journal: figures with a width approximately equal to the width of 1 column ( $\pm 80$  mm width), width of 2 columns ( $\pm 170$  mm width) or width of 1.5 columns ( $\pm 130$  mm width);
- figures should be designed so that their size is not disproportionately large in relation to the content;
- the text on the figures should be minimal and the font used should be the same on all figures (Arial, Times New Roman, Symbol);
- figures should be placed next to the appropriate text in the manuscript and marked with numbers in the order in which they appear in the text;
- each figure should have a caption that is placed below the figure - the caption should not be on the figure itself. In cases of inadequate quality of reproduction, the author should be required to submit figures as separate files. In this case, the figure should be saved in TIFF (or JPG) format with a minimum resolution of 500 dpi.

### **TABLES**

- tables should be in the form of editable text (not in the format of figures);
- tables should be placed next to the appropriate text in the manuscript and marked with numbers in the order in which they appear in the text;
- each table should have a caption that is placed below the table;
- the tables should not show the results that are already presented elsewhere in the manuscript - duplicating the presentation of results should be avoided;
- tables are without vertical lines as boundaries between cells and shading cells.

### **REFERENCES**

#### **Citation in the text**

Each reference cited in the text should be in the reference list (and vice versa). It is not recommended to list unpublished results or personal communications in the reference list, but they can be listed in the text. If they are still listed in the reference list, the journal style references are used, with 'Unpublished results' or 'Personal communication' instead of the date of publication. Citing a reference as 'in press' means that it is accepted for publication.

#### **Web references**

Web references are minimally listed with the full URL and the date when the site was last accessed. These references can be included in the reference list, but can also be given in a separate list after the reference list.

## **Reference style**

In text: References are given in the text by a number in square brackets in the order in which they appear in the text. Authors may also be referred to directly, but the reference number should always be given.

In reference list: References marked with a number in square brackets are sorted by numbers in the list.

## **Examples**

Reference to a journal publication:

[1] V.W.Y. Tam, M. Soomro, A.C.J. Evangelista, A review of recycled aggregate in concrete applications (2000-2017), *Constr. Build. Mater.* 172 (2018) 272-292. <https://doi.org/10.1016/j.conbuildmat.2018.03.240>.

Reference to a book:

[3] A.H. Nilson, D. Darwin, C.W. Dolan, *Design of Concrete Structures*, thirteenth ed., Mc Graw Hill, New York, 2004.

Reference to a chapter in an edited book:

[4] J.R. Jimenez, Recycled aggregates (RAs) for roads, in: F Pacheco-Torgal, V.W.Y. Tam, J.A. Labrincha, Y. Ding, J. de Brito (Eds.), *Handbook of recycled concrete and demolition waste*, Woodhead Publishing Limited, Cambridge, UK, 2013, pp. 351–377.

Reference to a website:

[5] WBCSD, The Cement Sustainability Initiative, World. Bus. Council. Sustain. Dev. <http://www.wbcscement.org/pdf/CSIRecyclingConcrete-FullReport.pdf>, 2017 (accessed 7 July 2016).

## **SUPPLEMENTARY MATERIAL**

Supplementary material such as databases, detailed calculations and the like can be published separately to reduce the workload. This material is published 'as received' (Excel or PowerPoint files will appear as such online) and submitted together with the manuscript. Each supplementary file should be given a short descriptive title.

## **ETHICS IN PUBLISHING**

Authors are expected to respect intellectual and scientific integrity in presentation of their work. The journal publishes manuscripts that have not been previously published and are not in the process of being considered for publication elsewhere. All co-authors as well as the institution in which the research was performed should agree to the publication in the journal.

Authors are expected to submit completely original research; if the research of other researchers is used, it should be adequately cited. Authors who wish to include in their manuscript images, tables or parts of text that have already been published somewhere, should obtain permission from the Copyright owner and provide a proof in the process of submitting the manuscript. All material for which there is no such evidence will be considered the original work of the author. To determine the originality of the manuscript, it can be checked using the [Crossref Similarity Check](#) service. For more information, please see our [Ethics and Malpractice Statement](#).

The Journal and Publishers imply that all authors, as well as responsible persons of the institute where the research was performed, agreed with the content of the submitted manuscript before submitting it. The Publishers will not be held legally responsible should there be any claims for compensation.

## **PEER REVIEW**

This journal uses a single blind review process, which means that the authors do not know the names of the reviewers, but the reviewers know who the authors are. In the review process, the Editor-in-Chief first assesses whether the contents of the manuscript comply with the scope of the journal. If this is the case, the paper is sent to at least two independent experts in the field, with the aim of assessing its scientific quality and making recommendation regarding publication. If the manuscript needs to be revised, the authors are provided with the reviewers' remarks. The authors are obliged to correct the manuscript in accordance with the remarks, submit the revised manuscript and a special file with the answers to the reviewers within the given deadline. The final decision, whether the paper will be published in journal or not, is made by the Editor-in-Chief.

## **AFTER ACCEPTANCE**

Once accepted for publication, the manuscript is set in the journal format. Complex manuscript is sent to the authors in the form of proof, for proof reading. Then, authors should check for typesetting errors, and whether the text, images, and tables are complete and accurate. Authors are asked to do this carefully, as subsequent corrections will not be considered. In addition, significant changes to the text and authorship at this stage are not allowed without the consent of the Editor-in-Chief. After online publication, changes are only possible in the form of Erratum which will be hyperlinked to manuscript.

## **COPYRIGHT**

Authors retain copyright of the published papers and grant to the publisher the non-exclusive right to publish the article, to be cited as its original publisher in case of reuse, and to distribute it in all forms and media.

The published articles will be distributed under the Creative Commons Attribution ShareAlike 4.0 International license ([CC BY-SA](https://creativecommons.org/licenses/by-sa/4.0/)). It is allowed to copy and redistribute the material in any medium or format, and remix, transform, and build upon it for any purpose, even commercially, as long as appropriate credit is given to the original author(s), a link to the license is provided, it is indicated if changes were made and the new work is distributed under the same license as the original.

Users are required to provide full bibliographic description of the original publication (authors, article title, journal title, volume, issue, pages), as well as its DOI code. In electronic publishing, users are also required to link the content with both the original article published in *Building Materials and Structures* and the license used.

Authors are able to enter into separate, additional contractual arrangements for the non-exclusive distribution of the journal's published version of the work (e.g., post it to an institutional repository or publish it in a book), with an acknowledgement of its initial publication in this journal.

## **OPEN ACCESS POLICY**

Journal *Building Materials and Structures* is published under an Open Access license. All its content is available free of charge. Users can read, download, copy, distribute, print, search the full text of articles, as well as to establish HTML links to them, without having to seek the consent of the author or publisher.

The right to use content without consent does not release the users from the obligation to give the credit to the journal and its content in a manner described under *Copyright*.

## **Archiving digital version**

In accordance with law, digital copies of all published volumes are archived in the legal deposit library of the National Library of Serbia in the Repository of SCIndeks - The Serbian Citation Index as the primary full text database.

## **Cost collection to authors**

Journal *Building Materials and Structures* does not charge authors or any third party for publication. Both manuscript submission and processing services, and article publishing services are free of charge. There are no hidden costs whatsoever.

## **DISCLAIMER**

The views expressed in the published works do not express the views of the Editors and the Editorial Staff. The authors take legal and moral responsibility for the ideas expressed in the articles. Publisher shall have no liability in the event of issuance of any claims for damages. The Publisher will not be held legally responsible should there be any claims for compensation.

Financial support



**MINISTRY OF EDUCATION, SCIENCE AND  
TECHNOLOGICAL DEVELOPMENT OF  
REPUBLIC OF SERBIA**

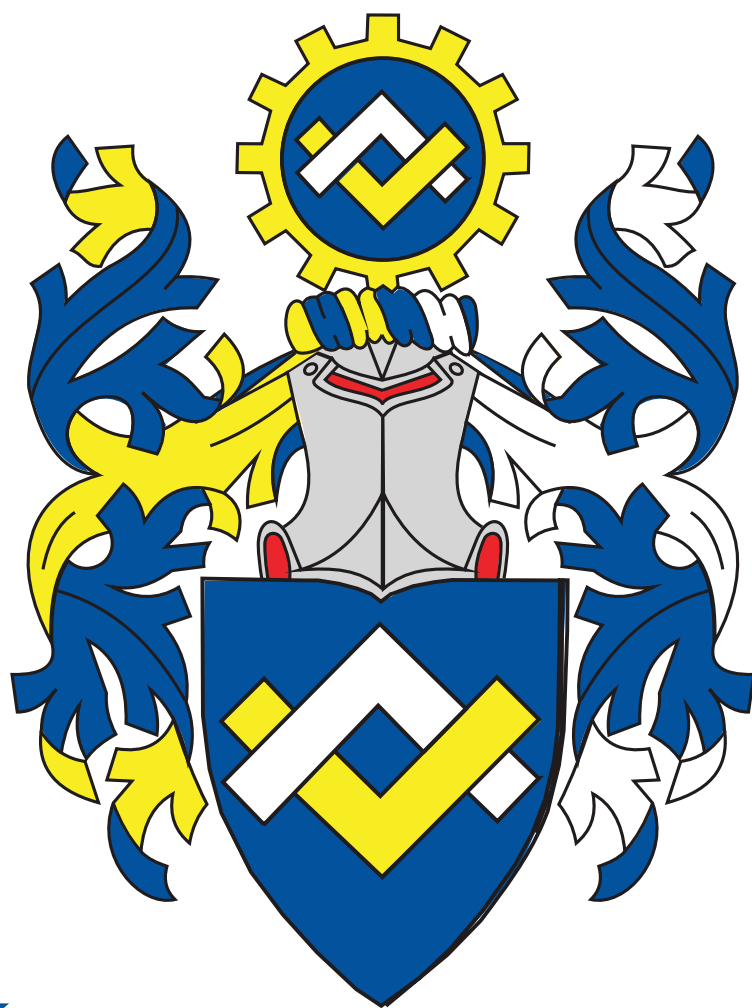


**INSTITUTE FOR TESTING OF MATERIALS-  
IMS INSTITUTE, BELGRADE**



**SERBIAN CHAMBER OF ENGINEERS**





**INŽENJERSKA  
KOMORA  
SRBIJE**



# Ringlock

Doka modularni sistem skela.

Bezbedno i efikasno rešenje za skele. Široka oblast primena.

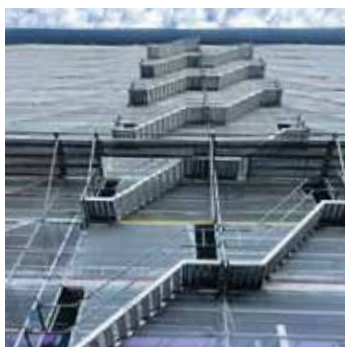
**doka**



**AT-PAC**  
COMPLETE SCAFFOLDING SOLUTIONS

PROVIDING

**Pristupne skele**



**Skele za stambene objekte**



**Skele za poslovne objekte**



**Stepenišni toranj**



**ADING**  
sastojak svake građevine



## ADITIVI ZA BETONE VISOKIH PERFORMANSI

Adresa: Nehruova 82, 11070 Novi Beograd Tel/Fax: + 381 11 616 05 76 email: [ading@ading.rs](mailto:ading@ading.rs)

[www.ading.rs](http://www.ading.rs)

# ACO. The future of drainage.



train



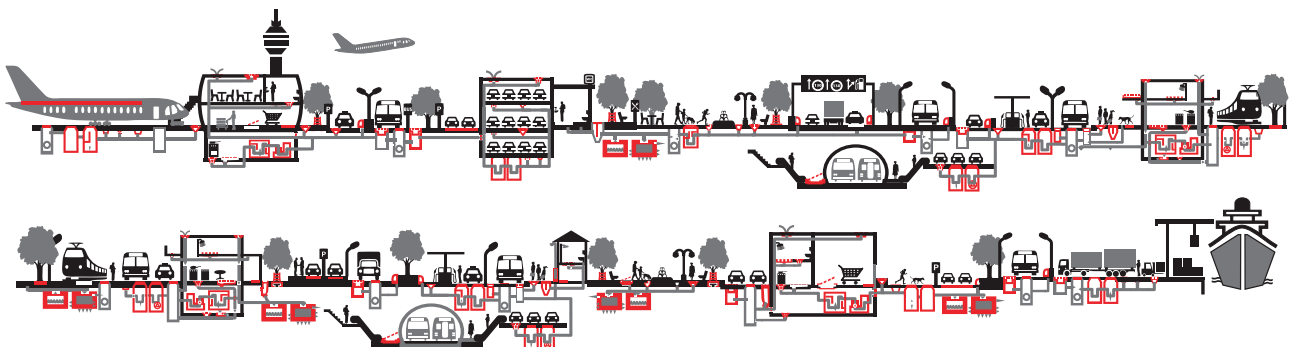
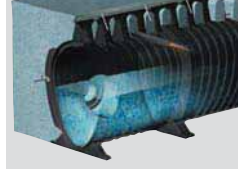
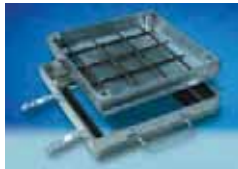
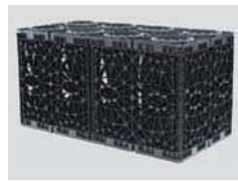
design



support



care



aco.rs

## **CENTAR ZA PUTEVE I GEOTEHNIKU**

U okviru centra posluju odeljenja za geotehniku, nadzor i terenska ispitivanja, projektovanje saobraćajnica, laboratorija za puteve i geotehniku. Značajna aktivnost centra usmerena je ka terenskim i laboratorijskim geološko - geotehničkim istraživanjima i ispitivanjima terena za potrebe izrade projektno - tehničke dokumentacije, za različite faze i nivoe projektovanja objekata visokogradnje, niskogradnje, saobraćaja i hidrogradnje, kao i za potrebe prostornog planiranja i zaštite životne sredine. Stručni nadzor, kontrola kvaliteta tokom građenja, rekonstrukcije i sanacije objekata različite namene, izrada studija, ekspertiza, konsultantske usluge, kompletan konsalting u oblasti geotehničkog inženjeringa, neke su od delatnosti centra.



### **Ispitivanje šipova**

- SLT metoda (Static load test)
- DLT metoda (Dynamic load test)
- PDA metoda (Pile driving analysis)
- PIT (SIT) metoda (Pile (Sonic) integrity testing)
- CSL - Crosshole Sonic Logging



- Ispitivanje šipova
  - Geotehnička istraživanja i ispitivanja – in situ
    - Laboratorija za puteve i geotehniku
      - Projektovanje puteva i sanacija klizišta
        - Nadzor

# Najlepši krov u komšiluku



Continental Plus Natura je premium crep u natur segmentu! Dobro poznatog oblika, trajan i veoma otporan, a povrh svega pristupačan, naprosto oduzima dah svima. Čak i vašim komšijama!

Continental Plus Natura crep potražite kod ovlašćenih Tondach partnera.

## PUT INŽENJERING



Put inženjering d.o.o punih 25 godina radi kao specijalizovano preduzeće za izgradnju infrastrukture u niskogradnji i visokogradnji, kao i proizvodnjom kamenog agregata i betona. Preduzeće se bavi i transportom, uslugama građevinske mehanizacije i specijalne opreme.

Koristeći inovativne tehnike i kvalitetan građevinski materijal iz sopstvenih resursa, spremni smo da odgovorimo na mnoge zahteve naših klijenata iz oblasti niskogradnje.



Osnovna prednost prefabrikovane konstrukcije jeste brzina kojom konstrukcija može biti projektovana, proizvedena, transportovana i namontirana.



Izvodimo hidrograđevinske radove u izgradnji kanalizacionih mreža za odvođenje atmosferskih, otpadnih i upotrebljenih voda, izvođenjem hidrograđevinskih radova u okviru regulacije rečnih tokova, kao i izvođenjem hidrotehničkih objekata.



Površinski kop udaljen je 35 km od Niša. Savremene drobilice, postrojenje za separaciju i sejalice efikasno usitnjavaju i razdvajaju kamene agregate po veličinama. Tehnički kapacitet trenutne primarne drobilice je 300 t/h.



Za spravljanje betona koristimo drobljeni krečnjački agregat sa našeg kamenoloma, deklariranih frakcija, kontrolisane vlažnosti. Kompletan proces proizvodnje i kontrole kvaliteta vršimo prema važećim standardima.



Obradu armature vršimo brzo, stručno i kvalitetno, sa kompjuterskom preciznošću i dimenzijama po projektu.



Naša kompanija u oblasti visokogradnje primenjuje sistem prefabrikovanih betonskih elemenata koji u odnosu na klasičnu gradnju ima brojne prednosti.



Prednapregnute šuplje ploče su konstruktivni elementi visokog kvaliteta, proizvedeni u fabrički kontrolisanim uslovima.



Izrađujemo betonske "New Jersey profile" koji se u svetu koriste za preusmeravanje saobraćaja i zaštitu pešaka u toku izgradnje puta, kao i Betonblock sistem betonskih blokova.



Uslugu transporta vršimo automikserima, kapaciteta bubnja od 7 m<sup>3</sup> do 10 m<sup>3</sup> betonske mase. Za ugradnju betona posedujemo auto-pumpu za beton, radnog učinka 150 m<sup>3</sup>/h, sa dužinom strele od 36 m.



Kao generalni izvođač radova, vršimo koordinaciju svih učesnika na projektu, planiranje, praćenje i nabavku materijala, kontrolu kvaliteta izvedenih radova, poštujući zadate vremenske rokove i finansijski okvir investitora.



Osnovi princip našeg poslovanja zasniva se na individualnom pristupu svakom klijentu i pronalaženje najoptimalnijeg rešenja za njegove transportne i logističke potrebe.



Usluge građevinske mehanizacijom vršimo tehnički ispravnim mašinama, sa potrebnim sertifikatima kako za rukovoce građevinskim mašinama tako i za same mašine.



Raspoložemo opremom i mašinama za sve zemljane radove, kipere i dampere za rad u teškim terenskim uslovima, automiksere i pumpe za beton, autodizalice, podizne platforme.



Sakupljanje i privremeno skladištenje otpada vršimo našim specijalizovanim vozilima i deponujemo na našu lokaciju sa odgovarajućom dozvolom. Kapacitet mašine je 250 t/h građevinskog neopasnog otpada.



### NIŠ

Knjaževačka bb, 18000 Niš - Srbija  
+381 18 215 355  
office@putinzenjering.com

### BEOGRAD

Jugoslovenska 2a, 11250 Beograd - Železnik  
+381 11 25 81 111  
beograd@putinzenjering.com



# ŽIVOT JE LEPŠI KADA BIRATE KVALITETNO



Mapei proizvodi i rešenja su izbor onih koji znaju da prepoznaju kvalitet, posvećenost svakom detalju i višedecenijsko iskustvo u građevinskoj industriji.

**Zato birajte pažljivo. Birajte kvalitet.**

Mapei, svetski lider u proizvodnji građevinskih lepкова, hidroizolacija i masa za fugovanje.



Saznaj više na [www.mapei.rs](http://www.mapei.rs)



**ŽIVI KVALITETNO**

## MATEST "IT TECH" KONTROLNA JEDINICA



### JEDNA TEHNOLOGIJA MNOGO REŠENJA

IT Touch Technology je Matestov najnoviji koncept koji ima za cilj da ponudi inovativna i user-friendly tehnologiju za kontrolu i upravljanje najmodernijom opremom u domenu testiranja građevinskih materijala

Ova tehnologija je srž Matestove kontrolne jedinice, software baziran na Windows platformi i touch screen sistem koji je modularan, fleksibilan i obavlja mnoge opcije

- IT TECH pokriva | INOVATIVNOST
- | INTERNET KONEKCIJA
- | INTERFEJS SA IKONICAMA
- | INDUSTRIJALNA TEHNOLOGIJA

### SISTEM JEDNOG RAZMIŠLJANJA JEDNOM SHVATIŠ - SVE TESTIRAŠ



#### NAPREDNA TEHNOLOGIJA ISPITIVANJA ASFALTA

- | GYROTRONIC - Gyrotory Compactor
- | ARC - Electromechanical Asphalt Roller Compactor
- | ASC - Asphalt Shear Box Compactor
- | SMARTRACKER™ - Multiwheels Hamburg Wheel Tracker, DRY + WET test environment
- | SOFTMATIC - Automatic Digital Ring & Ball Apparatus
- | Ductilometers with data acquisition system

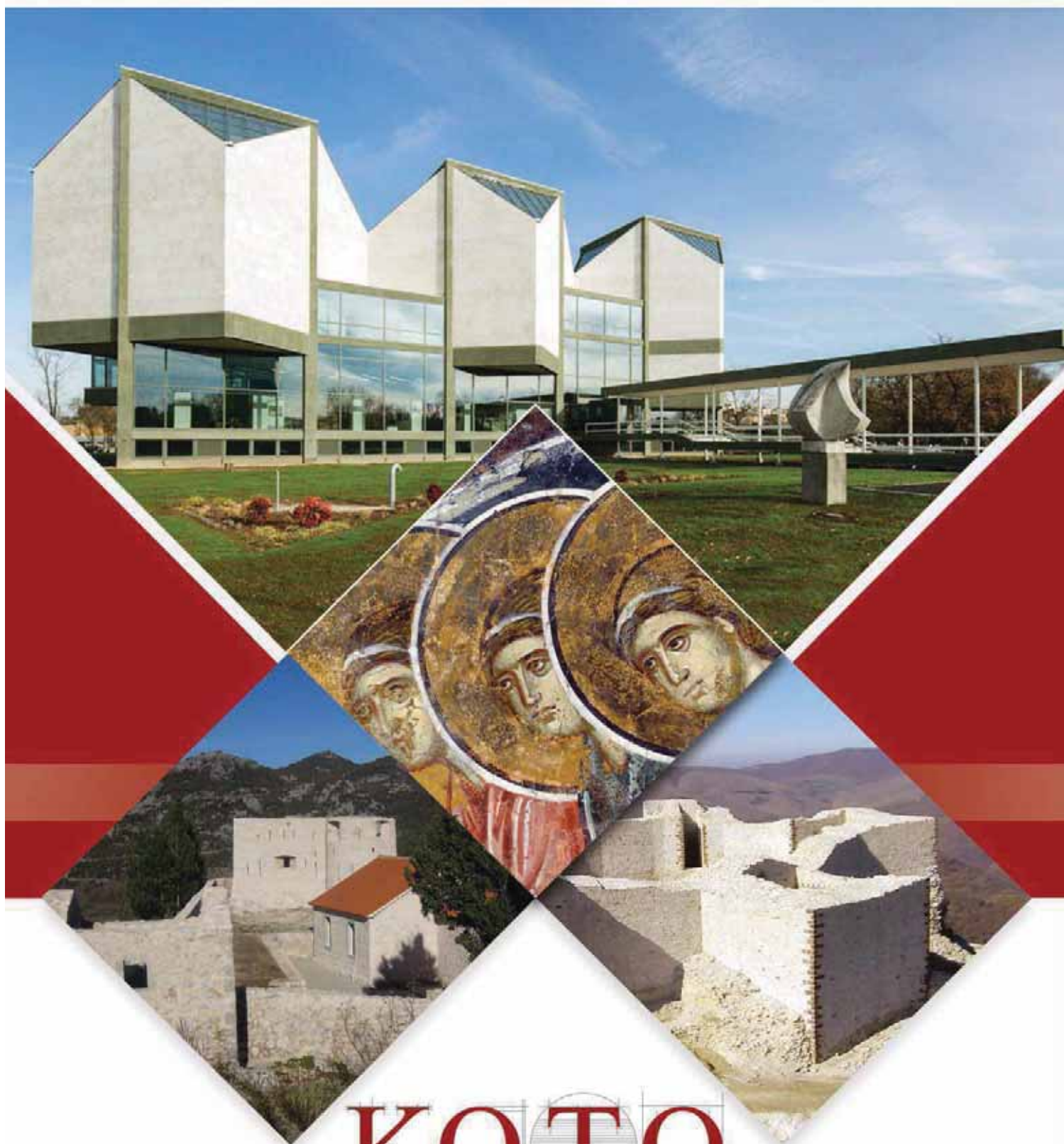
#### MULTIFUNKCIONALNI RAMOVI ZA TESTIRANJE

- | CBR/Marshall digital machines
- | Universal multispeed load frames
- | UNITRONIC 50kN or 200kN Universal multipurpose compression/flexural and tensile frames

#### OPREMA ZA GEOMEHANIČKO ISPITIVANJE

- | EDOTRONIC - Automatic Consolidation Apparatus
- | SHEARLAB - AUTOSHEARLAB - SHEARTRONIC
- Direct / Residual shear testing systems
- | Triaxial Load Frame 50kN

**MIXMATIC** - Automatic Programmable Mortar Mixer



# KOTO

[www.koto.rs](http://www.koto.rs) | [office@koto.rs](mailto:office@koto.rs) | 011 309 7410 | Vojvode Stepe br. 466, Beograd